Springer Theses
Recognizing Outstanding Ph.D. Research

Taro Noguchi

Development of Chemistry-Based Screening Platform for Access to Mirror-Image Library of Natural Products

Springer

Springer Theses

Recognizing Outstanding Ph.D. Research

Aims and Scope

The series "Springer Theses" brings together a selection of the very best Ph.D. theses from around the world and across the physical sciences. Nominated and endorsed by two recognized specialists, each published volume has been selected for its scientific excellence and the high impact of its contents for the pertinent field of research. For greater accessibility to non-specialists, the published versions include an extended introduction, as well as a foreword by the student's supervisor explaining the special relevance of the work for the field. As a whole, the series will provide a valuable resource both for newcomers to the research fields described, and for other scientists seeking detailed background information on special questions. Finally, it provides an accredited documentation of the valuable contributions made by today's younger generation of scientists.

Theses are accepted into the series by invited nomination only and must fulfill all of the following criteria

- They must be written in good English.
- The topic should fall within the confines of Chemistry, Physics, Earth Sciences, Engineering and related interdisciplinary fields such as Materials, Nanoscience, Chemical Engineering, Complex Systems and Biophysics.
- The work reported in the thesis must represent a significant scientific advance.
- If the thesis includes previously published material, permission to reproduce this must be gained from the respective copyright holder.
- They must have been examined and passed during the 12 months prior to nomination.
- Each thesis should include a foreword by the supervisor outlining the significance of its content.
- The theses should have a clearly defined structure including an introduction accessible to scientists not expert in that particular field.

More information about this series at http://www.springer.com/series/8790

Taro Noguchi

Development of Chemistry-Based Screening Platform for Access to Mirror-Image Library of Natural Products

Doctoral Thesis accepted by
Kyoto University, Japan

Springer

Author
Dr. Taro Noguchi
Graduate School of Pharmaceutical Sciences
Kyoto University
Kyoto
Japan

Supervisors
Prof. Shinya Oishi
Graduate School of Pharmaceutical Sciences
Kyoto University
Kyoto
Japan

Prof. Nobutaka Fujii
Graduate School of Pharmaceutical Sciences
Kyoto University
Kyoto
Japan

Prof. Hiroaki Ohno
Graduate School of Pharmaceutical Sciences
Kyoto University
Kyoto
Japan

ISSN 2190-5053 ISSN 2190-5061 (electronic)
Springer Theses
ISBN 978-981-10-6622-1 ISBN 978-981-10-6623-8 (eBook)
https://doi.org/10.1007/978-981-10-6623-8

Library of Congress Control Number: 2017953817

© Springer Nature Singapore Pte Ltd. 2018
This work is subject to copyright. All rights are reserved by the Publisher, whether the whole or part of the material is concerned, specifically the rights of translation, reprinting, reuse of illustrations, recitation, broadcasting, reproduction on microfilms or in any other physical way, and transmission or information storage and retrieval, electronic adaptation, computer software, or by similar or dissimilar methodology now known or hereafter developed.
The use of general descriptive names, registered names, trademarks, service marks, etc. in this publication does not imply, even in the absence of a specific statement, that such names are exempt from the relevant protective laws and regulations and therefore free for general use.
The publisher, the authors and the editors are safe to assume that the advice and information in this book are believed to be true and accurate at the date of publication. Neither the publisher nor the authors or the editors give a warranty, express or implied, with respect to the material contained herein or for any errors or omissions that may have been made. The publisher remains neutral with regard to jurisdictional claims in published maps and institutional affiliations.

Printed on acid-free paper

This Springer imprint is published by Springer Nature
The registered company is Springer Nature Singapore Pte Ltd.
The registered company address is: 152 Beach Road, #21-01/04 Gateway East, Singapore 189721, Singapore

Supervisor's Foreword

It is my pleasure to introduce Dr. Taro Noguchi's thesis for the Springer Theses, as an outstanding doctoral work in one of the internationally top-ranked universities. Dr. Noguchi started his research career at Kyoto University as an undergraduate student under the supervision of Prof. Nobutaka Fujii, Prof. Hiroaki Ohno, and myself in April 2011. At the beginning of his career, before he started this thesis project, he engaged in a structure–activity relationship study of neuropeptide derivatives to regulate reproductive neuroendocrine systems. During this period, he practiced a series of solid-phase techniques for peptide synthesis. In the spring of 2012, he initiated his doctoral study, developing a mirror-image screening process for drug discovery, at the Graduate School of Pharmaceutical Sciences, Kyoto University. His original concern was for the synthesis of natural products by organic chemistry. To determine the synthetic target(s) for his natural product project, he had to perform a protein synthesis study. After 1 year of investigations, he achieved the total synthesis of mirror-image L- and D-proteins of MDM2 and MDMX through a simple solid-phase peptide synthesis without particular ligation technologies. Although this research group did not have specific expertise concerning the synthesis of large protein molecules, he acquired many useful techniques and significant experience through numerous experiments. He also established synthetic protocols for the SH2 domain of the Grb2 protein, which is the first example of the chemical synthesis of SH2 domain proteins. With several synthetic mirror-image proteins in hand, his research was extended to screening projects in collaboration with Dr. Hiroyuki Osada and colleagues (RIKEN, Japan). Among a number of lead compounds from the first chemical array-based screening and second biochemical assays, he focused on the bioactivity profile of a tocopherol derivative, NP843, as a D-MDM2-selective inhibitor. The synthesis and biological evaluations of the mirror-image compound of NP843 (*ent*-NP843) identified its selective inhibitory activity against L-MDM2. As such, he demonstrated that the drug discovery process from virtual mirror-image compounds of chiral natural products worked successfully using mirror-image synthetic proteins.

This thesis is very comprehensive (including protein synthetic chemistry, medicinal chemistry, and drug discovery technologies) and informative for the

development of novel screening strategies using synthetic proteins as well as for drug discovery from natural product resources. Three outstanding articles related to this thesis have been published in the top journals of bioorganic chemistry. His work concerning mirror-image screening for MDM2 inhibitors was highlighted in the cover art of an issue of *Chemical Communications*, as well as in *Chemistry World*, by the Royal Society of Chemistry. I very much appreciate the continuous efforts by Dr. Noguchi to accomplish his projects.

Kyoto, Japan
June 2017

Prof. Shinya Oishi

Parts of this thesis have been published in the following journal articles:

Taro Noguchi, Shinya Oishi, Kaori Honda, Yasumitsu Kondoh, Tamio Saito, Tatsuhiko Kubo, Masato Kaneda, Hiroaki Ohno, Hiroyuki Osada, and Nobutaka Fujii, Affinity-based Screening of MDM2/MDMX−p53 Interaction Inhibitors by Chemical Array: Identification of Novel Peptidic Inhibitors. *Bioorganic & Medicinal Chemistry Letters* **2013**, *23*, 3802–3805.

Taro Noguchi, Shinya Oishi, Kaori Honda, Yasumitsu Kondoh, Tamio Saito, Hiroaki Ohno, Hiroyuki Osada, and Nobutaka Fujii, Screening of a Virtual Mirror-image Library of Natural Products. *Chemical Communications* **2016**, *52*, 7653–7656.

Taro Noguchi, Hiroyuki Ishiba, Kaori Honda, Yasumitsu Kondoh, Hiroaki Ohno, Nobutaka Fujii, and Shinya Oishi, Synthesis of Grb2 SH2 Domain Proteins for Mirror-image Screening Systems. *Bioconjugate Chemistry* **2017**, *28*, 609–619.

Acknowledgements

The author would like to express his sincere and wholehearted appreciation to Prof. Nobutaka Fujii (Kyoto University) for his kind guidance, constructive discussions, and constant encouragement during this study.

The author also expresses his sincere and heartfelt gratitude to Dr. Shinya Oishi and Prof. Hiroaki Ohno (Graduate School of Pharmaceutical Sciences, Kyoto University) for their valuable discussions and encouragement throughout this study.

The author is profoundly grateful to Prof. Hiroyuki Osada, Dr. Yasumitsu Kondoh, Dr. Tamio Saito, and Dr. Kaori Honda (RIKEN Center for Sustainable Resource Science) for their professional guidance as well as technical support to accomplish this research.

The author also expresses thanks to Prof. Hiroshi Takeshima and Dr. Miyuki Nishi and all the other colleagues (Graduate School of Pharmaceutical Sciences, Kyoto University) for their warm encouragement.

The support and advice from Prof. Yoshiji Takemoto (Graduate School of Pharmaceutical Sciences, Kyoto University) and Prof. Kiyosei Takasu (Graduate School of Pharmaceutical Sciences, Kyoto University) are greatly appreciated.

The author also wishes to express his gratitude to all the colleagues in the Department of Bioorganic Medicinal Chemistry/Department of Chemogenomics (Graduate School of Pharmaceutical Sciences, Kyoto University) for their valuable comments and for their assistance and cooperation in various experiments.

The author would like to thank the Japan Society for the Promotion of Science (JSPS) for financial support, and all the staffs at the Elemental Analysis Center, Kyoto University.

Finally, the author thanks his parents, Hiromi and Hiromi Noguchi, and sister and brother, Tomomi and Kosuke Noguchi, for their understanding and constant encouragement throughout this study.

Contents

Abbreviations

Abl	Abelson murine leukemia viral oncogene homologue 1
Bcr	Breakpoint cluster region protein
CD	Circular dichroism
DIPCI	*N*,*N*′-diisopropylcarbodiimide
EDT	1,2-ethanedithiol
ELISA	Enzyme-linked immunosorbent assay
FAM	Carboxyfluorescein
FP	Fluorescence polarization
Gab1	Grb2-associated binder 1
Grb2	Growth factor receptor-bound protein 2
GST	Glutathione *S*-transferase
Gu	Guanidine
HBTU	*O*-(1*H*-benzotriazol-1-yl)-*N*,*N*,*N*′,*N*′-tetramethyluronium hexafluorophosphate
HOBt	1-hydroxy-1*H*-benzotriazole
HRP	Horseradish peroxidase
HTS	High-throughput screening
MDM2	Mouse double minute 2 homologue
MDMX	Mouse double minute X homologue
MES	2-mercaptoethanesulfonic acid
MFD	Metal-free-desulfurization
MPAA	4-mercaptophenylacetic acid
NCL	Native chemical ligation
PALC	Photoaffinity linker-coated
PEG	Polyethylene glycol
PI3K	Phosphoinositide 3-kinase
PPI	Protein−protein interaction
RAS	Rat sarcoma
SA	Streptavidin
SH2	Src homology 2

SH3	Src homology 3
SPPS	Solid-phase peptide synthesis
SPR	Surface plasmon resonance
TBTU	*N*,*N*,*N*′,*N*′-tetramethyl-*O*-(benzotriazol-1-yl)uronium tetrafluoroborate
TCEP	Tris(2-carboxyethyl)phosphine
TMB	3,3′,5,5′-tetramethylbenzidine
TMR	Tetramethylrhodamine

Chapter 1
Introduction

Abstract Natural products and their derivatives are valuable resources for drug discovery. While most of chiral natural products are produced as single enantiomeric form in nature, mirror-image isomers of them are also potential resources for drug discovery because they have identical physicochemical properties and different biological properties. To screen the mirror-image library of chiral natural products, mirror-image screening strategy has been developed. In this strategy, the screening of chiral natural products using a chemically synthesized d-protein corresponds to that of mirror-image natural products using a native protein (l-protein) in a mirror. In an effort to identify anticancer agents from the mirror-image natural products, chemical protein syntheses of some target oncoproteins, MDM2, MDMX and Grb2, and their applications to the chemical array screening process were achieved.

Keywords Chemical protein synthesis · Chemical array screen · Mirror-image protein technology · Natural products-based drug discovery

Natural products and their derivatives have been valuable resources for drug discovery. Today, more than half of the approved medicines are derived from natural products. Natural products are originally produced from natural resources such as plants, fungi, bacteria, or others as secondary metabolites for defensive and reproductive behaviors, and some of them are used in clinical practice, especially as anticancer, antibacterial, and immunosuppressive agents [1]. For example, fidaxomicin, which was isolated from the fermentation broth of *Dactylosporangium aurantiacum* subspecies *hamdenensis*, is a bactericidal agent against *Clostridium difficile* [2]. Romidepsin, isolated from the bacterium *Chromobacterium violaceum*, has been used as an anticancer agent for T-cell lymphoma [3]. Cyclosporin A, isolated from *Trichoderma polysporum* as an antibiotic, is currently used to prevent rejection following organ transplantation [4]. The desirable biological activities are attributed to the unique, complex, and sp^3-carbon-rich scaffolds (Fig. 1.1).

To expand the library of natural product-like scaffolds to provide lead compounds for drug discovery and tool compounds for basic scientific research, a variety of methods have been developed (Fig. 1.2). Recently, using complex natural product structures as starting materials, a variety of natural product-like scaffolds were

© Springer Nature Singapore Pte Ltd. 2018

T. Noguchi, *Development of Chemistry-Based Screening Platform for Access to Mirror-Image Library of Natural Products*, Springer Theses,
https://doi.org/10.1007/978-981-10-6623-8_1

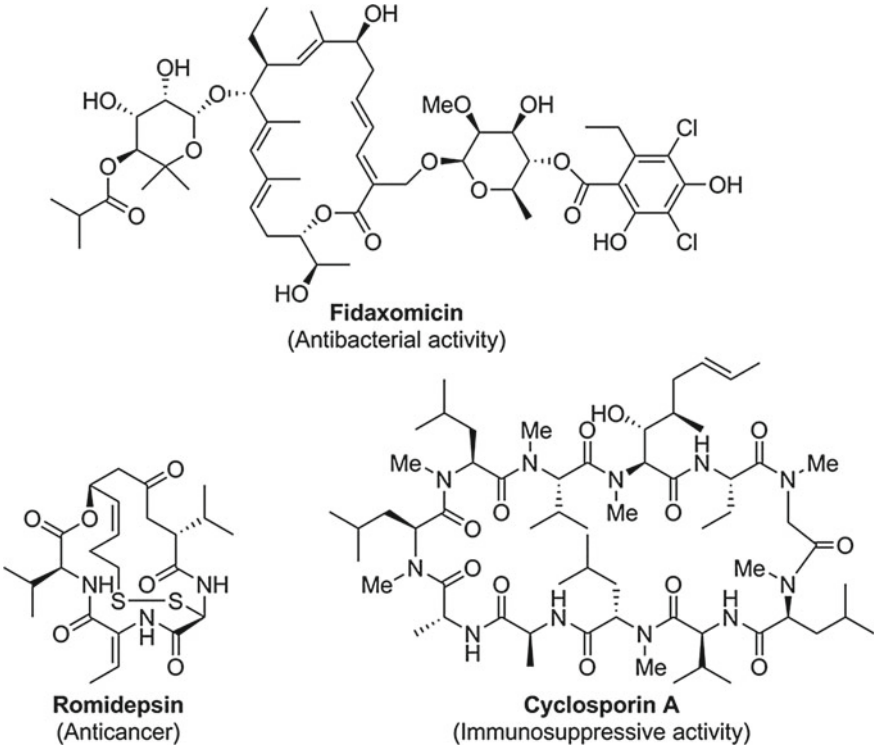

Fig. 1.1 Structures of natural products in clinical practice

prepared via a ring-distortion strategy using chemical modifications [5]. Similarly, the component sesquiterpenes in the extract from *Curcuma zedoria* were converted into a variety of derivatives with unprecedented scaffolds by treatment with oxidizing agents [6]. Manipulation of the biosynthetic pathway by modification of culture conditions or co-cultivation of two or more microorganisms increases the chemical diversity of metabolite products [7]. Epigenetic remodeling via activation of silent gene cluster(s) by cultivation in the presence of epigenetic regulatory agents also leads to the production of unprecedented natural products from fungi [8].

These chemistry- or biology-based approaches are useful to construct novel natural product-based scaffolds. However, the stereochemical outcomes of the newly obtained scaffolds from these approaches are highly dependent on those of the parent substrates. While many natural products are produced as a single enantiomer when bearing a chiral structure(s), in some limited cases, two enantiomeric forms of chiral natural products are produced by a single or various species [9]. The two mirror-image isomers with identical chemical and physicochemical properties often exhibit different functions and/or biological activities (Fig. 1.3). For example, L-serine is a proteinogenic amino acid, while D-serine, which is produced from L-serine by serine racemase (SR), works as a neuromodulator for NMDA receptors in brain [10].

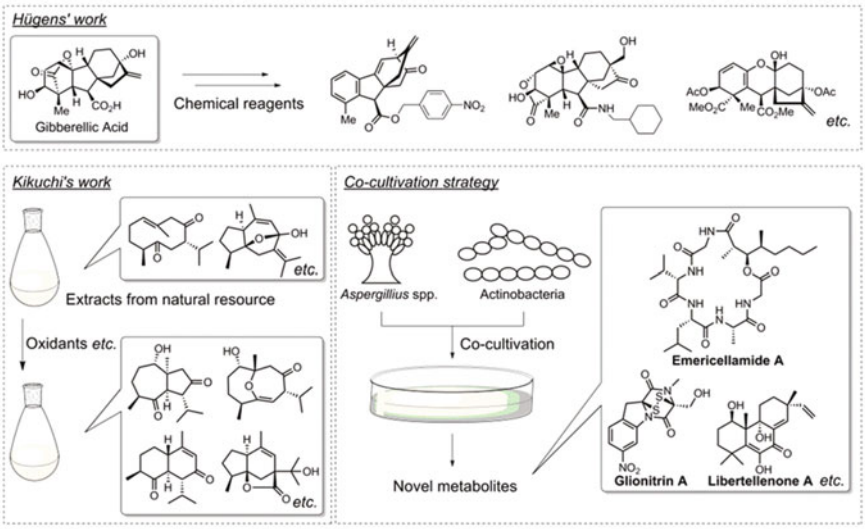

Fig. 1.2 Some recent strategies for expansion of natural product-like scaffolds

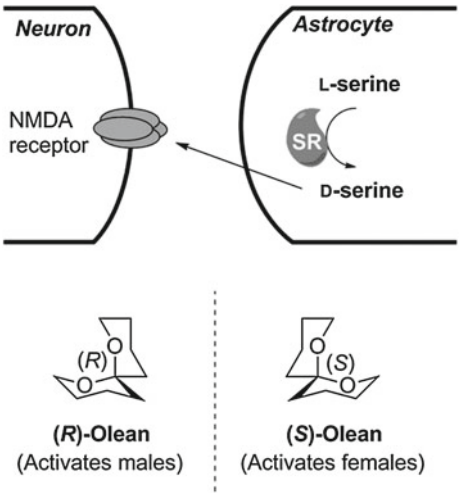

Fig. 1.3 Different biological activities of chiral natural products between their two mirror-image isomers

The insect pheromones (*R*)-(−)-olean and (*S*)-(+)-olean are selective sex attractants for male and female olive fruit flies (*Dacusoleae*), respectively [11]. Therefore, mirror-image natural products and their derivatives are expected to have potentially bioactivities as valuable resources in drug discovery.

The major obstacle to utilize enantiomers of chiral natural products as resources is that they are rarely obtained from natural resources. Construction of the corresponding library by chemical synthesis is hardly realized as well. To improve access to

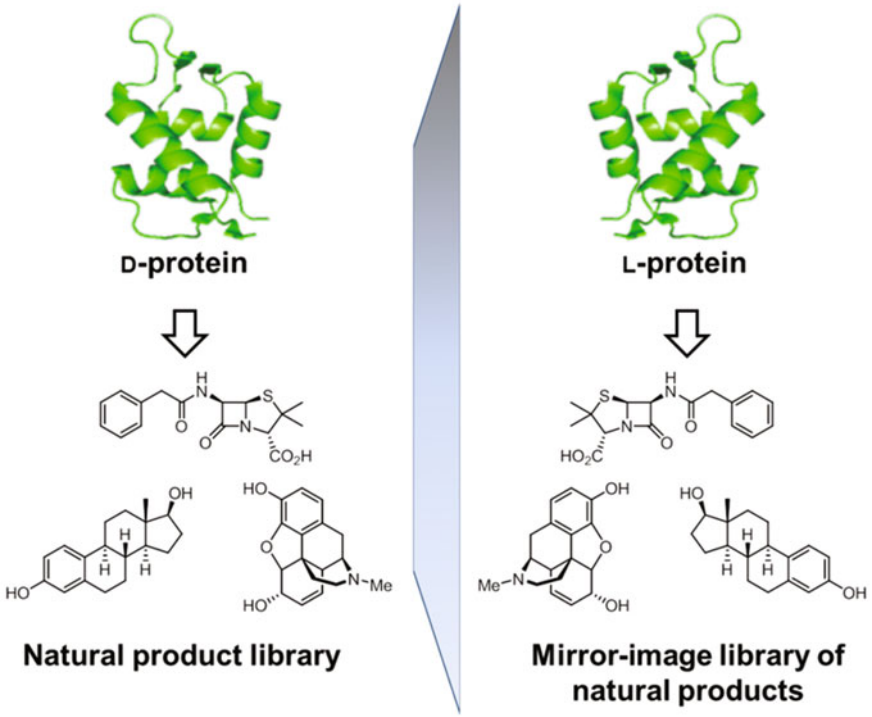

Fig. 1.4 Concept of screening strategy for a virtual mirror-image library of natural products. Screening of chiral natural products using D-protein corresponds to that of mirror-image natural products using L-protein in a mirror

mirror-image natural products and their derivatives with potentially desirable bioactivities as valuable resources, a complementary approach needs to be developed. For this purpose, the author designed a new screening strategy for a virtual mirror-image library of chiral natural products, taking advantage of the mirror-image protein (named D-protein, in which all chirality centers are mirror-inverted) technology. In this strategy, the screening of chiral natural product derivatives using a chemically synthesized D-protein corresponds to that of mirror-image natural products using a native protein (L-protein) in a mirror (Fig. 1.4). This process involves the following: Initially, (1) the D-protein of the target molecule is prepared by chemical protein synthesis; (2) using the synthetic D-protein, chiral natural products are screened to identify hit compound(s); (3) the mirror-image structure(s) of the hit compound(s) is synthesized; and (4) the biological activities for the native target molecule (L-protein) would be assessed. In this strategy, screening of the mirror-image library could be performed only by syntheses of mirror-image substances including a target protein and hit compound(s) without syntheses of numerous mirror-image natural products.

Recent progress in chemical protein synthesis has facilitated preparation of small to medium-sized biomolecules. Taking advantage of unique solid support materials,

longer peptide sequences can be synthesized by stepwise Fmoc-based solid-phase peptide synthesis (SPPS) [12]. Additionally, a number of novel methods, including native chemical ligation (NCL), have been established [13]. Developments of novel strategies for peptide thioester preparations [14] and the desulfurization reaction [15] have also facilitated a wide variety of NCL processes at a preferable position(s). Using these technologies, a variety of D-proteins have also been synthesized to understand and elucidate biological phenomena. For example, the molecular basis of the antifreeze properties of the snow flea antifreeze protein was elucidated via chemical synthesis of both protein enantiomers and racemic protein crystallography [16]. Crystal structures of the poly-ubiquitin-K27 were also obtained by using racemic proteins [17]. Moreover, D-protein technology has been applied for elucidation of molecular recognition of biologically important proteins. Ambidextrous chiral recognition of GroEL/ES for molecular chaperone activity was assessed using a mirror-image protein of DapA [18]. The stereoselectivity of the GroEL-GroES interaction was revealed by using a mirror-image protein of GroES [19]. Flexible chiral recognition of cargo-based transport across the cellular membrane by a protective antigen was also revealed using mirror-image polypeptides combined with the lethal factor in native form [20].

The mirror-image protein technology was also used for identification of novel functional molecules (Fig. 1.5). Mirror-image phage display (MIFD) led to identification of antiviral and anticancer D-peptides with resistance against peptidase-mediated degradation [21]. Schumacher et al. identified D-peptide ligands for Src homology 3 (SH3) domain of c-Src in an initial proof-of-concept study [21a]. HIV-1 entry inhibitors targeting the gp41 coiled-coil pocket were identified in the MIFD method [21b,c]. Spiegelmers, which are nuclease-resistant L-RNA aptamers, were identified by screening an RNA library using target D-proteins, and some of them are now in clinical trials [22]. In the mirror-image screening process, the hit peptides and RNAs are easily characterized by gene amplification and by phage polymerases, respectively. Small quantities of synthetic D-proteins are sufficient for screening a large number of peptides and RNAs with high diversity. However, for screening of natural products, these amplification techniques cannot be used. Preparation of significantly larger quantities of synthetic D-proteins is required for screening chiral natural products and their derivatives. To overcome these limitations, an effective detection and identification process of small-molecules hits via a high-throughput screening (HTS) process should be designed.

Chemical array screening is one of the effective approaches for the identification of small-molecule ligand-protein interactions [23]. This approach could explore protein-protein interaction (PPI) inhibitors against previously recognized binding pockets as well as search for potential binding molecules that interact with alternative or unexpected pockets present in the target proteins. In 2003, Kanoh and Osada et al. developed photo-crosslinked chemical array (Fig. 1.6) [24]. On the photo-crosslinked chemical array (76 $\times$ 25 mm), more than 3000 small molecules are immobilized at a variety of positions to a carbene-based photo-cross linker without specific functional groups on the immobilized molecules. Fluorescence-labeled proteins are applied to the array and the hit compounds are

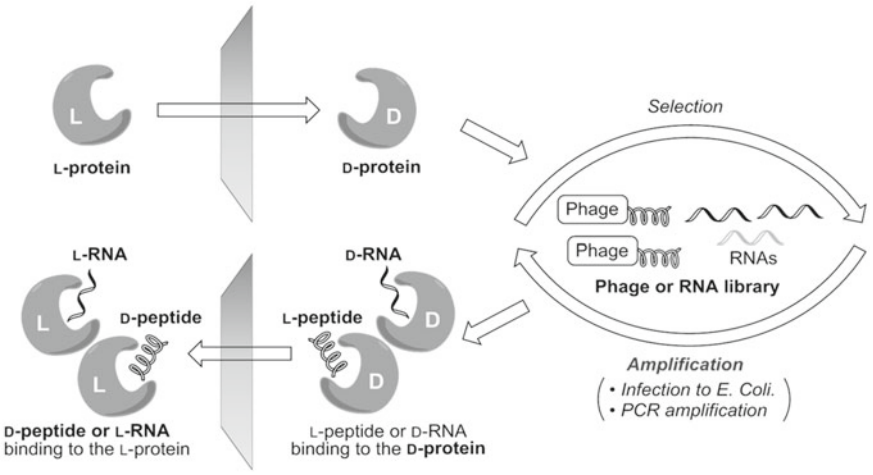

Fig. 1.5 Illustration showing the generation of D-peptides and/or L-RNAs against L-proteins. Initially, a D-protein is synthesized. Naturally occurring phage or RNA molecules from a library that bind to the D-protein are then identified. Subsequently, amplification, cloning and sequencing of bound phages or RNAs are performed. Identified sequences are finally synthesized using D-amino acids or L-ribonucleotides

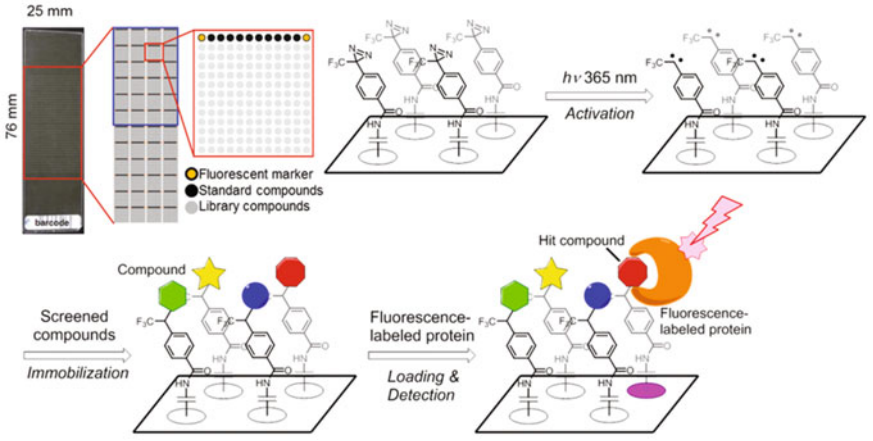

Fig. 1.6 Schematic representation of the photo-crosslinked chemical array technology. Carbene produced by 365 nm ultraviolet light radiation immobilizes compounds in a functional-group-independent manner. The immobilized compounds are screened with fluorescence-labeled proteins, and the hit compounds are detected by fluorescent signals using microarray scanner

detected by fluorescent signals using a microarray scanner. By using this technology, there have been some examples that have identified bioactive compounds [25]. Because the compounds were spotted on microarray in a small volume and screened in HTS manner using minimal quantity of the synthetic fluorescent protein(s), the

author expected screening process by using chemical array technology would be effective to identify novel hits from a virtual mirror-image library of natural products. Thus, the author decided to synthesize some domains of oncoproteins for the screening to identify novel anticancer agents.

In this thesis, the author describes development of screening process from a virtual mirror-image library of chiral natural products by using chemically synthesized mirror-image proteins.

In chap. 2, Sect. 1, the author describes the chemical synthesis of L-MDM2 and L-MDMX proteins and development of screening process using chemical array and fluorescence polarization (FP) assay to identify novel peptidic inhibitors from in-house compound library.

In chap. 2, Sect. 2, the author describes identification of a novel inhibitor against MDM2-p53 interaction from mirror-image library of natural products using D-MDM2 protein.

In Chap. 3, the author describes the chemical synthesis of both enantiomers of Grb2 SH2 domains and development of screening systems using chemical array and ELISA-based competitive assay.

References

1. (a) Bulter MS, Robertson AB, Cooper M (2014) Natural product and natural product derived drugs in clinical trials. A Nat Prod Rep 31:1612–1661; (b) Newman DJ, Cragg GM (2016) Natural products as sources of new drugs from 1981 to 2014. J Nat Prod 79:629–661
2. Theriault RJ, Karwowski JP, Jackson M, Girolami RL, Sunga GN, Vojtko CM, Coen LL (1987) Tiacumicins, a novel complex of 18-membered macrolide antibiotics. I. Taxonomy, fermentation and antibacterial activity. J Antibiot 40:567–574
3. Ueda H, Nakajima H, Hori Y, Fujita T, Nishimura M, Goto T, Okuhara M (1994) FR901228, a novel antitumor bicyclic depsipeptide produced by Chromobacterium violaceum No. 968. I. Taxonomy, fermentation, isolation, physico-chemical and biological properties, and antitumor activity. J Antibiot 47:301–310
4. Rüegger A, Kuhn M, Lichti H, Loosli HR, Huguenin R, Quiguerez C, von Wartburg A (1976) [Cyclosporin A, a peptide metabolite from *Trichoderma polysporum* (Link ex Pers.) Rifai, with a remarkable immunosuppressive activity]. Helv Chim Acta 59:1075–1092
5. Hüigens RW, Morrison KC, Hicklin RW, Flood TA, Richter MF, Hergenrother PJ (2013) A ring-distortion strategy to construct stereochemically complex and structurally diverse compounds from natural products. Nat. Chem. 5:195–202
6. Kikuchi H, Sakurai K, Oshima Y (2014) Development of diversity-enhanced extracts of Curcuma zedoaria and their new sesquiterpene-like compounds. Org Lett 16:1916–1919
7. (a) Takahashi JA, Teles APC, De Almeida Pinto Bracarense A, Gomes DC (2013) Classical and epigenetic approaches to metabolite diversification in filamentous fungi. Phytochem Rev 12:773–789; (b) Marmann A, Aly AH, Lin W, Wang B, Proksch P (2014) Co-cultivation–a powerful emerging tool for enhancing the chemical diversity of microorganisms. Mar Drugs 12:1043–1065; (c) Rutledge PJ, Challis GL (2015) Discovery of microbial natural products by activation of silent biosynthetic gene clusters. Nat Rev Microbiol 13:509–523
8. Williams RB, Henrikson JC, Hoover AR, Lee AE, Cichewicz RH (2008) Epigenetic remodeling of the fungal secondary metabolome. Org Biomol Chem 6:1895–1897
9. Finefield JM, Sherman DH, Kreitmann M, William RM (2012) Enantiomeric natural products: occurrence and biogenesis. Angew Chem Int Ed 51:4802–4836

10. Wolosker H, Dumin E, Balan L, Foltyn VN (2008) D-amino acids in the brain: D-serine in neurotransmission and neurodegeneration. FEBS J 275:3514–3526
11. Haniotakis G, Francke W, Mori K, Redlich H, Schurig V (1986) Sex-specific activity of (R)-(-)- and (S)- (+)-1,7-dioxaspiro [5.5] undecane, the major pheromone of Dacus oleae. J Chem Ecol 12:1559–1568
12. (a) Kempe M, Barany G (1996) CLEAR: A novel family of highly cross-linked polymeric supports for solid-phase peptide synthesis. J Am Chem Soc 118:7083–7093; (b) García-Romas Y, Paradís-Bas M, Tulla-Puche J, Albericio F (2010) ChemMatrix(®) for complex peptides and combinatorial chemistry. J Pept Sci 16:675–678
13. (a) Dawson PE, Muir TW, Clark-Lewis I, Kent SBH (1994) Synthesis of proteins by native chemical ligation. Science 266:776–779; (b) Saxon E, Armstrong JI, Bertozzi CR (2000) A "traceless" Staudinger ligation for the chemoselective synthesis of amide bonds. Org Lett 2:2141–2134; (c) Hondal RJ, Nilsson BL, Raines RT (2001) Selenocysteine in native chemical ligation and expressed protein ligation. J Am Chem Soc 123:5140–5141; (d) Bode JW, Fox RM, Baucom KD (2006) Chemoselective amide ligations by decarboxylative condensations of N-alkylhydroxylamines and alpha-ketoacids. Angew Chem Int Ed 45:1248–1252; (e) Lee CL, Li X (2014) Serine/threonine ligation for the chemical synthesis of proteins. Curr Opin Chem Biol 22:108–114
14. (a) Hojo H, Onuma Y, Akimoto Y, Nakahara Y, Nakahara Y (2007) N-Alkyl cysteine-assisted thioesterification of peptides. Tetrahedron Lett 48:25–28; (b) Blanco-Canosa JB, Dawson PE (2008) An efficient Fmoc-SPPS approach for the generation of thioester peptide precursors for use in native chemical ligation. Angew Chem Int Ed 47:6851–6855; (c) Tsuda S, Shigenaga A, Bando K, Otaka A (2009) N–>S acyl-transfer-mediated synthesis of peptide thioesters using anilide derivatives. Org Lett 11:823–826; (d) Olliver N, Dheur J, Mhida R, Blanpain A, Melnyk O (2010) Bis(2-sulfanylethyl) amino native peptide ligation. Org Lett 12:5238–5241; (e) Hou W, Zhang XH, Li FP, Liu CF (2011) Peptidyl N, N-bis(2-mercaptoethyl)-amides as thioester precursors for native chemical ligation. Org Lett 13:386–389; (f) Fang GM, Li YM, Shen F, Huang YC, Li JB, Lin Y, Cui HK, Liu L (2011) Protein chemical synthesis by ligation of peptide hydrazides. Angew Chem Int Ed 50:7645–7649
15. (a) Yan LZ, Dawson PE (2001) Synthesis of peptides and proteins without cysteine residues by native chemical ligation combined with desulfurization. J Am Chem Soc 123:526–533; (b) Wan Q, Danishefky SJ (2007) Free-radical-based, specific desulfurization of cysteine: a powerful advance in the synthesis of polypeptides and glycopolypeptides. Angew Chem Int Ed 46:9248–9252
16. (a) Pentelute BL, Gates ZP, Tereshko V, Dashnau JL, Vanderkooi JM, Kossiakoff AA, Kent SBH (2008) X-ray structure of snow flea antifreeze protein determined by racemic crystallization of synthetic protein enantiomers. J Am Chem Soc 130:9695–9701; (b) Pentelute BL, Gates ZP, Dashnau JL, Vanderkooi JM, Kent SBH (2008) Mirror image forms of snow flea antifreeze protein prepared by total chemical synthesis have identical antifreeze activities. J Am Chem Soc 130:9702–9707
17. Pan M, Gao S, Zheng Y, Tan X, Lan H, Tan X, Sun D, Lu L, Wang T, Zheng Q, Huang Y, Wang J, Liu L (2016) Quasi-Racemic X-ray Structures of K27-Linked Ubiquitin Chains Prepared by Total Chemical Synthesis. J Am Chem Soc 138:7429–7435
18. Weinstock MT, Jacobsen MT, Kay MS (2014) Synthesis and folding of a mirror-image enzyme reveals ambidextrous chaperone activity. Proc Natl Acad Sci U S A 111:11679–11684
19. Jacobsen MT, Petersen ME, Ye X, Galibert M, Lorimer GH, Aucagne V, Kay MS (2016) A helping hand to overcome solubility challenges in chemical protein synthesis. J Am Chem Soc 138:11775–11782
20. Rabideau AE, Liao X, Pentelute BL (2015) Delivery of mirror image polypeptides into cells. Chem Sci 6:648–653
21. (a) Schumacher TNM, Mayr LM, Minor DL, Milhollen MA, Burgess MW, Kim PS (1996) Identification of D-peptide ligands through mirror-image phage display. Science 271:1854–1857; (b) Eckert DM, Malashkevich VN, Hong LH, Carr PA, Kim PS (1999) Inhibiting HIV-1 entry: discovery of D-peptide inhibitors that target the gp41 coiled-coil pocket. Cell 99:103–115;

(c) Welch BD, VanDemark AP, Heroux A, Hill CP, Kay MS (2007) Potent D-peptide inhibitors of HIV-1 entry. Proc Natl Acad Sci U S A 104:16828–16833; (d) Wiesehan K, Buder K, Linke RP, Patt S, Stoldt M, Unger E, Schmitt B, Bucci E, Willbold D (2003) Selection of D-amino-acid peptides that bind to Alzheimer's disease amyloid peptide Aβ1-42 by mirror image phage display. ChemBioChem 4:748–753; (e) van Groen T, Wiesehan K, Funke SA, Kadish I, Nagel-Steger L, Willbold D (2008) Reduction of Alzheimer's disease amyloid plaque load in transgenic mice by D3, a D-enantiomeric peptide identified by mirror image phage display. ChemMedChem 3:1848–1852; (f) Liu M, Pazgier M, Li C, Yuan W, Li C, Lu W (2010) A left-handed solution to peptide inhibition of the p53-MDM2 interaction. Angew Chem Int Ed 49:3649–3652; (g) Liu M, Li C, Pazgier M, Li C, Mao Y, Lv Y, Gu B, Wei G, Yuan W, Zhan C, Lu WY, Lu W (2010) D-peptide inhibitors of the p53-MDM2 interaction for targeted molecular therapy of malignant neoplasms. Proc Natl Acad Sci U S A 107:14321–14326

22. Vater A, Klussmann S (2015) Turning mirror-image oligonucleotides into drugs: the evolution of Spiegelmer(®) therapeutics. Drug Discov. Today 20:147–155 and the references cited therein
23. (a) MacBeath G, Koehler AN, Schreiber SL (1999) Printing Small Molecules as Microarrays and Detecting Protein-Ligand Interactions en Masse. J Am Chem Soc 121:7967–7968; (b) Uttamchandani M, Walsh DP, Yao SQ, Chang YT (2005) Small molecule microarrays: recent advances and applications. Curr Opin Chem Biol 9:4–13
24. Kanoh N, Kumashiro S, Simizu S, Kondoh Y, Hatakeyama S, Tashiro H, Osada H (2003) Immobilization of natural products on glass slides by using a photoaffinity reaction and the detection of protein-small-molecule interactions. Angew Chem Int Ed 42:5584–5587
25. (a) Miyazaki I, Simizu S, Ichiyama H, Kawatani M, Osada H (2008) Robust and systematic drug screening method using chemical arrays and the protein library: identification of novel inhibitors of carbonic anhydrase II. Biosci Biotechnol Biochem 72:2739–2749; (b) Hagiwara K, Kondoh Y, Ueda A, Yamada K, Goto H, Watanabe T, Nakata T, Osada H, Aida H (2010) Discovery of novel antiviral agents directed against the influenza A virus nucleoprotein using photo-cross-linked chemical arrays. Biochem Biophys Res Commun 394:721–727; (c) Hagiwara K, Murakami T, Xue G, Shimizu Y, Takeda E, Hashimoto Y, Honda K, Kondoh Y, Osada H, Tsunetsugu-Yokota Y, Aida H (2010) Identification of a novel Vpr-binding compound that inhibits HIV-1 multiplication in macrophages by chemical array. Biochem Biophys Res Commun 403:40–45; (d) Miyazaki I, Simizu S, Ichiyama H, Okumura H, Takagi S, Osada H (2010) A small-molecule inhibitor shows that pirin regulates migration of melanoma cells. Nat Chem Biol 6:667–773; (e) Minagawa S, Kondoh Y, Sueoka K, Osada H, Nakamoto H (2011) Cyclic lipopeptide antibiotics bind to the N-terminal domain of the prokaryotic Hsp90 to inhibit the chaperone activity. Biochem J 435:237–246; (f) Bürger M, Zimmermann TJ, Kondoh Y, Stege P, Watanabe N, Osada H, Waldmann H, Vetter IR (2012) Crystal structure of the predicted phospholipase LYPLAL1 reveals unexpected functional plasticity despite close relationship to acyl protein thioesterases. J Lipid Res 53:43–50; (g) Zimmermann TJ, Bürger M, Tashiro E, Kondoh Y, Martinez NE, Görmer K, Rosin-Steiner S, Shimizu T, Ozaki S, Mikoshiba K, Watanabe N, Hall D, Vetter IR, Osada H, Hedberg C, Waldmann H (2013) Boron-based inhibitors of acyl protein thioesterases 1 and 2. Chembiochem 14:115–122; (h) Nakajima Y, Kawamura T, Maeda K, Ichikawa H, Motoyama T, Kondoh Y, Saito T, Kobayashi T, Yoshida M, Osada H, Kimura M (2013) Identification and characterization of an inhibitor of trichothecene 3-O-acetyltransferase, TRI101, by the chemical array approach. Biosci Biotechnol Biochem 77:1958–1960; (i) Yao R, Kondoh Y, Natsume Y, Yamanaka H, Inoue M, Toki H, Takagi R, Shimizu T, Yamori T, Osada H, Noda T (2014) A small compound targeting TACC3 revealed its different spatiotemporal contributions for spindle assembly in cancer cells. Oncogene 33:4242–4252; (j) Kawatani M, Fukishima Y, Kondoh Y, Honda K, Sekine T, Yamaguchi Y, Taniguchi N, Osada H (2015) Identification of matrix metalloproteinase inhibitors by chemical arrays. Biosci Biotechnol Biochem 79:1597–1602

Chapter 2
Development of a Mirror-Image Screening System for Chiral Natural Products

Abstract In this section, a novel approach for identifying MDM2-p53 and MDMX-p53 protein–protein interactions (PPIs) inhibitors by using chemically synthesized MDM2 and MDMX proteins has been established. MDM2 and MDMX are oncoproteins that negatively regulate the activity and stability of the tumor suppressor protein p53. The inhibitors of PPIs of MDM2-p53 and MDMX-p53 represent potential anticancer agents. Affinity-based chemical array screening is one of the efficient methods for identification of binding agents toward various pockets of proteins. To establish chemistry-based screening platform for identification of MDM2 and MDMX inhibitors, synthetic strategy of MDM2 and MDMX proteins and application of these proteins for chemical array screening were performed. MDM2 and MDMX proteins were prepared by Fmoc-based solid-phase peptide synthesis (SPPS), and binding candidates for them were identified from an in-house compound library by chemical array screening. The subsequent fluorescence polarization (FP) assay identified peptidic compounds that inhibited MDM2-p53 and MDMX-p53 interactions.

Keywords MDM2/MDMX proteins · Chemical protein synthesis · Chemical array screen · Mirror-image protein technology · Natural products-based drug discovery

2.1 Establishment of Screening Process Using Synthetic MDM2 and MDMX Proteins

MDM2 and MDMX are negative regulators of the tumor suppressor protein p53, and therefore confer tumor development and survival [1]. MDM2 and MDMX bind to the N-terminal transactivation domain of p53 with high affinity to inhibit functions associated with regulating responsive gene expression [2]. MDM2 has E3 ubiquitin ligase activity and thus also regulates the stability of p53 by proteasomal degradation, thereby conferring effective down-regulation of cellular p53 protein levels [3]. MDMX has no ubiquitin ligase activity, yet forms a MDMX-MDM2 heterodimer via interaction between their C-terminal RING finger domains. This heterodimer stimulates MDM2-mediated ubiquitination of the p53 and subsequent degradation

© Springer Nature Singapore Pte Ltd. 2018

T. Noguchi, *Development of Chemistry-Based Screening Platform for Access to Mirror-Image Library of Natural Products*, Springer Theses,
https://doi.org/10.1007/978-981-10-6623-8_2

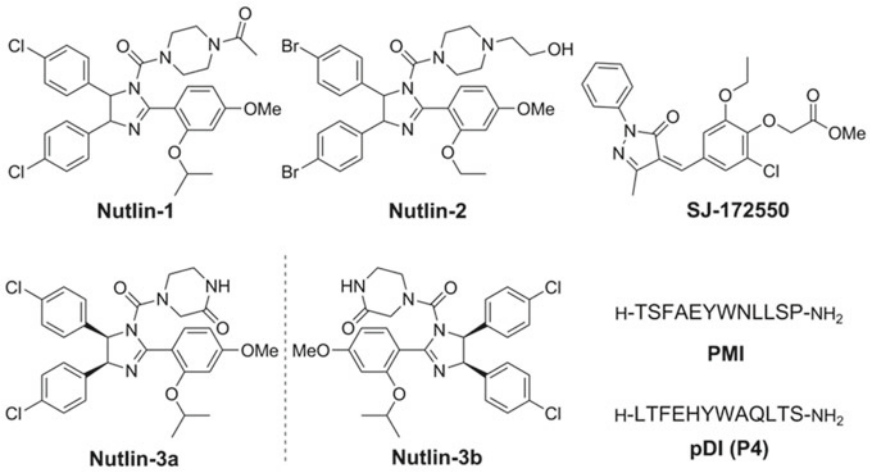

Fig. 2.1 Structures of MDM2–p53 and/or MDMX–p53 interaction inhibitors

[4]. As such, high expression of MDM2 and MDMX results in a reduction in the activity and expression level of the p53 in cancer cells, and PPI inhibitors against MDM2-p53 and/or MDMX-p53 interactions are expected as anticancer agents.

Inhibitory compounds that block the interaction between MDM2-p53 and MDMX-p53 have been identified using various types of screening technologies (Fig. 2.1) [5]. For example, MDM2-p53 interaction inhibitors, nutlin-1, -2, and -3, were identified by surface plasmon resonance (SPR) analysis [6]. SJ-172550 is an MDMX-p53 interaction inhibitor, which was identified by an FP assay [7]. p53-like peptide, PMI and pDI (also named P4), were identified as MDM2 and MDMX inhibitors by phage display [8]. These facile technologies are based on the evaluation of inhibitory effects by compounds against p53 binding to MDM2 and MDMX. Among the inhibitors, some chiral compounds have different activities between their enantiomers. For example, nutlin-3a potently binds to MDM2 (IC_{50}: 0.09 μM), while nutlin-3b (enantiomer of nutlin-3a) shows significantly less activity (IC_{50}: 13.6 μM). For identifying novel inhibitors from mirror-image natural products, strong enantiomeric recognitions of target proteins would be needed. Therefore, the author expected MDM2 and MDMX would have strong enantiomeric recognitions to small-molecules.

The author designed screening process using affinity-based chemical array screening and subsequent competitive FP assay to identify MDM2-p53 and MDMX-p53 interaction inhibitors efficiently. In this section, to investigate the feasibility of synthetic MDM2 and MDMX proteins for identification of their inhibitors, chemical synthesis of L-MDM2 and L-MDMX and application of the screening systems were performed.

Initially, the author investigated synthesis of MDM2 and MDMX and their fluorescent derivatives, which were used for chemical array screening. There have been a report on the synthesis of MDM2 and MDMX proteins by combining Boc-based

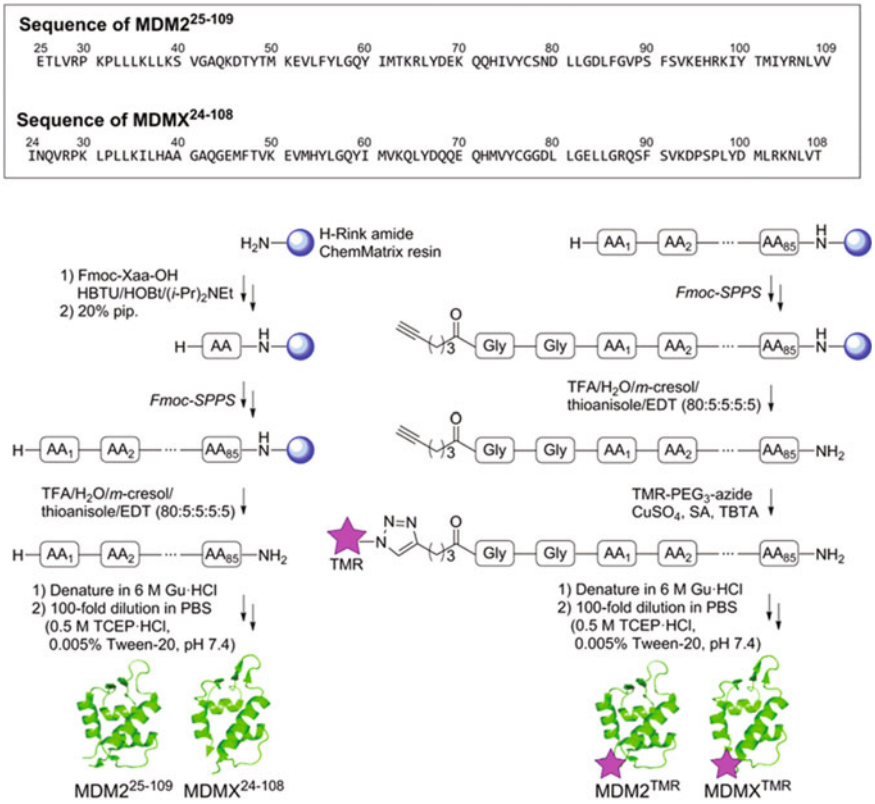

Scheme 2.1 Synthesis of MDM2 and MDMX proteins

SPPS with native chemical ligation [8]. Although this approach would be applicable to mid-sized protein synthesis, a more facile stepwise Fmoc-based SPPS approach was undertaken in this study (Scheme 2.1).

The p53-binding domain of MDM2 and MDMX (designated $MDM2^{25-109}$ and $MDMX^{24-108}$, respectively) were synthesized by standard Fmoc-based SPPS on an H-Rink Amide ChemMatrix resin using HBTU/HOBt/(*i*-Pr)$_2$NEt activation. After chain assembly, deprotection of the side chain protecting groups and cleavage from the resin with the cocktail [TFA/thioanisole/*m*-cresol/EDT/H_2O (80:5:5:5:5)], followed by RP-HPLC purification afforded the expected peptides. For the preparation of fluorescent MDM2 and MDMX proteins bearing a single tetramethylrhodamine moiety (designated $MDM2^{TMR}$ and $MDMX^{TMR}$, respectively), 5-hexynoic acid was conjugated via a diglycine linker on the resin. After purification of $MDM2^{25-109}$ and $MDMX^{24-108}$ with an N-terminal alkyne tag, treatment with TMR-$(PEG)_3$-azide in the presence of $CuSO_4$, sodium ascorbate (SA) and tris[(1-benzyl-1*H*-1,2,3-triazol-4-yl)methyl]amine (TBTA) provided fluorescent $MDM2^{TMR}$ and $MDMX^{TMR}$, respectively. The synthetic MDM2 and MDMX

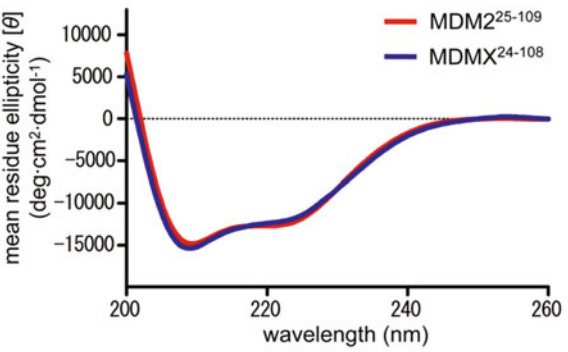

Fig. 2.2 CD spectra of $MDM2^{25-109}$ and $MDMX^{24-108}$. CD spectra of $MDM2^{25-109}$ and $MDMX^{24-108}$ were measured at room temperature in PBS containing 0.1 mM TCEP (pH 7.4)

proteins and their fluorescent derivatives, $MDM2^{TMR}$ and $MDMX^{TMR}$, were denatured in 6 M guanidine hydrochloride (Gu · HCl) solution and refolded by 100-fold dilution of the solution to PBS buffer (pH 7.4) containing 0.5 mM tris(2-carboxyethyl)phosphine (TCEP) and 0.005% Tween-20.

To validate the structures of the synthetic proteins, the author evaluated circular dichroism (CD) spectra of $MDM2^{25–109}$ and $MDMX^{24–108}$ (Fig. 2.2). Negative bands at 208 and 222 nm indicated the presence of α-helix secondary structure elements, which is characteristic for MDM2 and MDMX, and supported by previous crystal structure and CD analyses [9].

To further verify the biological activity of the synthetic proteins, binding affinities of MDM2 and MDMX towards the p53 peptide sequence were evaluated by SPR analysis. Varying concentrations of MDM2 and MDMX proteins were analyzed by a NeutrAvidin-coated NLC sensor chip (BioRad) on which the biotinylated wild-type p53 peptide (biotinyl-aminocaproyl-GSGSSQETFSDLWKLLPEN-NH_2) was immobilized (Fig. 2.3). $MDM2^{25–109}$ and $MDMX^{24–108}$ bound the p53 peptide with KD values of 0.803 and 2.22 μM, respectively, which supported the correct folding of these proteins [7]. The binding affinities (KD values) of $MDM2^{TMR}$ and $MDMX^{TMR}$ towards the p53 peptide were 0.616 and 2.14 μM, respectively, indicating that N-terminal modification of synthetic MDM2 and MDMX had no effect on the folding of these proteins or the biological functions [10].

The author next assessed the binding ability of $MDM2^{TMR}$ and $MDMX^{TMR}$ to the p53-like peptide (designated L-P4: H-LTFEHYWAQLTS-NH_2) immobilized on a microarray via carbene-mediated covalent bond formation. The enantiomer peptide (designated D-P4) was used as a negative control. $MDM2^{TMR}$ and $MDMX^{TMR}$ bound to L-p53 in a highly selective manner (Fig. 2.4). Higher MDM2–p53 binding compared with the MDMX–p53 interaction was observed, which is consistent with the more potent binding affinity of MDM2 to the p53 peptide in the SPR analysis.

To identify the inhibitor candidates for MDM2–p53 and MDMX–p53 interactions, the author next carried out chemical array screening using the $MDM2^{TMR}$ and $MDMX^{TMR}$ proteins (Fig. 2.5). Fifty-four hit compounds were identified from the 7600 compounds of the in-house chemical library that were immobilized on the

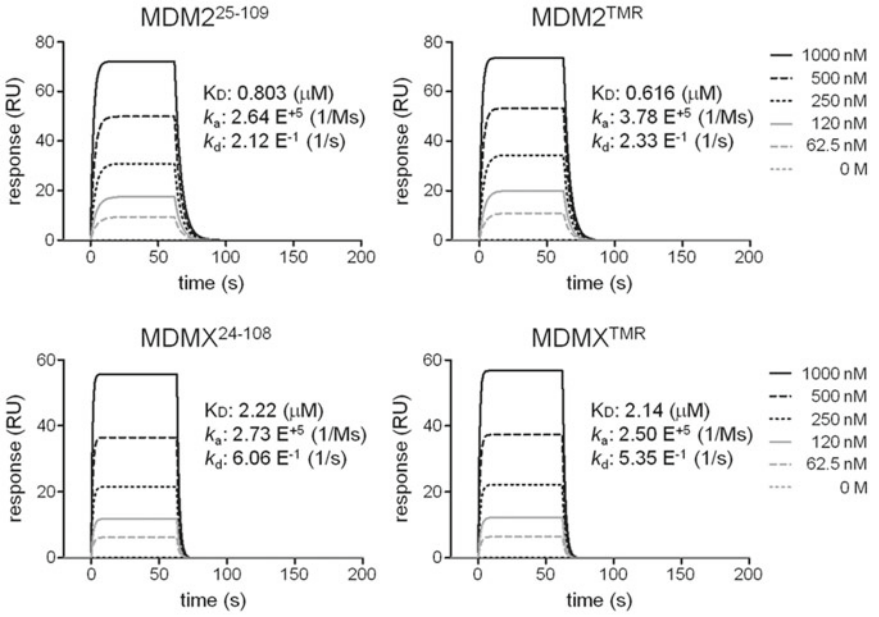

Fig. 2.3 SPR analysis of MDM2$^{25-109}$, MDM2^{TMR}, MDMX$^{24-108}$ and MDMX^{TMR} towards p53 peptide. KD values were determined by the calculation of k_a/k_d

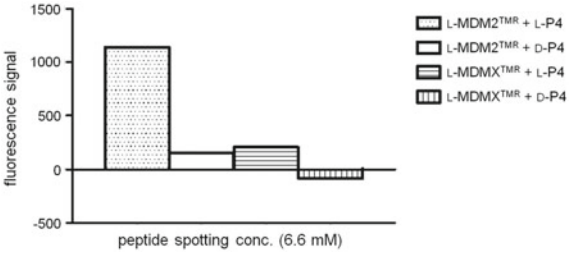

Fig. 2.4 Chemical array analysis of MDM2^{TMR} and MDMX^{TMR} proteins using both enantiomers of p53-like peptide (P4). MDM2^{TMR} and MDMX^{TMR} binding (1 μM in 1% skim-milk-TBS-T) were assessed using a chemical array, on which L-P4 (H-LTFEHYWAQLTS-NH_2) or D-P4 was spotted at the concentration of 6.6 mM

chemical array using 5 mM solutions. Of these, 6 compounds and 10 compounds showed selective binding to MDM2 and MDMX, respectively. The other 38 compounds exhibited binding to both MDM2 and MDMX.

To select small molecules that bind to the p53 binding pocket(s) in MDM2 and MDMX, the inhibitory effects on MDM2–p53 and MDMX–p53 interactions were further evaluated for the 54 hit compounds by a FP assay using a fluorescein-labeled P4 peptide (FAM-LTFEHYWAQLTS-NH_2) [11]. Three dual inhibitors against both interactions were obtained (Fig. 2.6): KPYA52218 (**1**), KPYB00497

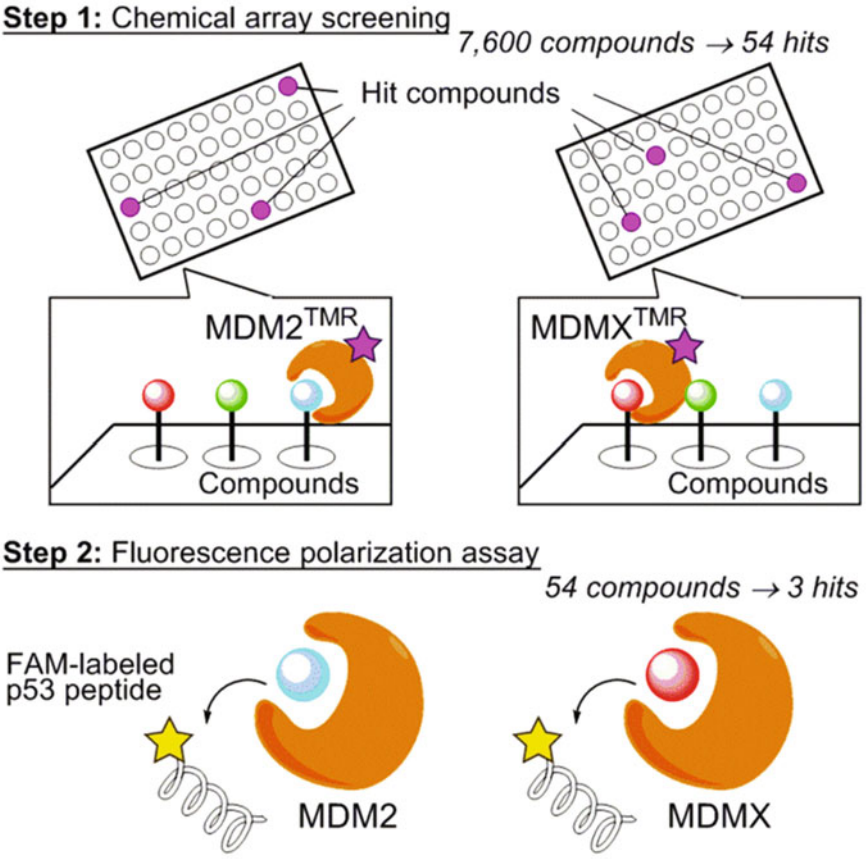

Fig. 2.5 Two-step screening process using $MDM2^{25-109}$ and $MDMX^{24-108}$ proteins

(**2**) and KPYB00556 (**3**) [IC_{50} (**1**) = 8.51 μM for MDM2, 32.4 μM for MDMX; IC_{50} (**2**) = 22.2 μM for MDM2, 42.1 μM for MDMX; IC_{50} (**3**) = 21.3 μM for MDM2, 52.5 μM for MDMX]. In the initial chemical array analysis, these compounds **1–3** were also identified to show dual binding to MDM2 and MDMX. Although MDM2 and MDMX share homologous sequences in their p53-binding domains, many of the known MDM2–p53 inhibitors do not effectively interact with MDMX–p53 probably because of the shallower and wider p53-binding pocket in MDMX [12]. Agents that disrupt MDM2-p53 interaction could inhibit tumor growth, but they are less effective in cancer cells that express high level of MDMX [13]. These dual inhibitors represent promising anticancer agent leads against cancer cells in which MDM2 and MDMX are overexpressed [14]. To gain insight into the effect on cell proliferation, growth inhibition by compounds **1–3** against human lung carcinoma-derived A549 cells was assessed. Compounds **1** and **3** showed no effect on cell growth, whereas cell growth was inhibited by compound **2** (EC_{50} = 13.7 μM).

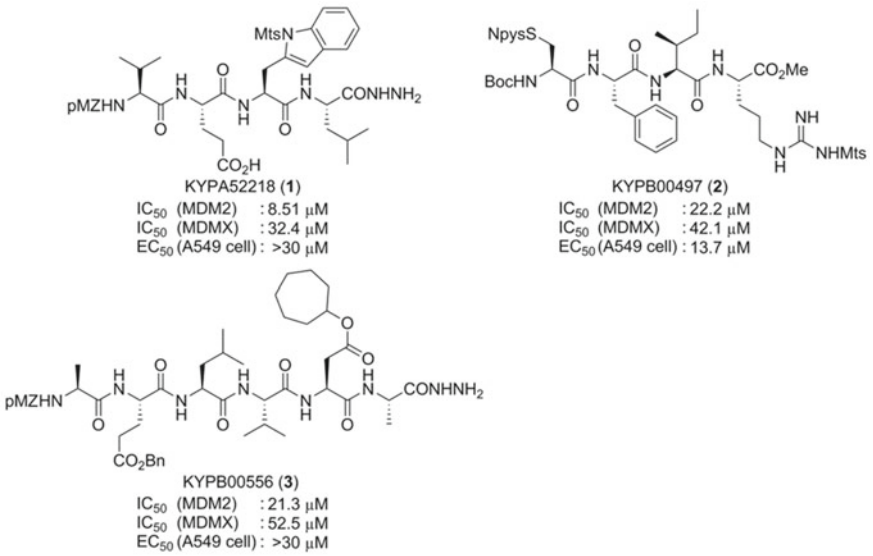

Fig. 2.6 Structures and biological activities of the hit compounds

Of note, in this screening process, the biological data from FP assays did not necessarily correspond to the binding ability obtained in the initial microarray screening, possibly owing to structural modification of the molecules bound to the microarray and potential binding to other binding site(s) than the p53 binging pocket. However, the microarray technology successfully facilitated the selection process for the identification of potential MDM2/MDMX-p53 interaction inhibitors.

In conclusion, the author has established screening protocols for binding molecules of MDM2 and MDMX by chemical array technology using synthetic fluorescent proteins. The preliminary screening of an in-house chemical library identified a number of peptidic binding molecules towards MDM2 and MDMX. The subsequent FP assay identified three dual inhibitors of MDM2–p53 and MDMX–p53 interactions. This new screening strategy for MDM2 and MDMX proteins using the affinity-based chemical array and subsequent FP assay should facilitate the identification process of MDM2–p53 and MDMX–p53 inhibitors.

2.1.1 Experimental Section

General Methods

Fmoc-protected amino acids were purchased from Watanabe Chemical Industries, Ltd. (Hiroshima, Japan), Kokusan Chemical Co. Ltd. (Kanagawa, Japan) or Sigma-Aldrich JAPAN (Tokyo, Japan). Other chemicals were purchased from Nacalai Tesque Inc. (Kyoto, Japan). For analytical HPLC for MDM2 and MDMX proteins,

Cosmosil 5C18-AR300 (4.6 × 250 mm, Nacalai Tesque Inc.) was employed with a linear gradient of CH_3CN containing 0.1% (v/v) TFA at a flow rate of 1 mL/min. Cosmosil 5C18-ARII column (4.6 × 250 mm, Nacalai Tesque Inc.) was employed for the analysis of the other peptides and peptidic compounds. ^{1}H NMR and ^{13}C NMR spectra were recorded using a JEOL ECA-500 spectrometer. ^{1}H NMR spectra were tabulated as follows: chemical shift, multiplicity (br: broad, s: singlet, d: doublet, t: triplet, q: quartet, m: multiplet), number of protons, and coupling constants.

Synthesis of MDM2$^{25–109}$ and MDMX$^{24–108}$

MDM2$^{25–109}$ and MDMX$^{24–108}$ were synthesized using automatic peptide synthesizer (PSSM-8, Shimadzu Corporation Ltd.) by Fmoc-based SPPS on H-Rink Amide ChemMatrix resin (0.4–0.6 mmol/g). For the side-chain protection, *t*-Bu ester for Asp and Glu; 2,2,4,6,7-pentamethyldihydrobenzofuran-5-sulfonyl (Pbf) for Arg; *t*-Bu for Thr, Tyr and Ser; Boc for Lys and Trp; and Trt for Gln, Asn, His, and Cys were employed for side-chain protection. Fmoc-Phe-OH (5 eq) was coupled by using HBTU (5 eq), HOBt (5 eq) and $(i\text{-Pr})_2$NEt (10 eq) in DMF-NMP, and the other Fmoc-protected amino acids were coupled by using HBTU (5 eq), HOBt (5 eq), $(i\text{-Pr})_2$NEt (10 eq) in DMF. In each coupling of amino acid, coupling reaction was carried out for 45 min twice. Fmoc-protecting group was removed by treating the resin with 20% piperidine in DMF. After chain assembly, the resulting protected peptide resin was treated with TFA/thioanisole/*m*-cresol/EDT/H_2O (80:5:5:5:5) at room temperature for 2 h. After removal of the resin by filtration, the filtrate was poured into ice-cold dry Et_2O. The resulting powder was collected by centrifugation and then washed three times with ice-cold dry Et_2O. The crude product was purified by HPLC on a Cosmosil 5C18-AR300 preparative column (Nacalai Tesque, 20 × 250 mm) with a linear gradient of CH_3CN containing 0.1% TFA at a flow rate of 8 mL/min, affording the expected peptides as white powder. The polypeptides were characterized by ESI-MS and purity was calculated as >95% by HPLC.

MS (ESI) for MDM2$^{25–109}$: Calcd for $C_{462}H_{739}N_{117}O_{123}S_4$: 10027.42; observed: $[M+12H]^{12+}$ *m/z* = 836.80, $[M+11H]^{11+}$ *m/z* = 912.45, $[M+10H]^{10+}$ *m/z* = 1003.91, $[M+9H]^{9+}$ *m/z* = 1115.26, $[M+8H]^{8+}$*m/z* = 1254.33, $[M+7H]^{7+}$ *m/z* = 1443.55, $[M+6H]^{6+}$ *m/z* = 1672.32.

MS (ESI) for MDMX$^{24–108}$: Calcd for $C_{438}H_{701}N_{117}O_{121}S_6$: 9733.08; observed: $[M+12H]^{12+}$ *m/z* = 811.68, $[M+11H]^{11+}$ *m/z* = 885.91, $[M+10H]^{10+}$ *m/z* = 974.42, $[M+9H]^{9+}$ *m/z* = 1082.62, $[M+8H]^{8+}$*m/z* = 1217.89, $[M+7H]^{7+}$ *m/z* = 1391.30, $[M+6H]^{6+}$ *m/z* = 1623.57.

Synthesis of MDM2^{TMR} and MDMX^{TMR}

Protected MDM2$^{25–109}$ and MDMX$^{24–108}$ were synthesized according to the identical procedure for the synthesis of MDM2$^{25–109}$ and MDMX$^{24–108}$. After assembling the full length sequence, two glycine residues (5 eq) and 5-hexynoic acid (5 eq) were coupled with HBTU (5 eq), HOBt (5 eq) and $(i\text{-Pr})_2$NEt (10 eq) in DMF. The resulting protected peptides were subjected to the deprotection, cleavage from resin, and HPLC purification. 200 mM $CuSO_4$ in H_2O (20 μL, 4 μmol) and 200 mM tris[(1-benzoyl-1*H*-1,2,3-triazol-4-yl)methyl]amine (TBTA) in DMSO (20 μL, 4 μmol) were added to H_2O-DMSO-*t*-BuOH (15:5:27, 470 μL) and the solution was stirred for 3 min.

Then, a sodium ascorbate solution (200 mM, 40 μL, 8 μmol) was added to the mixture in several pulses. This reagent cocktail was added to the mixture of MDM2 or MDMX (200 nmol) and TMR-$(PEG)_3$-azide (1 μmol) in DMSO (100 μL). After 15 min, the reaction mixture was purified by RP-HPLC on a Cosmosil 5C18-AR300 preparative column (Nacalai Tesque, 20 × 250 mm) with a linear gradient of CH_3CN containing 0.1% TFA at a flow rate of 8 mL/min. This purification afforded the TMR-labeled polypeptide dimer with a disulfide bond via the Cys residues (Cys^{82} in MDM2; Cys^{81} in MDMX). The collected TMR-labeled polypeptide dimer was dissolved in 10 mM TCEP · HCl in 6 M Gu · HCl/H_2O solution at 37 °C for 5 h, followed by RP-HPLC purification on a Cosmosil 5C18-AR300 preparative column (Nacalai Tesque, 20 × 250 mm) with a linear gradient of CH_3CN containing 0.1% TFA at a flow rate of 8 mL/min. This purification procedure afforded the monomer polypeptide as a pink powder (80 nmol, 40%).

MS (ESI) for $MDM2^{TMR}$: Calcd for $C_{505}H_{789}N_{125}O_{133}S_4$: 10865.79; observed: $[M+13H]^{13+}$ *m/z* = 836.55, $[M+12H]^{12+}$ *m/z* = 906.36, $[M+11H]^{11+}$ *m/z* = 989.10, $[M+10H]^{10+}$ *m/z* = 1087.60, $[M+9H]^{9+}$ *m/z* = 1208.20, $[M+8H]^{8+}$ *m/z* = 1359.00, $[M+7H]^{7+}$ *m/z* = 1553.07 $[M+6H]^{6+}$ *m/z* = 1812.23.

MS (ESI) for $MDMX^{TMR}$: Calcd for $C_{481}H_{751}N_{125}O_{131}S_6$: 10571.44; observed: $[M+14H]^{14+}$ *m/z* = 756.19, $[M+13H]^{13+}$ *m/z* = 814.28, $[M+12H]^{12+}$ *m/z* = 881.98, $[M+11H]^{11+}$ *m/z* = 962.15, $[M+10H]^{10+}$ *m/z* = 1058.36, $[M+9H]^{9+}$ *m/z* = 1175.58, $[M+8H]^{8+}$ *m/z* = 1322.82, $[M+7H]^{7+}$ *m/z* = 1511.24, $[M+6H]^{6+}$ *m/z* = 1762.70.

Folding of Synthetic MDM2 and MDMX Proteins

Lyophilized polypeptide (1 mg/mL) was dissolved in 6 M Gu · HCl containing 1 mM TCEP · HCl, followed by 100-fold dilution with PBS (pH 7.4) containing 0.5 mM TCEP · HCl and 0.005% Tween-20 at 4 °C. The solution was stored at 4 °C overnight, and the solution was concentrated using a MWCO 3000 centrifugal filtration membrane (Millipore, Amicon-Ultra 3 kDa).

Synthesis of p53 Peptides and Their Derivatives

All p53 and p53-like peptides were synthesized by Fmoc-based SPPS on Rink-amide resin (0.66 mmol/g, 45.5 mg, 0.025 mmol). Fmoc-protected amino acids (3 eq) were coupled by using DIPCI (3 eq) and HOBt (3 eq) in DMF. The Fmoc-protecting group was removed by treating the resin with 20% piperidine in DMF. Coupling of biotin (0.125 mmol) was carried out with HBTU (5 eq), HOBt (5 eq) and $(i\text{-Pr})_2NEt$ (10 eq) in DMF. Coupling of 5-carboxyfluorescein (5 eq) was carried out with DIPCI (5 eq) and HOBt (10 eq) in DMF. The resulting protected peptide resin was treated with TFA/thioanisole/*m*-cresol/EDT/H_2O (80:5:5:5:5) at room temperature for 2 h. After removal of the resin by filtration, the filtrate was poured into ice-cold dry Et_2O. The resulting powder was collected by centrifugation and then washed three times with ice-cold dry Et_2O. The crude product was purified by HPLC on a Cosmosil 5C18-ARII preparative column (Nacalai Tesque, 20 × 250 mm). All peptides were characterized by ESI-MS or MALDI-TOF-MS and the purity was ascertained by HPLC as >95%.

Biotin-labeled p53 peptide: MS (MALDI-TOF) calcd for $C_{108}H_{166}N_{27}O_{35}S$ $[M+H]^+$ 2434.18; found 2434.23.

L-P4: MS (MALDI-TOF) calcd for $C_{71}H_{100}N_{17}O_{19}$ $[M+H]^+$ 1494.74; found 1494.61.

D-P4: MS (MALDI-TOF) calcd for $C_{71}H_{100}N_{17}O_{19}$ $[M+H]^+$ 1494.74; found 1494.67.

Fluorescein-labeled P4 peptide: MS (ESI) calcd for $C_{92}H_{110}N_{17}O_{25}$ $[M+H]^+$ 1852.79, found 1852.95.

SPR Analysis

Binding kinetics analysis was carried out on a ProteOn XRP360 instrument using an N-terminal biotinylated wild-type p53 peptide immobilized on a NeutrAvidin-coated NLC sensor chip (43 RUs) at 20 °C. PBS (pH 7.4) containing 0.005% Tween-20 was used as the running buffer.

Screening by the Chemical Array

The photoaffinity linker-coated (PALC) slides were prepared according to previous reports using amine-coated slides and the photoaffinity linker [15]. A solution of compounds (5 mM in DMSO) from the in-house chemical library was immobilized onto the PALC glass slides with a chemical arrayer equipped with 24 stamping pins. The slides were exposed to UV irradiation of 4 J/cm^2 at 365 nm using a CL-1000L UV crosslinker (UVP, CA). The slides were washed successively with DMSO, DMF, acetonitrile, THF, dichloromethane, EtOH, and ultra-pure water (5 min, 3 times each), and dried. MDM2^{TMR} (1 μM in 1% skim-milk-TBS-T) and MDMX^{TMR} (1 μM in 1% skim-milk-TBS-T) were incubated with the glass slide for 1 h, and then washed with TBS-T (10 mM Tris-HCl, pH 8.0, 150 mM NaCl, 0.05% Tween-20) (5 min, 3 times). The slides were dried and scanned at 532 nm on a GenePix scanner. The fluorescence signals were quantified with GenePixPro.

Fluorescence Polarization Assay

Fluorescence polarization assays were carried out in PBS containing 0.005% Tween-20 using a fluorescein-labeled P4 peptide (0.5 nM) and MDM2$^{25–109}$ (10 nM) or MDMX$^{24–108}$ (50 nM) in black 96-well non-binding surface assay plates (Corning). For the inhibitor assays, compounds were preincubated with the synthetic protein for 30 min. The fluorescein-labeled P4 peptide was then added and incubated for 30 min. The unlabeled L-P4 peptide was used as the positive control. FP signals were analyzed using an EnVision Xcite plate reader with a 480-nm excitation filter and a 535-nm emission filter.

Cell Growth Inhibition Assay

A549 cells were cultured in DMEM medium (Sigma) supplemented with 10% (v/v) FBS at 37 °C in a 5% CO_2-incubator. Cell based assays using A549 cells were performed in 96-well plates (BD Falcon). A549 cells were seeded at 500 cells/well in 50 μL of DMEM, and placed for 6 h. Chemical compounds in DMSO were diluted 250-fold with the culture medium in advance. Following the addition of the fresh culture medium (40 μL), the chemical diluents (30 μL) were also added to the cell cultures. The final volume of DMSO in the medium was equal to 0.1% (v/v). The cells under chemical treatment were incubated for a further 72 h. The wells in the plates were washed twice with the cultured medium without phenol-red. After 1 h

incubation with 100 μL of the medium, the cell culture in each well was supplemented with the MTS reagent (20 μL, Promega), followed by incubation for an additional 40 min. Absorbance at 490 nm of each well was measured using a Wallac 1420 ARVO SX multilabel counter (Perkin Elmer).

Characterization Data of Hit Compounds (1–3)

KPYA 52218 (**1**). ^{1}H NMR (500 MHz, DMSO-d_6) δ 0.77 (t, J = 7.7 Hz, 6H), 0.85 (d, J = 6.3 Hz, 3H), 0.90 (d, J = 6.9 Hz, 3H), 1.45 (m, 1H), 1.56 (m, 1H), 1.64 (m, 1H), 1.74 (m, 1H), 1.87 (m, 1H), 1.95 (m, 1H), 2.21 (dd, J = 5.7, 10.3 Hz, 2H), 2.25 (s, 3H), 2.40 (s, 6H), 2.91 (dd, J = 10.3, 14.9 Hz, 1H), 3.10 (d, J = 6.0, 12.0 Hz, 1H), 3.73 (s, 3H), 3.88 (dd, J = 6.9, 8.6 Hz, 1H), 4.32 (m, 1H), 4.38 (m, 1H), 4.64 (m, 1H), 4.92 (q, J = 12.4 Hz, 2H), 6.88 (d, J = 8.6 Hz, 2H), 7.08 (s, 2H), 7.17–7.28 (m, 5H), 7.67 (s, 1H), 7.77 (dd, J = 2.3, 6.3 Hz, 1H), 7.82 (d, J = 8.0 Hz, 1H), 8.17 (d, J = 8.0 Hz, 1H), 8.42 (d, J = 8.0 Hz, 1H), 10.85 (br, 1H); ^{13}C NMR (500 MHz, DMSO-d_6) δ 17.9, 19.1, 20.4, 21.4, 21.9, 22.8, 24.0, 26.8, 29.7, 30.1, 40.6, 49.6, 51.3, 52.1, 55.0, 60.1, 65.3, 111.6, 113.7, 115.5, 120.0, 122.5, 124.3, 125.0, 128.7, 129.6, 129.8, 132.3, 133.8, 139.5, 144.2, 156.2, 158.9, 170.9, 171.3, 174.0; MS (MALDI-TOF) calcd for $C_{45}H_{59}N_7NaO_{11}S$ $[M+Na]^+$ 928.39, found 928.37.

KPYB 00497 (**2**). ^{1}H NMR (500 MHz, DMSO-d_6) δ 0.78 (t, J = 7.4 Hz, 3H), 0.82 (d, J = 6.9 Hz, 3H), 1.04 (m, 1H), 1.2–1.4 (m, 3H), 1.38 (s, 9H), 1.56 (m, 1H), 1.66 (m, 2H), 2.21 (s, 3H), 2.57 (s, 6H), 2.79 (dd, 1H), 2.9–3.1 (m, 5H), 3.59 (s, 3H), 4.1–4.2 (m, 3H), 4.59 (m, 1H), 6.47 (br, 1H), 6.91 (s, 2H), 7.1–7.2 (m, 5H), 7.24 (d, J = 8.0 Hz, 1H), 7.60 (dd, J = 4.6, 8.0 Hz, 1H), 7.87 (d, J = 8.0 Hz, 1H), 7.97 (d, J = 8.0 Hz, 1H), 8.35 (d, J = 8.0 Hz, 1H), 8.64 (dd, J = 1.1, 8.6 Hz, 1H), 8.89 (dd, J = 1.1, 4.6 Hz, 1H); ^{13}C NMR (500 MHz, DMSO-d_6) δ 10.8, 15.0, 20.3, 22.4, 24.1, 27.9, 28.1, 36.9, 37.4, 40.3, 51.7, 51.8, 53.2, 54.1, 56.3, 78.5, 122.0, 126.2, 127.8, 129.3, 131.0, 134.5, 136.9, 137.2, 139.6, 142.6, 154.1, 155.0, 155.1, 156.3, 170.0, 170.1, 171.0, 172.1; MS (MALDI-TOF) calcd for $C_{44}H_{61}N_9NaO_{11}S_3$ $[M+Na]^+$ 1010.35, found 1010.52.

KPYB 00556 (**3**). ^{1}H NMR (500 MHz, DMSO-d_6) δ 0.7–0.9 (m, 12H), 1.17 (d, J = 6.9 Hz, 3H), 1.21 (d, J = 7.4 Hz, 3H), 1.3–1.6 (m, 13H), 1.80 (m, 3H), 1.92 (m, 2H), 2.38 (m, 2H), 2.52 (dd, J = 1.78, 10.9 Hz, 1H), 2.75 (dd, J = 4.9, 16.3 Hz, 1H), 3.74 (s, 3H), 4.03 (m, 1H), 4.13 (dd, J = 6.9, 8.6 Hz, 1H), 4.23 (m, 1H), 4.30 (m, 1H), 4.35 (m, 1H), 4.60 (m, 1H), 4.80 (m, 1H), 4.92 (dd, J = 11.7, 30.6 Hz, 2H), 5.08 (s, 2H), 6.90 (d, J = 8.0 Hz, 2H), 7.27 (d, J = 8.6 Hz, 2H), 7.3–7.4 (m, 5H), 7.41 (d, J = 8.0 Hz, 1H), 7.77 (d, J = 8.0 Hz, 1H), 7.92 (d, J = 8.0 Hz, 1H), 7.96–7.98 (m, 2H), 8.24 (d, J = 8.0 Hz, 1H), 10.07 (br, 1H); ^{13}C NMR (500 MHz, DMSO-d_6) δ 17.9, 18.0, 19.0, 21.5, 22.3, 23.1, 24.0, 27.2, 27.7, 30.0, 30.7, 33.1, 36.0, 40.3, 47.1, 49.2, 50.1, 51.0, 51.5, 55.1, 57.4, 65.2, 65.4, 74.7, 113.7, 127.8, 127.9, 128.4, 128.8, 129.7, 136.2, 155.8, 159.0, 169.3, 169.9, 170.7, 170.8, 171.4, 171.7, 172.2, 172.5; MS (MALDI-TOF) calcd for $C_{49}H_{72}N_8NaO_{13}$ $[M+Na]^+$ 1003.51, found 1003.61.

2.2 Development of a Mirror-Image Screening Process by Using Synthetic Proteins

2.2.1 Screening of a Virtual Mirror-Image Library of Natural Products

Summary

The author established a novel screening approach for access to an unexplored mirror-image library of chiral natural product derivatives using D*-protein technology. Natural products and their derivatives are valuable resources for drug discovery. While most of chiral natural products are produced as single enantiomeric form in nature, mirror-image isomers of them are also potential resources for drug discovery because they have identical physicochemical properties and different biological properties. To screen the mirror-image library of chiral natural products, mirror-image screening strategy has been developed. Mirror-image MDM2 protein (named* D*-MDM2) was prepared by Fmoc-based solid phase peptide synthesis. By using* D*-MDM2 for screening, NP843, which was an α-tocopherol derivative, was ideintified as* D*-MDM2–*D*-p53 interaction inhibitors. The biological activities of ent-NP843 toward* L*-MDM2–*L*-p53 were also evaluated after preparing ent-NP843 by chiral pool synthesis. In this strategy, two chemical syntheses of mirror-image substances including a target protein and hit compound(s) allow the lead discovery from a virtual mirror-image library without synthesis of numerous mirror-image compounds.*

To screen the mirror-image library of chiral natural products and their derivatives for MDM2–p53 interaction inhibitors, the author performed the designed screening process using chemical array screening and subsequent FP assay with synthetic proteins [16]: (1) the D-protein of the target molecule is prepared by chemical protein synthesis; (2) using the synthetic D-protein, chiral natural products are screened to identify hit compound(s); (3) the mirror-image structure(s) of the hit compound(s) is synthesized; and (4) the biological activities for the native target molecule (L-protein) would be assessed (Fig. 2.7).

Initially, the author synthesized D-MDM2$^{25-109}$ by standard Fmoc-based solid-phase peptide synthesis (SPPS) according to the identical protocol described in Sect. 1 of Chap. 2. The tetramethylrhodamine (TMR)-labeled protein (D-MDM2^{TMR}) was also prepared by conjugation of TMR-$(PEG)_3$-azide onto the N-terminal alkyne tag of D-MDM2$^{25-109}$. The folded L-MDM2$^{25-109}$ and D-MDM2$^{25-109}$ had symmetric circular dichroism (CD) spectra, supporting the presence of mirror-image α-helices (Fig. 2.8).

To verify the biological activity of the synthetic MDM2 proteins, the binding affinities toward biotinylated p53 peptides (biotinyl-aminocaproyl-GSGSSQETFSDLWKLLPEN-NH_2) were evaluated by surface plasmon resonance (SPR) analysis (Fig. 2.9). The high-affinity bindings of L-MDM2–L-p53 peptide and D-MDM2–D-p53 peptide were observed [KD (L-MDM2–L-p53): 0.75 ± 0.04 μM; KD (D-MDM2–D-p53): 0.51 ± 0.02 μM], while the binding activities of

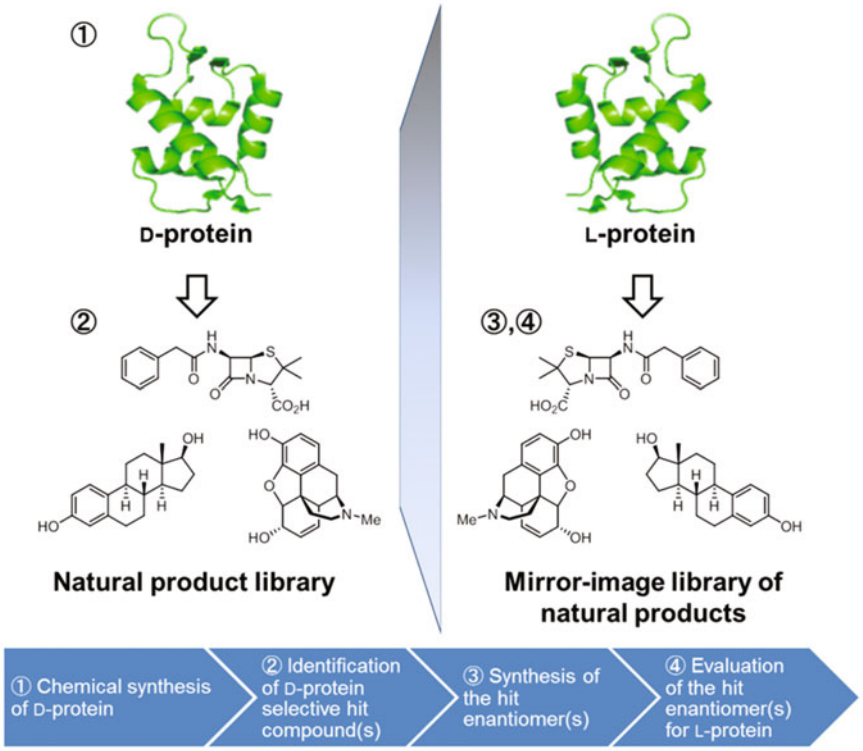

Fig. 2.7 Concept of mirror-image screening of chiral natural products

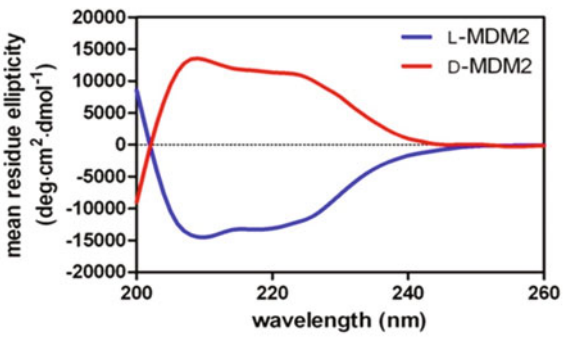

Fig. 2.8 CD spectra of synthetic L-MDM2 and D-MDM2 proteins. Spectra of L-MDM2$^{25–109}$ and D-MDM2$^{25–109}$ were measured at 25 °C in PBS containing 0.5 mM tris(2-carboxyethyl)phosphine (TCEP) and 0.005% Tween-20 (pH 7.4)

L-MDM2–D-p53 peptide and D-MDM2–L-p53 peptide were practically nil, suggesting high enantiomeric recognition of MDM2 toward p53.

The author next performed screening of natural products and their derivatives using both enantiomers of MDM2 protein. Chemical array screening of 22,293 compounds including natural products and their derivatives from RIKEN NPDepo

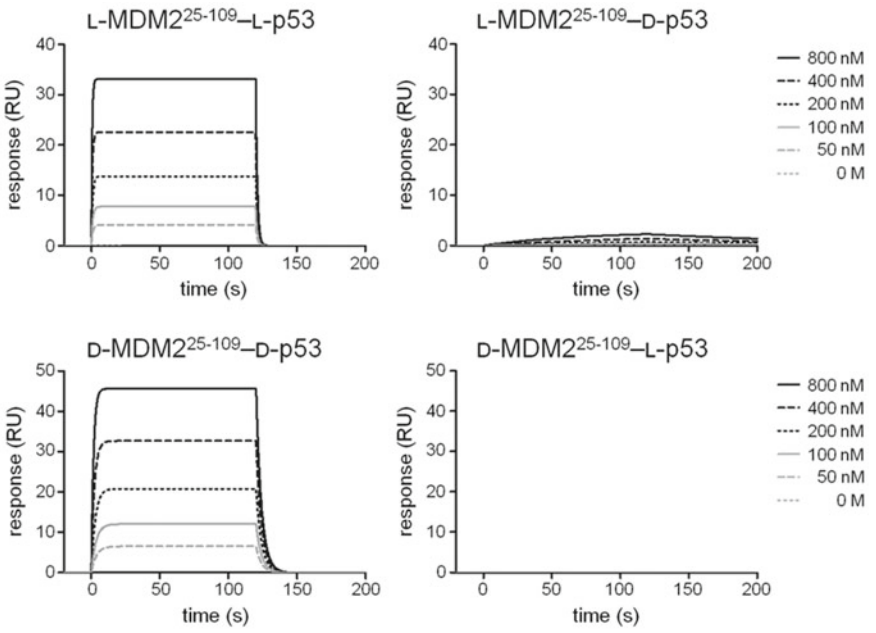

Analyte/Ligand	k_a (1/Ms)	k_d (1/s)	KD (mol/L)
L-MDM2$^{25-109}$/L-p53	$1.1 \pm 0.75\ E^{+6}$	$8.5 \pm 0.16\ E^{-1}$	$7.5 \pm 0.40\ E^{-7}$
D-MDM2$^{25-109}$/D-p53	$5.6 \pm 0.69\ E^{+5}$	$2.8 \pm 0.24\ E^{-1}$	$5.1 \pm 0.21\ E^{-7}$

Fig. 2.9 SPR analysis of p53 binding to synthetic MDM2$^{25–109}$. KD values were determined by the calculation of k_a/k_d

was carried out using L-MDM2^{TMR} and D-MDM2^{TMR}. Among 43 initial hit compounds, four compounds showed inhibitory activity against L-MDM2–L-p53 or D-MDM2–D-p53 interactions in the competitive binding inhibition assay by fluorescence polarization (FP) (Fig. 2.10). Of these, a chiral α-tocopherol derivative NP843 (**1a**) was identified to be a selective inhibitor against D-MDM2–D-p53 interaction (Fig. 2.11).

The next step was to verify the bioactivity of the enantiomeric form of **1a** (*ent*-NP843, **1b**) toward L-MDM2–L-p53 interaction. Compound **1b** was prepared by chiral pool synthesis from three commercially available optically pure components (Scheme 2.2). Initially, (*R*)-Roche ester-derived tosylate **2** was reacted with Grignard reagent **3**, prepared from (*S*)-citronellyl bromide, in the presence of copper catalyst. The subsequent deprotection of trityl-group gave alcohol **4**, after treatment with 1N NaOH for hydrolysis of the formyl ester derived from **4**. C1 elongation of **4** was then performed via tosylation and cyanation followed by reductions to give an alcohol **6**, which was converted into phosphonium salt **8**. (*R*)-Trolox-derived aldehyde **9** was employed as a chiral chromane component for Wittig reaction. The

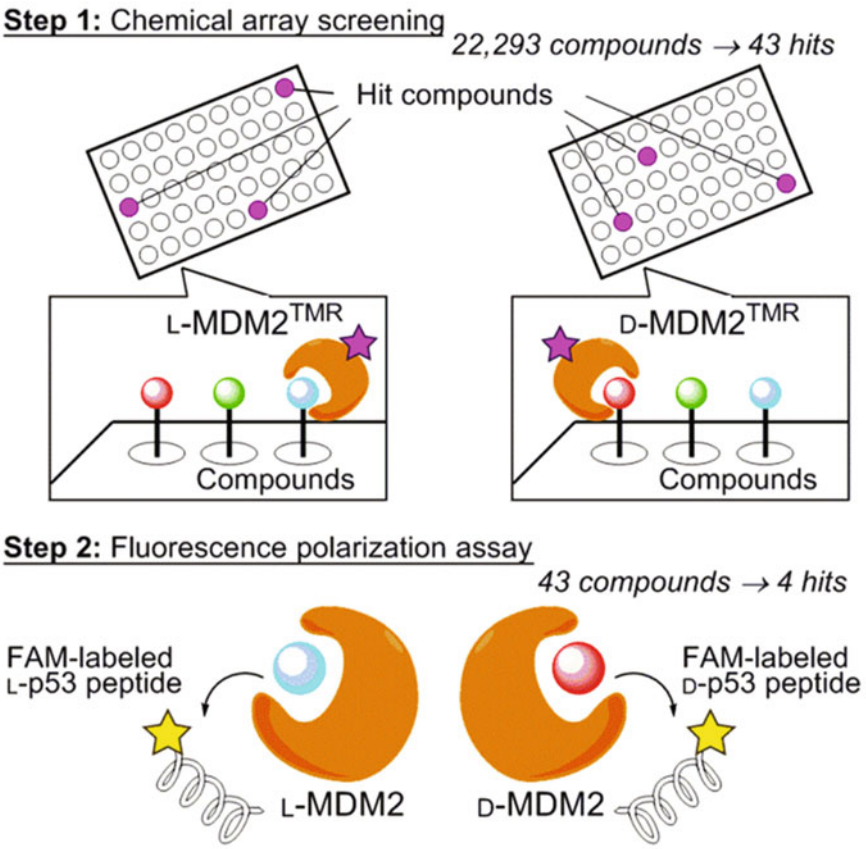

Fig. 2.10 Two-step screening process using D-MDM2$^{25-109}$

subsequent two-step catalytic reduction including PtO_2-mediated hydrogenation of olefins and subsequent Pd/C-mediated hydrogenolysis of the benzyl group provided the L-α-tocopherol (**10b**) in 84% yield. Alkylation of **10b** with bromide **11** followed by deprotection gave ketone **12b**. Construction of the left-part of the chromone substructure by treatment of **12b** with *N,N*-dimethylformamide dimethyl acetal (DMF-DMA) afforded **1b**.

The inhibitory activity of mirror-image compound **1b** against interaction between MDM2 and p53 peptide was evaluated by FP assay (Table 2.1). Compound **1b** inhibited L-MDM2–L-p53 interaction [IC_{50} (**1b**) = 7.6 ± 1.9 μM for L-MDM2–L-p53], while no inhibition was observed against D-MDM2–D-p53 interaction at 30 μM of **1b**. This corresponded with the inhibitory activities of the original hit **1a** against D-MDM2–D-p53 and L-MDM2–L-p53 interactions, respectively [IC_{50} (**1a**) = 6.5 ± 0.5 μM for D-MDM2–D-p53]. The similar inhibitory activities of **1b** were observed by SPR analysis and enzyme-linked immunosorbent assay (ELISA)

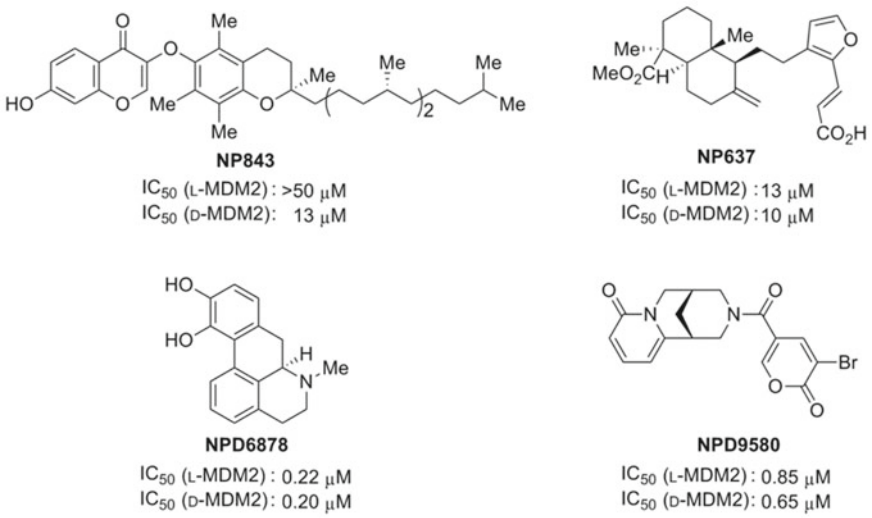

Fig. 2.11 Structures and biological activities of MDM2-p53 inhibitors from mirror-image screening. IC_{50} values were measured by FP assay using 0.5 nM FAM-labeled P4 peptide and 10 nM MDM2 protein

Table 2.1 Biological activities of NP843 and *ent*-NP843

Compounds	IC_{50} (μM)[a]		GI_{50} (μM)[b]	
	L-MDM2	D-MDM2	SJSA-1 cells	H1299 cells
Nutlin-3a	0.32 ± 0.03	>30	5.2 ± 0.19	>30
NP843 (**1a**)	>30	6.5 ± 0.5	>30	>30
ent-NP843 (**1b**)	7.6 ± 1.9	>30	>30	>30

[a]IC_{50} values for L/D-MDM2 were measured by FP assay using 1.0 nM fluorescein-labeled P4 peptide and 10 nM MDM2
[b]GI_{50} values for SJSA-1 and H1299 cells were measured by MTS assay

using synthetic and recombinant L-MDM2 proteins, respectively (Table 2.2). These data identified the mirror-image α-tocopherol derivative **1b** (*ent*-NP843) as a selective inhibitor of the L-MDM2–L-p53 interaction. Furthermore, the antiproliferative activity of *ent*-NP843 was investigated using cancer cells, SJSA-1 cells (MDM2 overexpressed) [17] and H1299 cells (no p53 expression) [18]. Unfortunately, no antiproliferative activities of *ent*-NP843 against SJSA-1 and H1299 cells were observed at 30 μM (Table 2.1).

Further structure–activity study of compound **1b** and the derivatives revealed the structural requirements for inhibition of L-MDM2–L-p53 interaction (Table 2.3). The author designed two diastereomers of compound **1b**: epimer **1c** at the tetrasubstituted carbon on the chromane scaffold, and diastereomer **1d** with two epimeric methyl groups on the right-hand alkyl chain (mirror-image of **1c**) (Fig. 2.12). Com-

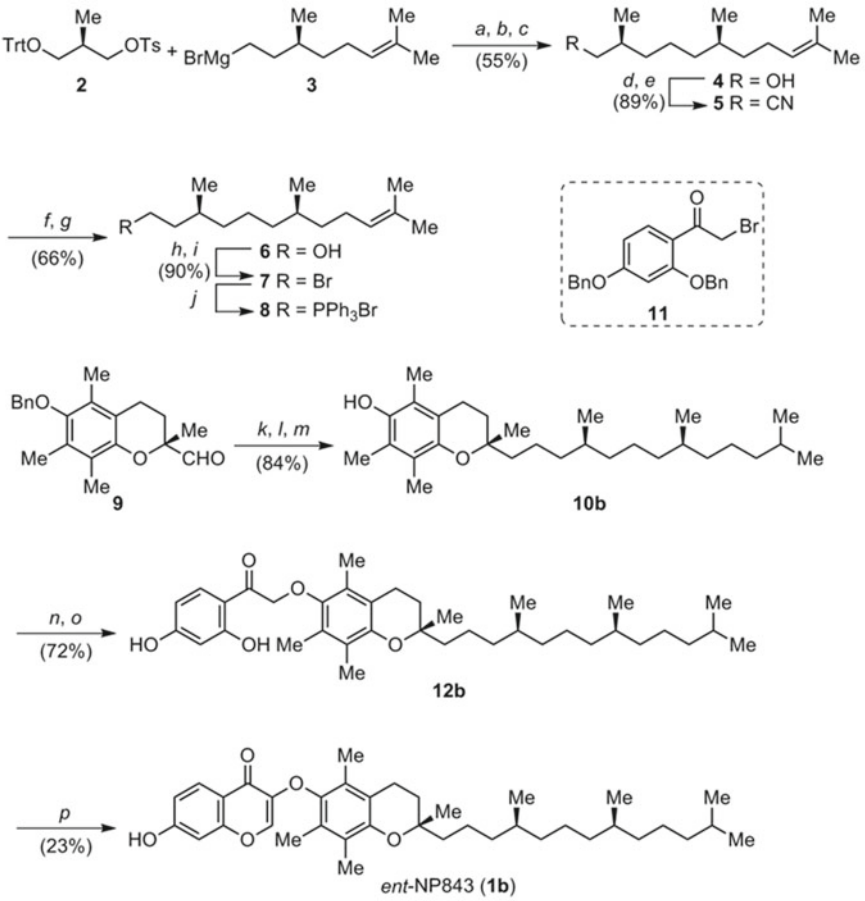

Scheme 2.2 Synthetic scheme for *ent*-NP843. *Reagents and condition*: *a* Li_2CuCl_4, THF, 0 °C; *b* HCO_2H, Et_2O, rt; *c* NaOH, MeOH/H_2O, rt; *d* TsCl, pyridine, 0 °C; *e* NaCN, DMSO, rt; *f* DIBAL-H, THF/CH_2Cl_2, −78 °C, then H_3O^+; *g* DIBAL-H, THF/CH_2Cl_2, −78 °C; *h* TsCl, pyridine, 0 °C; *i* LiBr, acetone, reflux; *j* PPh_3, neat, 100 °C; *k* LHMDS, **8**, THF, −40 °C to rt; *l* H_2, PtO_2, TBME, rt; *m* H_2, Pd/C, MeOH, rt; *n* **11**, K_2CO_3, DMF, rt; *o* H_2, Pd/C, EtOAc, rt; *p* DMF-DMA, THF, reflux

pound **1d**, having a tetrasubstituted carbon with (*S*)-configuration on the chromane skeleton (identical to that of compound **1b**) reproduced the bioactivity of **1b** against L-MDM2–L-p53 interaction [IC_{50} (**1d**) = 6.9 ± 1.9 μM for L-MDM2–L-p53], while compound **1c** with (*R*)-configuration (identical to that of compound **1a**) showed no inhibition. However, for D-MDM2–D-p53 inhibition, compound **1c** was potent [IC_{50} (**1c**) = 7.8 ± 2.0 μM for D-MDM2–D-p53]. These results indicate that the stereochemistry of the tetrasubstituted carbon on the chromane skeleton is dominant in the chiral recognition by L-MDM2 protein when compared with the stereocenters on the extended alkyl chain. To demonstrate the significance of the aliphatic chain length

Table 2.2 Inhibitory Activities of NP843 and *ent*-NP843 by SPR Analysis and ELISA

Compound	IC_{50} (μM)[a]	
	SPR	ELISA
L-P4	0.011 ± 0.001	0.066 ± 0.007
D-P4	>1.0	>1.0
NP843 (**1a**)	>30	>30
ent-NP843 (**1b**)	3.1 ± 0.5	16.7 ± 1.1

[a]IC_{50} values were evaluated in triclicate assays

Table 2.3 Biological activity of NP843 derivatives

Compounds	IC_{50} (μM)[a]	
	L-MDM2	D-MDM2
1c	>30	7.8 ± 2.0
1d	6.9 ± 1.9	>30
13a	>30	>30
13b	>30	>30
14a	>30	>30
14b	>30	>30

[a]IC_{50} values for L/D-MDM2 were measured by FP assay using 1.0 nM fluorescein-labeled P4 peptide and 10 nM MDM2

of **1b**, the author also designed derivatives **13a**,**b** and **14a**,**b** with shorter isoprene units (Fig. 2.12). Derivatives **13a**,**b** and **14a**,**b** showed no inhibitory activity against L-MDM2–L-p53 interaction (nor against D-MDM2–D-p53 interaction). These results suggest a chain length of three isoprene units is indispensable for biological activity of compound **1b**.

In this study, isolated natural products and derivatives, which were immobilized on microarray slides, were used as a screening resource. This approach would be further applicable to the mirror-image screening of mixture samples from natural resources including crude plant extracts and fermentation broth extracts, which could provide unprecedented opportunity to explore diastereomeric interactions between the mirror-image structures of chiral ingredients and native proteins. Once the hit extract(s) is identified, structural determination of the active ingredient(s) and synthesis of its enantiomer(s) would be needed. In this way, novel hit compound(s) with "unnatural" chirality would be obtained with a high probability. It is the expectation that future analysis of screening data sets against a number of target molecules may give some insights into the value of mirror-image natural resources for drug discovery.

In this strategy, two chemical syntheses of mirror-image substances (target protein and initial hit compound), and chemical array technology using synthetic D-protein facilitated access to a variety of virtual mirror-image natural products. For further applications to other molecular targets, rapid and efficient preparations of mirror-

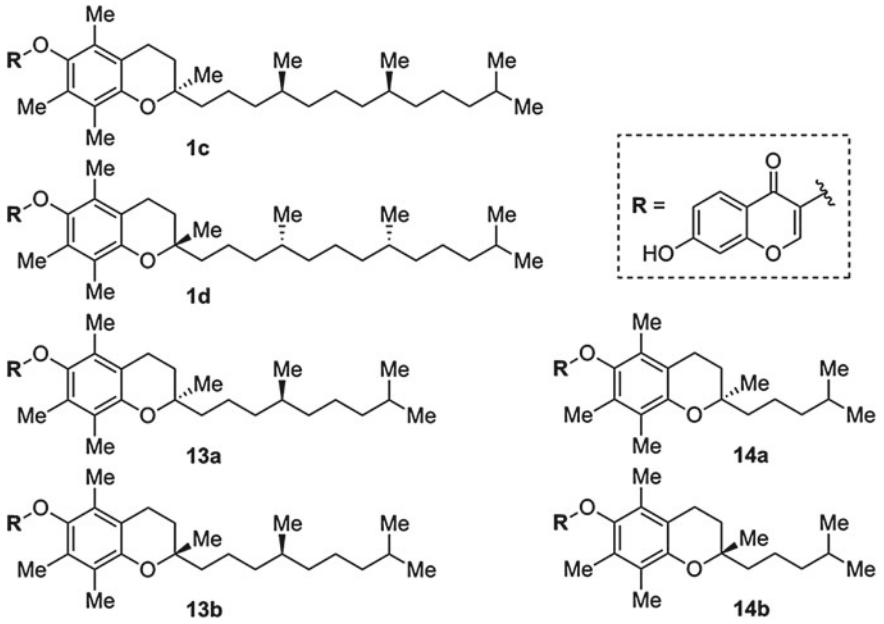

Fig. 2.12 Structures of NP843 derivatives

image biomolecules and natural product hit(s) are essential because these cannot be generated via protein expressions or conventional cultivations. Recent progress in chemical protein synthesis has increased the availability of synthetic proteins, even with highly functional modification(s) [19]. Although this study demonstrates mirror-image screening for protein–protein interaction inhibitors, the targets could be extended to enzyme inhibitors and receptor ligands once the counterpart mirror-image biomolecule(s) are available [20]. A number of recent advances in efficient synthetic strategies to access unique and complex frameworks in natural products should also contribute to the concise preparation of mirror-image structure(s) of natural product hit compounds. Thus, investigation of the bioactivities and functions of virtual mirror-image compounds is achievable only by using advanced synthetic organic chemistry technologies.

In summary, the author has established a novel screening process for a virtual mirror-image library of chiral natural products and derivatives. Chemically synthesized mirror-image MDM2 was applied for chemical array screening of a library of natural product derivatives, identifying novel tocopherol derivative NP843 (**1a**) as a D-MDM2–D-p53 interaction inhibitor. Chemical synthesis of the enantiomeric compound (**1b**) enabled the validation of the inhibitory activity of **1b** against L-MDM2–L-p53 interaction. The selective recognition by MDM2 was attributed to the stereochemistry of the tetrasubstituted carbon on the chromane skeleton of **1b**. The aliphatic side chain of three isoprene units was also needed for inhibition. In contrast to conventional screenings, this process could identify hit compounds from

unavailable mirror-image chiral natural products, thus providing unprecedented lead compounds for drug discovery. This is the first application of mirror-image protein technology to the screening of chiral small molecules including natural products.

2.2.2 *Experimental Section*

General Methods

^{1}H NMR and ^{13}C NMR spectra were recorded using a JEOL ECA-500 spectrometer. Chemical shifts are reported in δ (ppm) relative to Me_4Si (in $CDCl_3$). ^{13}C NMR spectra were referenced to the residual $CHCl_3$ (in $CDCl_3$). ^{1}H NMR spectra were tabulated as follows: chemical shift, multiplicity (br: broad, s: singlet, d: doublet, t: triplet, q: quartet, m: multiplet), number of protons, and coupling constants. Exact mass (HRMS) spectra were recorded on a JMS-HX/HX 110A mass spectrometer or Shimadzu LC-ESI-IT-TOF-MS equipment. Melting points were measured by a hot stage melting point apparatus (uncorrected). For flash chromatography, Wakogel C-300E (Wako) was employed. For analytical HPLC for MDM2 proteins, Cosmosil 5C18-AR300 (4.6 × 250 mm, Nacalai Tesque Inc.) was employed with a linear gradient of CH_3CN containing 0.1% (v/v) TFA aq. at a flow rate of 1 mL/min. Cosmosil 5C18-ARII column (4.6 × 250 mm, Nacalai Tesque Inc.) was employed for the analysis of the other peptides. The purity of all compounds for biological evaluations was determined by combustion analysis (>95%).

Synthesis of MDM2$^{25–109}$ and MDM2^{TMR} Proteins

L-MDM2$^{25–109}$, L-MDM2^{TMR}, D-MDM2$^{25–109}$ and D-MDM2^{TMR} proteins were synthesized by the identical protocol in Sect. 1 of Chap. 2. Briefly, protected MDM2$^{25–109}$ was synthesized by a standard protocol of Fmoc-based SPPS using automatic peptide synthesizer (PSSM-8, Shimadzu Corporation Ltd.) on H-Rink Amide ChemMatrix resin (0.4–0.6 mmol/g) using HBTU/HOBt/(i-Pr)$_2$NEt activation. The resulting protected peptide resin was treated with TFA/thioanisole/m-cresol/EDT/H_2O (80:5:5:5:5) at room temperature for 2 h. After removal of the resin by filtration, the filtrate was poured into ice-cold dry Et_2O. The resulting powder was collected by centrifugation and then washed with ice-cold dry Et_2O three times. The crude product was purified by HPLC to provide MDM2$^{25–109}$ proteins as white powder (Fig. 2.13).

For the synthesis of MDM2^{TMR} proteins, two glycines and 5-hexynoic acid were coupled with HBTU/HOBt/(i-Pr)$_2$NEt. The resulting protected peptides were treated with the deprotection cocktail as above to provide alkyne-conjugated proteins. Subsequently, treatment of the proteins with TMR-(PEG)$_3$-azide in the presence of Cu(I) provided TMR-labeled MDM2^{TMR} proteins as pink powder (Fig. 2.13).

ESI-MS for L-MDM2$^{25–109}$: Calcd for $C_{462}H_{739}N_{117}O_{123}S_4$: 10027.42; observed: $[M+12H]^{12+}$ m/z = 836.74, $[M+11H]^{11+}$ m/z = 912.76, $[M+10H]^{10+}$ m/z = 1003.86, $[M+9H]^{9+}$ m/z = 1115.39, $[M+8H]^{8+}$ m/z = 1254.76, $[M+7H]^{7+}$ m/z = 1434.00.[1]

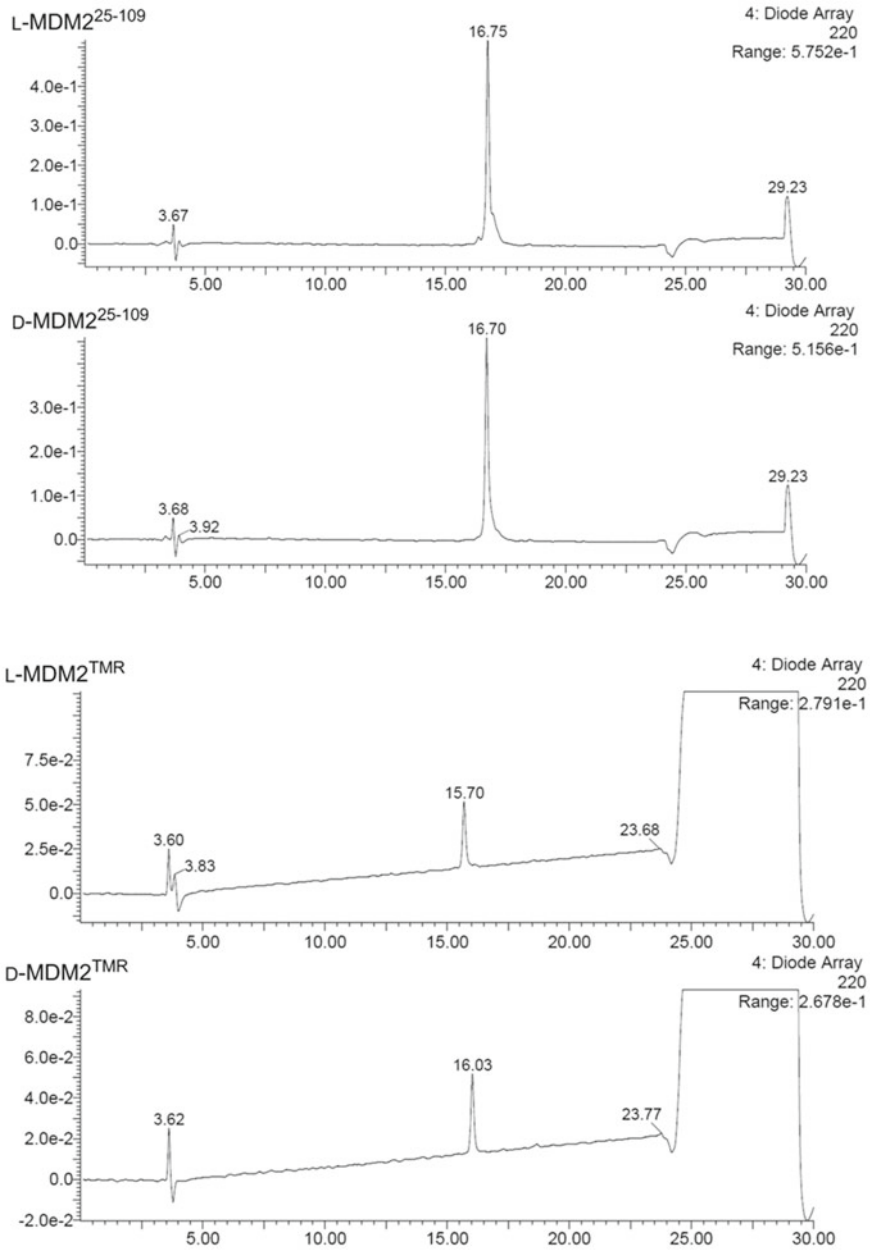

Fig. 2.13 LC–MS chromatograms of purified synthetic MDM2$^{25-109}$ and MDM2^{TMR} proteins. *HPLC conditions*: HPLC analysis was performed at 25 °C on a Cosmosil 5C18-AR300 preparative column (Nacalai Tesque, 4.5 × 250 mm) with a linear gradient of 30–50% CH_3CN containing 0.1% TFA at a flow rate of 1 mL/min over 20 min

ESI-MS for D-MDM2$^{25–109}$: Calcd for $C_{462}H_{739}N_{117}O_{123}S_4$: 10027.42; observed: $[M+12H]^{12+}$ m/z = 836.68, $[M+11H]^{11+}$ m/z = 912.77, $[M+10H]^{10+}$ m/z = 1003.94, $[M+9H]^{9+}$ m/z = 1115.46, $[M+8H]^{8+}$ m/z = 1254.85, $[M+7H]^{7+}$ m/z = 1433.42.

ESI-MS for L-MDM2^{TMR}: Calcd for $C_{505}H_{789}N_{125}O_{133}S_4$: 10865.79; observed: $[M+13H]^{13+}$ m/z = 836.94, $[M+12H]^{12+}$ m/z = 906.78, $[M+11H]^{11+}$ m/z = 989.03, $[M+10H]^{10+}$ m/z = 1087.90, $[M+9H]^{9+}$ m/z = 1208.38, $[M+8H]^{8+}$ m/z = 1359.59.[1]

ESI-MS for D-MDM2^{TMR}: Calcd for $C_{505}H_{789}N_{125}O_{133}S_4$: 10865.79; observed: $[M+13H]^{13+}$ m/z = 836.65, $[M+12H]^{12+}$ m/z = 906.65, $[M+11H]^{11+}$ m/z = 989.11, $[M+10H]^{10+}$ m/z = 1088.17, $[M+9H]^{9+}$ m/z = 1208.45, $[M+8H]^{8+}$ m/z = 1359.80.

Folding of Synthetic MDM2$^{25–109}$ and MDM2^{TMR} Proteins

Folding of synthetic MDM2 proteins were carried out by the identical protocol in Sect. 1 of Chap. 2 [16]. Lyophilized polypeptide was dissolved in 6 M guanidine hydrochloride (Gu · HCl) (1 mg/mL) followed by 100-fold dilution with PBS (pH 7.4) containing 0.5 mM TCEP · HCl and 0.005% Tween-20 at 4 °C. The solution was stored at 4 °C overnight, and the solution was concentrated using a MWCO 3000 centrifugal filtration membrane (Millipore, Amicon-Ultra 3 kDa) (3 times).

Synthesis of p53 Peptides and Their Derivatives

p53 peptides were synthesized by Fmoc-based SPPS on Rink-amide resin (0.66 mmol/g, 45.5 mg, 0.025 mmol) according to the identical protocol in the previous report [16]. Fmoc-protected amino acids (3 eq) were coupled by using DIPCI (3 eq) and HOBt (3 eq) in DMF. The Fmoc-protecting group was removed by treatment of the resin with 20% piperidine in DMF. Coupling of biotin (0.125 mmol) was carried out with HBTU (5 eq), HOBt (5 eq) and $(i\text{-Pr})_2$NEt (10 eq) in DMF. Coupling of 5-carboxyfluorescein (5 eq) was carried out with DIPCI (5 eq) and HOBt (10 eq) in DMF. The resulting protected peptide resin was treated with TFA/thioanisole/*m*-cresol/EDT/H_2O (80:5:5:5:5) at room temperature for 2 h. After removal of the resin by filtration, the filtrate was poured into ice-cold dry Et_2O. The resulting powder was collected by centrifugation and then washed with ice-cold dry Et_2O three times. The crude product was purified by HPLC on a Cosmosil 5C18-ARII preparative column (Nacalai Tesque, 20 × 250 mm). All peptides were characterized by MALDI-TOF-MS.

Biotin-labeled L-p53 peptide (biotinyl-aminocaproyl-GSGSSQETFSDLWKLLPEN-NH_2): MS (MALDI-TOF) calcd for $C_{108}H_{166}N_{27}O_{35}S$ $[M+H]^+$ 2434.19; found: 2434.13.

Biotin-labeled D-p53 peptide: MS (MALDI-TOF) calcd for $C_{108}H_{166}N_{27}O_{35}S$ $[M+H]^+$ 2434.19; found: 2434.12.

L-P4 (H-LTFEHYWAQLTS-NH_2): MS (MALDI-TOF) calcd for $C_{71}H_{100}N_{17}O_{19}$ $[M+H]^+$ 1494.74; found: 1494.75.

D-P4: MS (MALDI-TOF) calcd for $C_{71}H_{100}N_{17}O_{19}$ $[M+H]^+$ 1494.74; found: 1494.73.

5-Carboxyfluorescein-labeled L-P4 (5-FAM-LTFEHYWAQLTS-NH_2): MS (MALDI-TOF) calcd for $C_{92}H_{110}N_{17}O_{25}$ $[M+H]^+$ 1852.79; found: 1852.80.

5-Carboxyfluorescein-labeled D-P4: MS (MALDI-TOF) calcd for $C_{92}H_{110}N_{17}O_{25}$ $[M+H]^+$ 1852.79; found: 1852.76.

(2*S*,6*R*)-2,6,10-Trimethylundec-9-en-1-ol (4)
To a stirred mixture of Mg (1.00 g, 41.2 mmol) in THF (6.6 mL) was added dropwise (*S*)-citronellyl bromide (6.00 g, 27.4 mmol) in THF (16.8 mL) over 2 h using syringe pump at 60 °C to give Grignard reagent **3**. To a stirred solution of **2** [21] (6.9 g, 14.2 mmol) in THF (31.0 mL) were added the reagent **3** and 0.1 M Li_2CuCl_4 in THF (27.0 mL, 2.70 mmol) at −40 °C. The resulting mixture was stirred at −40 °C overnight and the reaction was quenched with saturated NH_4Cl at 0 °C. The whole was extracted with Et_2O and the extract was washed with H_2O and brine, and dried over $MgSO_4$. The filtrate was concentrated under reduced pressure. The oily residue was dissolved in hexane and the solution was filtrated through a short pad of silica gel and the filtrate was concentrated under reduced pressure. To a stirred solution of the residue in dry Et_2O (120 mL) was added HCO_2H (120 mL) dropwise at 0 °C under argon, and the stirring was continued for 1 h. After toluene (150 mL) was added, the solution was concentrated under reduced pressure. 1N NaOH in MeOH/H_2O (1:1, 100 mL) was added to the residue and the mixture was stirred for 10 min. The mixture was concentrated under reduced pressure. The residue was extracted with Et_2O and the extract was dried over $MgSO_4$. The filtrate was concentrated under reduced pressure, and the residue was purified by column chromatography to give the title compound **4** as a colorless oil (1.67 g, 55%). $[\alpha]_D^{25}$ −7.5 (*c* 1.10, $CHCl_3$); IR (neat): 3319 (OH), 1035 (C–O); ^{1}H NMR (500 MHz, $CDCl_3$) δ 0.86 (d, J = 6.3 Hz, 3H), 0.93 (d, J = 6.3 Hz, 3H), 1.04–1.42 (m, 9H), 1.60 (s, 3H), 1.58–1.65 (m, 1H), 1.68 (s, 3H), 1.89–2.03 (m, 2H), 3.42 (dd, J = 10.3, 6.3 Hz, 1H), 3.51 (dd, J = 10.6, 6.0 Hz, 1H), 5.09–5.11 (m, 1H); ^{13}C NMR (125 MHz, $CDCl_3$) δ 16.6, 17.6, 19.6, 24.3, 25.5, 25.7, 32.4, 33.4, 35.8, 37.1, 37.2, 68.4, 125.0, 131.0. HRMS (FAB) calcd for $C_{14}H_{29}O$ (MH^+): 213.2213; found: 213.2217.

(2*R*,6*S*)-2,6,10-Trimethylundec-9-en-1-ol (*ent*-4)
According to the procedure described for the preparation of **4**, compound *ent*-**2** (5.00 g, 10.3 mmol) was converted into *ent*-**4** with (*R*)-citronellyl bromide (6.40 g, 29.2 mmol) as a colorless oil (996 mg, 46%). $[\alpha]_D^{25}$ +7.4 (*c* 1.17, $CHCl_3$); IR (neat): 3357 (OH), 1034 (C-O); ^{1}H NMR (500 MHz, $CDCl_3$) δ 0.86 (d, J = 6.9 Hz, 3H), 0.92 (d, J = 6.3 Hz, 3H), 1.03–1.41 (m, 9H), 1.60 (s, 3H), 1.58–1.65 (m, 1H), 1.68 (s, 3H), 1.89–2.03 (m, 2H), 3.42 (dd, J = 10.3, 6.3 Hz, 1H), 3.51 (dd, J = 10.6, 6.3 Hz, 1H), 5.09–5.11 (m, 1H); ^{13}C NMR (125 MHz, $CDCl_3$) δ 16.6, 17.6, 19.6, 24.3, 25.5, 25.7, 32.4, 33.4, 35.8, 37.1, 37.2, 68.4, 125.0, 131.0. HRMS (FAB) calcd for $C_{14}H_{29}O$ (MH^+): 213.2213; found: 213.2223.

(3*S*,7*R*)-3,7,11-Trimethyldodec-10-enenitrile (5)
To a stirred solution of compound **4** (1.26 g, 5.93 mmol) in pyridine (4.3 mL) was added TsCl (1.40 g, 7.72 mmol) at 0 °C. After the mixture was stirred for 2 h, saturated aqueous solution of citric acid was added. The whole was extracted with Et_2O and the extract was washed with H_2O and brine, and dried over $MgSO_4$. The extract was concentrated under reduced pressure after filtration through a short pad of silica gel to give a crude sulfonate. To a stirred solution of the sulfonate in DMSO (13.0 mL) was added NaCN (0.581 g, 11.86 mmol) at room temperature. After the

mixture was stirred overnight, saturated aqueous solution of NH_4Cl was added. The whole was extracted with $CHCl_3$ and the extract was washed with H_2O and brine, and dried over $MgSO_4$. The filtrate was concentrated under reduced pressure, and the residue was purified by column chromatography to give the title cyanide **5** as a colorless oil (1.17 g, 89%). $[\alpha]_D^{25}$ +5.2 (*c* 1.02, $CHCl_3$); IR (neat): 2247 (C≡N); ^{1}H NMR (500 MHz, $CDCl_3$) δ 0.87 (d, *J* = 6.3 Hz, 3H), 1.07 (d, *J* = 6.9 Hz, 3H), 1.07–1.17 (m, 2H), 1.23–1.43 (m, 7H), 1.60 (s, 3H), 1.69 (s, 3H), 1.81–1.89 (m, 1H), 1.89–2.03 (m, 2H), 2.23 (dd, *J* = 16.6, 6.9 Hz, 1H), 2.32 (dd, *J* = 16.6, 5.7 Hz, 1H), 5.09–5.11 (m, 1H); ^{13}C NMR (125 MHz, $CDCl_3$) δ 17.6, 19.5 (2C), 24.2, 24.4, 25.5, 25.7, 30.5, 32.3, 36.2, 36.8, 37.0, 119.0, 124.9, 131.1. HRMS (FAB) calcd for $C_{15}H_{28}N$ (MH^+): 222.2216; found: 222.2224.

(3*R*,7*S*)-3,7,11-Trimethyldodec-10-enenitrile (*ent*-5)
According to the procedure described for the preparation of **5**, compound *ent*-**4** (950 mg, 4.47 mmol) was converted into *ent*-**5** as a colorless oil (948 mg, 96%). $[\alpha]_D^{25}$ −5.3 (*c* 1.08, $CHCl_3$); IR (neat): 2247 (C≡N); ^{1}H NMR (500 MHz, $CDCl_3$) δ 0.87 (d, *J* = 6.3 Hz, 3H), 1.07 (d, *J* = 6.9 Hz, 3H), 1.09-1.17 (m, 2H), 1.21–1.43 (m, 7H), 1.61 (s, 3H), 1.69 (s, 3H), 1.81–1.89 (m, 1H), 1.89–2.03 (m, 2H), 2.24 (dd, *J* = 16.6, 6.9 Hz, 1H), 2.32 (dd, *J* = 16.6, 5.7 Hz, 1H), 5.08–5.11 (m, 1H); ^{13}C NMR (125 MHz, $CDCl_3$) δ 17.6, 19.5 (2C), 24.2, 24.4, 25.5, 25.7, 30.5, 32.3, 36.2, 36.8, 37.0, 119.0, 124.9, 131.1. HRMS (FAB) calcd for $C_{15}H_{28}N$ (MH^+): 222.2216; found: 222.2224.

(3*S*,7*R*)-3,7,11-Trimethyldodec-10-en-1-ol (6)[6]
To a stirred solution of **5** (1.00 g, 4.52 mmol) in CH_2Cl_2 (5.0 mL) was added dropwise 1.0 M DIBAL-H in THF (4.97 mL, 4.97 mmol) at −78 °C under argon. After the mixture was stirred for 2 h, saturated aqueous solution of sodium potassium tartrate was added and the mixture was warmed to room temperature. The whole was extracted with Et_2O and the extract was dried over $MgSO_4$. The extract was concentrated under reduced pressure after filtration through a short pad of silica gel to give crude aldehyde. To a stirred solution of the aldehyde in CH_2Cl_2 (5.0 mL) was added dropwise DIBAL-H in THF (1.0 M, 4.97 mL, 4.97 mmol) at −78 °C under argon. After the mixture was stirred for 2 h, saturated aqueous solution of sodium potassium tartrate was added. The whole was extracted with Et_2O and the extract was dried over $MgSO_4$. The extract was concentrated under reduced pressure, and the residue was purified by column chromatography to give the title alcohol **6** as a colorless oil (0.848 g, 83%). $[\alpha]_D^{25}$ −2.3 (*c* 0.90, $CHCl_3$); IR (neat): 3299 (OH), 1058 (C-O); ^{1}H NMR (500 MHz, $CDCl_3$) δ 0.86 (d, *J* = 6.3 Hz, 3H), 0.90 (d, *J* = 6.3 Hz, 3H), 1.07–1.41 (m, 11H), 1.54–1.64 (m, 1H), 1.61 (s, 3H), 1.69 (s, 3H), 1.89-2.03 (m, 2H), 3.64–3.73 (m, 2H), 5.09–5.11 (m, 1H); ^{13}C NMR (125 MHz, $CDCl_3$) δ 17.6, 19.6, 19.7, 24.3, 25.6, 25.7, 29.5, 32.4, 37.0, 37.2, 37.5, 40.0, 61.3, 125.0, 124.9, 131.0. HRMS (FAB) calcd for $C_{15}H_{31}O$ (MH^+): 227.2369; found: 227.2363.

(3*R*,7*S*)-3,7,11-Trimethyldodec-10-en-1-ol (*ent*-6)
According to the procedure described for the preparation of **6**, compound *ent*-**5** (900 mg, 4.07 mmol) was converted into *ent*-**6** as a colorless oil (606 mg, 66%).

$[\alpha]_D^{25}$ +2.0 (*c* 1.05, $CHCl_3$); IR (neat): 3299 (OH), 1055 (C–O); ^{1}H NMR (500 MHz, $CDCl_3$) δ 0.86 (d, J = 6.3 Hz, 3H), 0.90 (d, J = 6.3 Hz, 3H), 1.04–1.41 (m, 11H), 1.52–1.63 (m, 1H), 1.60 (s, 3H), 1.68 (s, 3H), 1.89–2.03 (m, 2H), 3.64–3.73 (m, 2H), 5.08–5.12 (m, 1H); ^{13}C NMR (125 MHz, $CDCl_3$) δ 17.6, 19.6, 19.7, 24.3, 25.6, 25.7, 29.5, 32.4, 37.0, 37.2, 37.5, 39.9, 61.3, 125.0, 124.9, 131.0. HRMS (FAB) calcd for $C_{15}H_{31}O$ (MH^+): 227.2369; found: 227.2363.

(6*R*,10*S*)-12-Bromo-2,6,10-trimethyldodec-2-ene (7)
To a stirred solution of compound **6** (800 mg, 3.53 mmol) in pyridine (2.70 mL) was added TsCl (876 mg, 4.60 mmol) at 0 °C. After the mixture was stirred for 2 h, saturated aqueous solution of citric acid was added. The whole was extracted with Et_2O and the extract was washed with H_2O and brine, and dried over $MgSO_4$. The extract was concentrated under reduced pressure after filtration through a short pad of silica gel to give a crude sulfonate. To a stirred solution of the sulfonate in acetone (5 mL) was added LiBr (1.80 g, 17.7 mmol). After the mixture was stirred for 1 h under reflux, the whole was concentrated under reduced pressure. To the residue was added H_2O and the whole was extracted with Et_2O and dried over $MgSO_4$. The filtrate was concentrated under reduced pressure, and the residue was purified by column chromatography to give the title bromide **7** as a colorless oil (923 mg, 90%). $[\alpha]_D^{25}$ +5.8 (*c* 1.00, $CHCl_3$); ^{1}H NMR (500 MHz, $CDCl_3$) δ 0.86 (d, J = 6.9 Hz, 3H), 0.89 (d, J = 6.9 Hz, 3H), 1.04–1.41 (m, 9H), 1.61 (s, 3H), 1.68 (s, 3H), 1.61–1.68 (m, 2H), 1.85–2.03 (m, 3H), 3.38-3.49 (m, 2H), 5.09–5.11 (m, 1H); ^{13}C NMR (125 MHz, $CDCl_3$) δ 17.6, 19.0, 19.6, 24.1, 25.6, 25.7, 31.6, 32.3, 32.4, 36.8, 37.1 (2C), 40.0, 125.0, 131.0. Anal. calcd. for $C_{15}H_{29}Br$: C, 62.28; H, 10.10. Found: C, 62.31; H, 10.32.

(6*S*,10*R*)-12-Bromo-2,6,10-trimethyldodec-2-ene (*ent*-7)
According to the procedure described for the preparation of **7**, compound *ent*-**6** (580 mg, 2.56 mmol) was converted into *ent*-**7** as a colorless oil (669 mg, 90%). $[\alpha]_D^{25}$ −5.8 (*c* 1.01, $CHCl_3$); ^{1}H NMR (500 MHz, $CDCl_3$) δ 0.86 (d, J = 6.9 Hz, 3H), 0.89 (d, J = 6.9 Hz, 3H), 1.07–1.41 (m, 9H), 1.61 (s, 3H), 1.68 (s, 3H), 1.61–1.68 (m, 2H), 1.84–2.03 (m, 3H), 3.38–3.49 (m, 2H), 5.09–5.11 (m, 1H); ^{13}C NMR (125 MHz, $CDCl_3$) δ 17.6, 19.0, 19.6, 24.1, 25.6, 25.7, 31.6, 32.2, 32.4, 36.8, 37.1 (2C), 40.0, 125.0, 131.0. Anal. calcd. for $C_{15}H_{29}Br$: C, 62.28; H, 10.10. Found: C, 62.22; H, 10.08.

Triphenyl((3*S*,7*R*)-3,7,11-trimethyldodec-10-en-1-yl)phosphonium Bromide (8)
A mixture of the bromide **7** (757 mg, 2.61 mmol) and PPh_3 (750 mg, 2.87 mmol) was heated to 100 °C and the mixture was stirred for 15 h. After cooling, Et_2O was added to the mixture and the resulting white precipitate was washed with Et_2O to remove the excess PPh_3. The residue was dried under vacuum to give the title phosphonium salt **8**, which was used without further purification.

Triphenyl((3*S*,7*R*)-3,7,11-trimethyldodec-10-en-1-yl)phosphonium Bromide (*ent*-8)
According to the procedure described for the preparation of **8**, compound *ent*-**7** (600 mg, 2.07 mmol) was converted into *ent*-**8**.

(*S*)-2,5,7,8-Tetramethyl-2-((4*S*,8*S*)-4,8,12-trimethyltridecyl)chroman-6-ol (10b) [22]

To a stirred solution of phosphonium salt **8** (ca. 2.61 mmol) in THF (15.0 mL) was added LHMDS (1.0 M, 2.30 mL, 2.30 mmol) in THF dropwise at −40 °C under argon. After the mixture was stirred for 30 min, the aldehyde **9** [23] (675 mg, 2.08 mmol) in THF (5.0 mL) was added to the mixture. The stirring was continued for 30 min at the same temperature and for 1 h at 0 °C. After the reaction was quenched with saturated aqueous solution of NH_4Cl, the whole was extracted with Et_2O and the extract was washed with H_2O and brine, and dried over Na_2SO_4. The filtrate was concentrated under reduced pressure. The oily residue was dissolved in hexane and the solution was filtrated through a short pad of silica gel to remove phosphine oxide and the filtrated was concentrated under reduced pressure. To a stirred solution of the crude alkene in TBME (9.5 mL) was added PtO_2 (37.8 mg, 0.167 mmol). The mixture was stirred under an atmosphere of H_2 at room temperature. After 30 min, the reaction mixture was filtrated through Celite and the filtrate was concentrated. To a stirred solution of the residue in MeOH (35.0 mL) was added 10% Pd/C (222 mg, 0.208 mmol). The mixture was stirred under an atmosphere of H_2 at room temperature. After 30 min, the reaction mixture was filtrated through Celite. The filtrate was concentrated under reduced pressure, and the residue was purified by column chromatography to give the title compound **10b** as a pale yellow oil (759 mg, 84%). $[\alpha]_D^{25}$ −0.7 (*c* 1.01, $CHCl_3$); ^{1}H NMR (500 MHz, $CDCl_3$) δ 0.83–0.87 (m, 12H), 1.02–1.53 (m, 21H), 1.23 (s, 3H), 1.73–1.84 (m, 2H), 2.11 (s, 6H), 2.16 (s, 3H), 2.60 (t, J = 6.9 Hz, 2H), 4.17 (s, 1H); ^{13}C NMR (125 MHz, $CDCl_3$) δ 11.3, 11.8, 12.2, 19.6, 19.7, 20.7, 21.0, 22.6, 22.7, 23.8, 24.4, 24.8, 28.0, 31.5, 32.7, 32.9, 37.3, 37.4 (3C), 39.4, 39.8, 74.5, 117.3, 118.4, 121.0, 122.6, 144.5, 145.5. HRMS (ESI) calcd for $C_{29}H_{50}O_2$ (M^+): 430.3811; found: 430.3806.

(*R*)-2,5,7,8-Tetramethyl-2-((4*S*,8*S*)-4,8,12-trimethyltridecyl)chroman-6-ol (10c)

According to the procedure described for the preparation of **10b**, compound *ent*-**9** (675 mg, 2.07 mmol) was converted into compound **10c** by the reaction with **8** (ca. 2.61 mmol) as a pale yellow oil (573 mg, 57%) (Fig. 2.14). $[\alpha]_D^{25}$ +1.0 (*c* 1.10, $CHCl_3$); ^{1}H NMR (500 MHz, $CDCl_3$) δ 0.83–0.87 (m, 12H), 1.03–1.58 (m, 21H), 1.23 (s, 3H), 1.73–1.84 (m, 2H), 2.11 (s, 6H), 2.16 (s, 3H), 2.60 (t, J = 6.9 Hz, 2H), 4.17 (s, 1H); ^{13}C NMR (125 MHz, $CDCl_3$) δ 11.3, 11.8, 12.2, 19.7 (2C), 20.8, 21.0, 22.6, 22.7, 23.8, 24.4, 24.8, 28.0, 31.4, 32.7, 32.8, 37.3, 37.4 (2C), 37.5, 39.4, 39.8, 74.5, 117.3, 118.4, 121.0, 122.6, 144.5, 145.5. HRMS (ESI) calcd for $C_{29}H_{50}O_2$ (M^+): 430.3811; found: 430.3803.

Fig. 2.14 Structure of **10c**

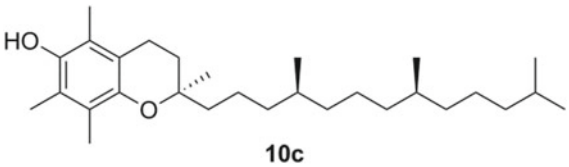

10c

Fig. 2.15 Structure of **10d**

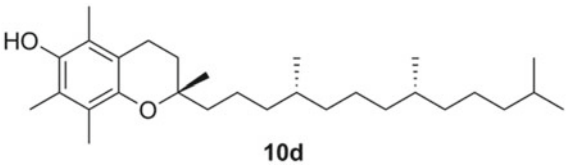

10d

(*S*)-2,5,7,8-Tetramethyl-2-((4*R*,8*R*)-4,8,12-trimethyltridecy)chroman-6-ol (10d) According to the procedure described for the preparation of **10b**, compound **9** (540 mg, 1.66 mmol) was converted into compound **10d** by the reaction with *ent*-**8** (ca. 2.08 mmol) as a pale yellow oil (573 mg, 80%) (Fig. 2.15). $[\alpha]_D^{25}$ −1.0 (*c* 1.00, $CHCl_3$); ^1H NMR (500 MHz, $CDCl_3$) δ 0.83–0.87 (m, 12H), 1.03–1.58 (m, 21H), 1.23 (s, 3H), 1.73-1.84 (m, 2H), 2.11 (s, 6H), 2.16 (s, 3H), 2.60 (t, J = 6.9 Hz, 2H), 4.17 (s, 1H); ^{13}C NMR (125 MHz, $CDCl_3$) δ 11.3, 11.8, 12.2, 19.7 (2C), 20.8, 21.0, 22.6, 22.7, 23.8, 24.4, 24.8, 28.0, 31.5, 32.7, 32.9, 37.3, 37.4 (2C), 37.5, 39.4, 39.8, 74.5, 117.3, 118.4, 121.0, 122.6, 144.5, 145.5. HRMS(ESI) calcd for $C_{29}H_{50}O_2$ (M^+): 430.3811; found: 430.3801.

1-(2,4-Dihydroxyphenyl)-2-{[(*S*)-2,5,7,8-tetramethyl-2-((4*S*,8*S*)-4,8,12-trimethyltridecyl)chroman-6-yl]oxy}ethan-1-one (12b)
To a stirred solution of compound **10b** (600 mg, 1.39 mmol) in DMF (1.4 mL) were added K_2CO_3 (385 mg, 2.78 mmol) and compound **11** (745 mg, 1.81 mmol) at room temperature. After the mixture was stirred overnight, the reaction was quenched with H_2O. The whole was extracted with Et_2O and the extract was washed with H_2O and brine, and dried over $MgSO_4$. The filtrate was concentrated under reduced pressure. To a stirred solution of the residue in EtOAc (15.0 mL) was added 10% Pd/C (149 mg, 0.140 mmol). The mixture was stirred under an atmosphere of H_2 at room temperature. After the reaction was completed, the reaction mixture was filtrated through Celite. Purification by column chromatography gave the title compound **12b** as pale yellow solid (583 mg, 72%): mp 87–88 °C; $[\alpha]_D^{25}$ −4.0 (*c* 1.01, $CHCl_3$); IR (neat): 3315 (OH), 1627 (C=O); ^1H NMR (500 MHz, $CDCl_3$) δ 0.84–0.87 (m, 12H), 1.04–1.57 (m, 21H), 1.24 (s, 3H), 1.73–1.85 (m, 2H), 2.09 (s, 3H), 2.14 (s, 3H), 2.18 (s, 3H), 2.58 (t, J = 6.6 Hz, 2H), 4.92 (s, 2H), 5.80 (br s, 1H), 6.36 (dd, J = 8.6, 2.3 Hz, 1H), 6.42 (d, J = 2.3 Hz, 1H), 7.52 (d, J = 7.7 Hz, 1H), 12.40 (s, 1H); ^{13}C NMR (125 MHz, $CDCl_3$) δ 11.8, 11.9, 12.8, 19.7 (2C), 20.6, 21.0, 22.6, 22.7, 23.8, 24.4, 24.8, 28.0, 31.2, 32.7, 32.8, 37.3, 37.4 (3C), 39.4, 40.0, 74.0, 75.0, 103.8, 108.0, 111.9, 117.8, 123.2, 125.7, 127.6, 130.9, 147.8, 148.3, 162.8, 165.3, 198.0. Anal. calcd. for $C_{37}H_{56}O_5$: C, 76.51; H, 9.72. Found: C, 76.41; H, 9.89.

1-(2,4-Dihydroxyphenyl)-2-{[(*R*)-2,5,7,8-tetramethyl-2-((4*S*,8*S*)-4,8,12-trimethyltridecyl)chroman-6-yl]oxy}ethan-1-one (12c)
According to the procedure described for the preparation of **12b**, compound **10c** (100 mg, 0.232 mmol) was converted into compound **12c** as pale yellow solid (88.9 mg, 66%) (Fig. 2.16): mp 86–87 °C; $[\alpha]_D^{25}$ +3.7 (*c* 0.55, $CHCl_3$); IR (neat):

Fig. 2.16 Structure of **12c**

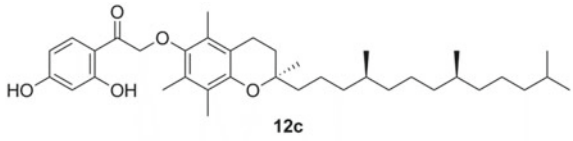

Fig. 2.17 Structure of **12d**

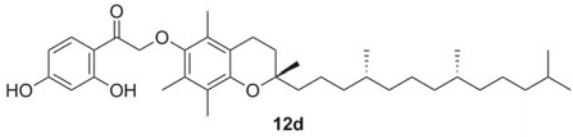

3351 (OH), 1626 (C=O); ^{1}H NMR (500 MHz, $CDCl_3$) δ 0.84–0.87 (m, 12H), 1.04–1.61 (m, 21H), 1.24 (s, 3H), 1.73–1.85 (m, 2H), 2.08 (s, 3H), 2.14 (s, 3H), 2.18 (s, 3H), 2.58 (t, J = 6.9 Hz, 2H), 4.92 (s, 2H), 6.36 (dd, J = 8.9, 2.6 Hz, 1H), 6.42 (d, J = 2.9 Hz, 1H), 7.51 (d, J = 9.2 Hz, 1H), 12.40 (s, 1H); ^{13}C NMR (125 MHz, $CDCl_3$) δ 11.8, 11.9, 12.8, 19.7 (2C), 20.6, 21.0, 22.6, 22.7, 23.8, 24.4, 24.8, 28.0, 31.1, 32.7, 32.8, 37.3, 37.4 (2C), 37.5, 39.4, 40.1, 74.0, 75.0, 103.8, 108.1, 111.9, 117.8, 123.2, 125.7, 127.6, 130.9, 147.8, 148.3, 162.9, 165.3, 198.0. Anal. Calcd. for $C_{37}H_{56}O_5$: C, 76.51; H, 9.72. Found: C, 76.35; H, 9.79.

1-(2,4-Dihydroxyphenyl)-2-{[(*S*)-2,5,7,8-tetramethyl-2-((4*R*,8*R*)-4,8,12-trimethyltridecyl)chroman-6-yl]oxy}ethan-1-one (12d)
According to the procedure described for the preparation of **12b**, compound **10d** (500 mg, 1.16 mmol) was converted into compound **12d** as pale yellow solid (483 mg, 72%) (Fig. 2.17): mp 86–87 °C; $[\alpha]_D^{25}$ −3.9 (*c* 1.11, $CHCl_3$); IR (neat): 3350 (OH), 1626 (C=O); ^{1}H NMR (500 MHz, $CDCl_3$) δ 0.84–0.87 (m, 12H), 1.04–1.61 (m, 21H), 1.24 (s, 3H), 1.73–1.85 (m, 2H), 2.08 (s, 3H), 2.14 (s, 3H), 2.18 (s, 3H), 2.58 (t, J = 6.9 Hz, 2H), 4.92 (s, 2H), 6.36 (dd, J = 8.9, 2.6 Hz, 1H), 6.42 (d, J = 2.9 Hz, 1H), 7.51 (d, J = 9.2 Hz, 1H), 12.40 (s, 1H); ^{13}C NMR (125 MHz, $CDCl_3$) δ 11.8, 11.9, 12.8, 19.7 (2C), 20.6, 21.0, 22.6, 22.7, 23.8, 24.4, 24.8, 28.0, 31.1, 32.7, 32.8, 37.3, 37.4 (2C), 37.5, 39.4, 40.1, 74.0, 75.0, 103.8, 108.1, 111.8, 117.8, 123.2, 125.7, 127.6, 130.9, 147.7, 148.3, 163.0, 165.3, 198.0. HRMS (ESI) calcd for $C_{37}H_{57}O_5$ (MH^+): 581.4201; found: 581.4207.

7-Hydroxy-3-{[(*R*)-2,5,7,8-tetramethyl-2-((4*R*,8*R*)-4,8,12-trimethyltridecyl)chroman-6-yl]oxy}-4*H*-chromen-4-one (1a, NP843)
mp 228–229 °C; $[\alpha]_D^{25}$ +5.0 (*c* 1.00, $CHCl_3$); IR (neat): 3163 (OH); ^{1}H NMR (500 MHz, $CDCl_3$) δ 0.84–0.87 (m, 12H), 1.03–1.59 (m, 21H), 1.25 (s, 3H), 1.75–1.85 (m, 2H), 2.02 (s, 3H), 2.06 (s, 3H), 2.09 (s, 3H), 2.58 (t, J = 6.9 Hz, 2H), 6.86 (d, J = 2.3 Hz, 1H), 7.07–7.10 (m, 2H), 8.22 (d, J = 9.2 Hz, 1H), 8.67 (br s, 1H); ^{13}C NMR (125 MHz, $CDCl_3$) δ 11.8 (2C), 12.6, 19.6, 19.7, 20.6, 21.0, 22.6, 22.7, 23.7, 24.4, 24.8, 28.0, 31.2, 32.7, 32.8, 37.3, 37.4 (3C), 39.4, 40.0, 75.3, 102.7, 115.5, 117.0, 118.2, 123.7, 125.3, 127.1, 127.6, 140.0, 142.8, 143.4, 149.0, 157.8, 162.2, 172.6. Anal. calcd. for $C_{38}H_{54}O_5$: C, 77.25; H, 9.21. Found: C, 77.13; H, 9.40.

7-Hydroxy-3-{[(*S*)-2,5,7,8-tetramethyl-2-((4*S*,8*S*)-4,8,12-trimethyltridecyl])chroman-6-yl]oxy}-4*H*-chromen-4-one (1b)

To a stirred solution of compound **12** (100 mg, 0.172 mmol) in THF (0.76 mL) was added DMF-DMA (27.7 μL, 0.260 mmol) under argon, and the mixture was stirred under reflux for 4 h. Then, aqueous 1N HCl (1 mL) and MeOH (1 mL) were added and the mixture was stirred overnight. The whole was extracted with Et_2O and dried over Na_2SO_4. The filtrate was concentrated under reduced pressure, and the residue was purified by column chromatography to give the title compound **1b** as white solid (23.3 mg, 23%): mp 228–229 °C; $[\alpha]_D^{25}$ −5.3 (*c* 1.00, $CHCl_3$); IR (neat): 3133 (OH); ^{1}H NMR (500 MHz, $CDCl_3$) δ 0.84–0.87 (m, 12H), 1.03–1.59 (m, 21H), 1.25 (s, 3H), 1.75–1.85 (m, 2H), 2.02 (s, 3H), 2.06 (s, 3H), 2.09 (s, 3H), 2.58 (t, *J* = 6.9 Hz, 2H), 6.86 (d, *J* = 2.3 Hz, 1H), 7.07–7.10 (m, 2H), 8.22 (d, *J* = 9.2 Hz, 1H), 8.55 (br s, 1H); ^{13}C NMR (125 MHz, $CDCl_3$) δ 11.8 (2C), 12.6, 19.6, 19.7, 20.6, 21.0, 22.6, 22.7, 23.8, 24.4, 24.8, 28.0, 31.2, 32.7, 32.8, 37.3, 37.4 (3C), 39.4, 40.0, 75.2, 102.7, 115.5, 117.0, 118.2, 123.7, 125.3, 127.1, 127.6, 140.0, 142.8, 143.4, 149.0, 157.8, 162.1, 172.6. Anal. calcd. for $C_{38}H_{54}O_5$: C, 77.25; H, 9.21. Found: C, 77.22; H, 9.43.

7-Hydroxy-3-{[(*R*)-2,5,7,8-tetramethyl-2-((4*S*,8*S*)-4,8,12-trimethyltridecyl])chroman-6-yl]oxy}-4*H*-chromen-4-one (1c)

According to the procedure described for the preparation of **1b**, compound **12c** (50.0 mg, 0.0861 mmol) was converted into compound **1c** as white solid (12.2 mg, 24%): mp 229–231 °C; $[\alpha]_D^{25}$ +5.4 (*c* 1.01, $CHCl_3$); IR (neat): 3125 (OH); ^{1}H NMR (500 MHz, $CDCl_3$) δ 0.84–0.87 (m, 12H), 1.03–1.64 (m, 21H), 1.25 (s, 3H), 1.75–1.85 (m, 2H), 2.02 (s, 3H), 2.06 (s, 3H), 2.09 (s, 3H), 2.58 (t, *J* = 6.9 Hz, 2H), 6.86 (d, *J* = 2.3 Hz, 1H), 7.07–7.10 (m, 2H), 8.22 (d, *J* = 8.6 Hz, 1H), 8.57 (br s, 1H); ^{13}C NMR (125 MHz, $CDCl_3$) δ 11.8 (2C), 12.6, 19.7 (2C), 20.6, 21.0, 22.6, 22.7, 23.7, 24.4, 24.8, 28.0, 31.1, 32.7, 32.8, 37.3, 37.4 (3C), 39.4, 40.0, 75.3, 102.7, 115.5, 117.0, 118.3, 123.7, 125.3, 127.1, 127.6, 140.0, 142.8, 143.4, 149.1, 157.8, 162.1, 172.6. Anal. calcd. for $C_{38}H_{54}O_5 \cdot 0.15$EtOAc: C, 76.75; H, 9.21. Found: C, 76.40; H, 9.21.

7-Hydroxy-3-{[(*S*)-2,5,7,8-tetramethyl-2-((4*R*,8*R*)-4,8,12-trimethyltridecyl])chroman-6-yl]oxy}-4*H*-chromen-4-one (1d)

According to the procedure described for the preparation of **1b**, compound **12d** (100 mg, 0.172 mmol) was converted into compound **1d** as white solid (23.5 mg, 23%): mp 229–231 °C; $[\alpha]_D^{25}$ −5.4 (*c* 0.95, $CHCl_3$); IR (neat): 3126 (OH); ^{1}H NMR (500 MHz, $CDCl_3$) δ 0.84–0.87 (m, 12H), 1.03–1.64 (m, 21H), 1.25 (s, 3H), 1.75–1.85 (m, 2H), 2.02 (s, 3H), 2.06 (s, 3H), 2.09 (s, 3H), 2.58 (t, *J* = 6.9 Hz, 2H), 6.86 (d, *J* = 2.3 Hz, 1H), 7.07–7.10 (m, 2H), 8.22 (d, *J* = 8.6 Hz, 1H), 8.51 (br s, 1H); ^{13}C NMR (125 MHz, $CDCl_3$) δ 11.8 (2C), 12.6, 19.7 (2C), 20.6, 21.0, 22.6, 22.7, 23.8, 24.4, 24.8, 28.0, 31.1, 32.7, 32.8, 37.3, 37.4 (3C), 39.4, 40.0, 75.3, 102.7, 115.4, 117.0, 118.3, 123.7, 125.3, 127.1, 127.6, 139.9, 142.8, 143.4, 149.1, 157.8, 162.1, 172.6. Anal. calcd. for $C_{38}H_{54}O_5$: C, 77.25; H, 9.21. Found: C, 77.36; H, 9.32.

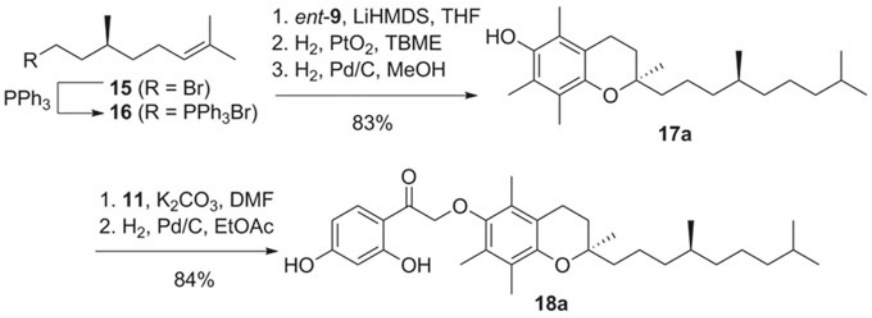

Scheme 2.3 Synthetic scheme for **18a**

(*S*)-(3,7-Dimethyloct-6-en-1-yl)triphenylphosphonium Bromide (16)
According to the procedure described for the preparation of **8**, (*S*)-citronellyl bromide **15** (3.99 g, 18.2 mmol) was converted into compound **16**, which was used without further purification.

(*R*)-2-((*S*)-4,8-Dimethylnonyl)-2,5,7,8-tetramethylchroman-6-ol (17a)
According to the procedure described for the preparation of **10b**, compound *ent*-**9** (800 mg, 2.47 mmol) was converted into compound **17a** using the phosphonium salt **16** (ca. 4.93 mmol) as a pale yellow oil (735 mg, 83%) (Scheme 2.3). $[\alpha]_D^{25}$ +0.4 (*c* 1.00, $CHCl_3$); ^{1}H NMR (500 MHz, $CDCl_3$) δ 0.83–0.88 (m, 9H), 1.05–1.53 (m, 14H), 1.23 (s, 3H), 1.73–1.84 (m, 2H), 2.11 (s, 6H), 2.16 (s, 3H), 2.60 (t, J = 6.9 Hz, 2H), 4.18 (s, 1H); ^{13}C NMR (125 MHz, $CDCl_3$) δ 11.3, 11.8, 12.2, 19.7 (2C), 21.0, 22.6, 22.7, 23.8, 24.7, 28.0, 31.5, 32.7, 37.2, 37.5, 39.3, 39.8, 74.5, 117.3, 118.4, 121.0, 122.6, 144.5, 145.5. HRMS (ESI) calcd for $C_{24}H_{40}O_2$ (M^+): 360.3028; found: 360.3026.

(*S*)-2-((*S*)-4,8-Dimethylnonyl)-2,5,7,8-tetramethylchroman-6-ol (17b)
According to the procedure described for the preparation of **10b**, compound **9** (800 mg, 2.47 mmol) was converted into compound **17b** using phosphonium salt **16** (ca. 4.93 mmol) as a pale yellow oil (730 mg, 82%). $[\alpha]_D^{25}$ +1.5 (*c* 1.00, $CHCl_3$); ^{1}H NMR (500 MHz, $CDCl_3$) δ 0.83–0.88 (m, 9H), 1.04–1.53 (m, 14H), 1.23 (s, 3H), 1.73–1.84 (m, 2H), 2.11 (s, 6H), 2.16 (s, 3H), 2.60 (t, J = 6.9 Hz, 2H), 4.18 (s, 1H); ^{13}C NMR (125 MHz, $CDCl_3$) δ 11.3, 11.8, 12.2, 19.6, 20.7, 21.0, 22.6, 22.7, 23.8, 24.8, 28.0, 31.5, 32.7, 37.3, 37.5, 39.3, 39.7, 74.5, 117.3, 118.4, 121.0, 122.6, 144.5, 145.5. HRMS (ESI) calcd for $C_{24}H_{40}O_2$ (M^+): 360.3028; found: 360.3035.

1-(2,4-Dihydoxyphenyl)-2-{[(*R*)-2-((*S*)-4,8-dimethylnonyl)-2,5,7,8-tetramethylchroman-6-yl]oxy}ethan-1-one (18a)
According to the procedure described for the preparation of **12b**, compound **17a** (700 mg, 1.94 mmol) was converted into compound **18a** as a pale yellow solid (916 mg, 84%): mp 89–91 °C; $[\alpha]_D^{25}$ +3.8 (*c* 0.70, $CHCl_3$); IR (neat): 3341 (OH), 1626 (C=O); ^{1}H NMR (500 MHz, $CDCl_3$) δ 0.84–0.87 (m, 9H), 1.06–1.61 (m, 14H), 1.24 (s, 3H), 1.73–1.85 (m, 2H), 2.09 (s, 3H), 2.14 (s, 3H), 2.18 (s, 3H), 2.57

(t, J = 6.6 Hz, 2H), 4.93 (s, 2H), 6.37 (dd, J = 8.9, 2.6 Hz, 1H), 6.42 (d, J = 2.9 Hz, 1H), 7.49 (d, J = 8.6 Hz, 1H), 12.37 (s, 1H); ^{13}C NMR (125 MHz, $CDCl_3$) δ 11.8, 11.9, 12.8, 19.6, 20.6, 21.0, 22.6, 22.7, 23.8, 24.7, 28.0, 31.1, 32.7, 37.2, 37.5, 39.3, 40.0, 73.9, 75.0, 103.8, 108.2, 111.7, 117.8, 123.2, 125.7, 127.6, 130.8, 147.7, 148.3, 163.2, 165.3, 198.0. HRMS (ESI) calcd for $C_{32}H_{47}O_5$ (MH^+): 511.3418; found: 511.3414.

1-(2,4-Dihydroxyphenyl)-2-{[(*S*)-2-((*S*)-4,8-dimethylnonyl)-2,5,7,8-tetramethylchroman-6-yl]oxy}ethan-1-one (18b)

According to the procedure described for the preparation of **12b**, compound **17b** (700 mg, 1.94 mmol) was converted into compound **18b** as a pale yellow solid (766 mg, 79%): mp 89–91 °C; $[\alpha]_D^{25}$ −3.7 (*c* 0.62, $CHCl_3$); IR (neat): 3363 (OH), 1626 (C=O); ^{1}H NMR (500 MHz, $CDCl_3$) δ 0.84-0.87 (m, 9H), 1.03–1.60 (m, 14H), 1.24 (s, 3H), 1.73–1.85 (m, 2H), 2.09 (s, 3H), 2.14 (s, 3H), 2.18 (s, 3H), 2.57 (t, J = 6.6 Hz, 2H), 4.93 (s, 2H), 6.26 (s, 1H), 6.37 (dd, J = 9.2, 2.3 Hz, 1H), 6.42 (d, J = 2.9 Hz, 1H), 7.50 (d, J = 9.2 Hz, 1H), 12.38 (s, 1H); ^{13}C NMR (125 MHz, $CDCl_3$) δ 11.8, 11.9, 12.8, 19.6, 20.6, 21.0, 22.6, 22.7, 23.8, 24.7, 28.0, 31.2, 32.7, 37.3, 37.5, 39.3, 40.0, 73.9, 75.0, 103.8, 108.2, 111.7, 117.8, 123.2, 125.7, 127.6, 130.9, 147.7, 148.3, 163.1, 165.3, 198.0. HRMS (ESI) calcd for $C_{32}H_{47}O_5$ (MH^+): 511.3418; found: 511.3419.

3-{[(*R*)-2-((*S*)-4,8-Dimethylnonyl)-2,5,7,8-tetramethylchroman-6-yl]oxy}-7-hydroxy-4*H*-chromen-4-one (13a)

According to the procedure described for the preparation of **1b**, compound **18a** (100 mg, 0.196 mmol) was converted into compound **13a** as a white solid (20.5 mg, 20%): mp 239–241 °C; $[\alpha]_D^{25}$ +5.4 (*c* 0.33, $CHCl_3$); IR (neat): 3116 (OH); ^{1}H NMR (500 MHz, $CDCl_3$) δ 0.84–0.87 (m, 9H), 1.06–1.61 (m, 14H), 1.25 (s, 3H), 1.75–1.85 (m, 2H), 2.02 (s, 3H), 2.05 (s, 3H), 2.09 (s, 3H), 2.58 (t, J = 6.7 Hz, 2H), 6.86 (d, J = 2.3 Hz, 1H), 7.07–7.10 (m, 2H), 8.22 (d, J = 8.7 Hz, 1H), 8.59 (br s, 1H); ^{13}C NMR (125 MHz, $CDCl_3$) δ 11.8 (2C), 12.7, 19.6, 20.6, 21.0, 22.6, 22.7, 23.8, 24.7, 28.0, 31.1, 32.7, 37.2, 37.5, 39.3, 39.9, 75.3, 102.7, 115.5, 117.0, 118.3, 123.7, 125.3, 127.1, 127.6, 140.0, 142.8, 143.4, 149.0, 157.8, 162.1, 172.6. Anal. calcd. for $C_{33}H_{44}O_5 \cdot 0.25$EtOAc: C, 75.24; H, 8.54. Found: C, 75.08; H, 8.60.

3-{[(*S*)-2-((*S*)-4,8-Dimethylnonyl)-2,5,7,8-tetramethylchroman-6-yl]oxy}-7-hydroxy-4*H*-chromen-4-one (13b)

According to the procedure described for the preparation of **1b**, compound **18b** (100 mg, 0.196 mmol) was converted into compound **13b** as a white solid (23.4 mg, 23%): mp 239–241 °C; $[\alpha]_D^{25}$ −5.6 (*c* 0.39, $CHCl_3$); IR (neat): 3131 (OH); ^{1}H NMR (500 MHz, $CDCl_3$) δ 0.86 (d, J = 6.3 Hz, 9H), 1.05–1.59 (m, 14H), 1.25 (s, 3H), 1.76–1.84 (m, 2H), 2.02 (s, 3H), 2.06 (s, 3H), 2.09 (s, 3H), 2.58 (t, J = 6.9 Hz, 2H), 6.85 (d, J = 1.7 Hz, 1H), 7.07 (dd, J = 9.2, 2.3 Hz, 1H), 7.09 (s, 1H), 8.22 (d, J = 8.6 Hz, 1H), 8.38 (br s, 1H); ^{13}C NMR (125 MHz, $CDCl_3$) δ 11.8 (2C), 12.6, 19.6, 20.6, 21.0, 22.6, 22.7, 23.7, 24.7, 28.0, 31.2, 32.7, 37.3, 37.5, 39.3, 39.9, 75.3, 102.7, 115.7, 116.7, 118.3, 123.6, 125.3, 127.1, 127.4, 140.2, 142.8, 143.3, 149.0, 157.9, 162.5, 172.7. Anal. calcd. For $C_{33}H_{44}O_5 \cdot 0.1$EtOAc: C, 75.76; H, 8.53. Found: C, 75.65; H, 8.58.

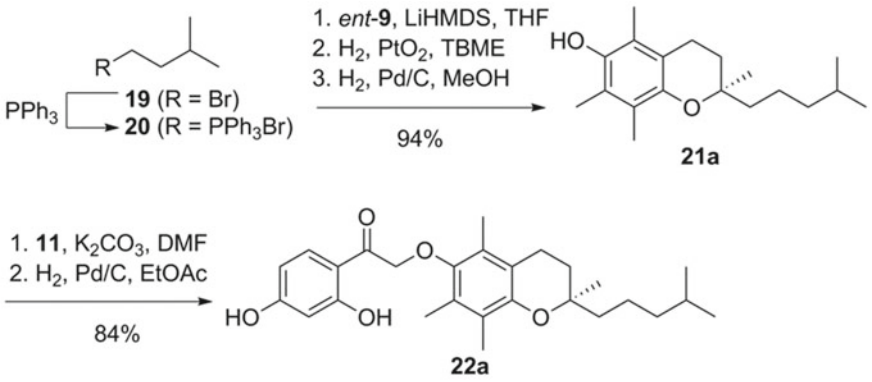

Scheme 2.4 Synthetic scheme for **22a**

(Isopentyl)triphenylphosphonium Bromide (19)
According to the procedure described for the preparation of **8**, 1-bromo-3-methylbutane **19** (1.99 g, 13.2 mmol) was converted into compound **20**, which was used without further purification.

(*R*)-2,5,7,8-Tetramethyl-2-(4-methylpentyl)chroman-6-ol (21a)
According to the procedure described for the preparation of **10b**, compound *ent*-**9** (800 mg, 2.47 mmol) was converted into compound **21a** using the phosphonium salt **20** (ca. 4.93 mmol) as a pale yellow oil (675 mg, 94%) (Scheme 2.4). $[\alpha]_D^{25}$ −0.9 (*c* 1.00, $CHCl_3$); ^{1}H NMR (500 MHz, $CDCl_3$) δ 0.87 (d, J = 6.9 Hz, 6H), 1.14–1.19 (m, 2H), 1.22 (s, 3H), 1.37–1.58 (m, 5H), 1.73–1.84 (m, 2H), 2.11 (s, 6H), 2.16 (s, 3H), 2.60 (t, J = 6.9 Hz, 2H), 4.17 (s, 1H); ^{13}C NMR (125 MHz, $CDCl_3$) δ 11.3, 11.8, 12.2, 20.7, 21.4, 22.6 (2C), 23.8, 27.9, 31.5, 39.4, 39.7, 74.5, 117.3, 118.4, 121.0, 122.6, 144.5, 145.5. HRMS (ESI) calcd for $C_{19}H_{30}O_2$ (M^+): 290.2246; found: 290.2245.

(*S*)-2,5,7,8-Tetramethyl-2-(4-methylpentyl)chroman-6-ol (21b)
According to the procedure described for the preparation of **10b**, compound **9** (800 mg, 2.47 mmol) was converted into compound **21b** using compound **20** (ca. 4.93 mmol) as a pale yellow oil (621 mg, 86%). $[\alpha]_D^{25}$ +0.9 (*c* 1.00, $CHCl_3$); ^{1}H NMR (500 MHz, $CDCl_3$) δ 0.87 (d, J = 6.9 Hz, 6H), 1.14–1.19 (m, 2H), 1.22 (s, 3H), 1.37–1.58 (m, 5H), 1.73–1.84 (m, 2H), 2.11 (s, 6H), 2.16 (s, 3H), 2.60 (t, J = 6.9 Hz, 2H), 4.17 (s, 1H); ^{13}C NMR (125 MHz, $CDCl_3$) δ 11.3, 11.8, 12.2, 20.7, 21.4, 22.6 (2C), 23.8, 27.9, 31.5, 39.4, 39.7, 74.5, 117.3, 118.4, 121.0, 122.6, 144.5, 145.5. HRMS (ESI) calcd for $C_{19}H_{30}O_2$ (M^+): 290.2246; found: 290.2239.

(*R*)-1-(2,4-Dihydroxyphenyl)-2-{[2,5,7,8-tetramethyl-2-(4-methylpentyl)chroman-6-yl]oxy}ethan-1-one (22a)
According to the procedure described for the preparation of **12b**, compound **21a** (600 mg, 2.07 mmol) was converted into compound **22a** as a pale yellow solid (765 mg, 84%): mp 86–87 °C; $[\alpha]_D^{25}$ +3.5 (*c* 0.78, $CHCl_3$); IR (neat): 3351 (OH), 1626 (C=O); ^{1}H NMR (500 MHz, $CDCl_3$) δ 0.87 (d, J = 6.9 Hz, 6H), 1.18 (dd,

J = 14.9, 6.9 Hz, 2H), 1.24 (s, 3H), 1.37–1.61 (m, 5H), 1.73–1.85 (m, 2H), 2.08 (s, 3H), 2.14 (s, 3H), 2.18 (s, 3H), 2.57 (t, *J* = 6.6 Hz, 2H), 4.93 (s, 2H), 6.36 (dd, *J* = 8.9, 2.3 Hz, 1H), 6.42 (d, *J* = 2.3 Hz, 1H), 6.52 (br s, 1H), 7.49 (d, *J* = 9.2 Hz, 1H), 12.37 (s, 1H); ^{13}C NMR (125 MHz, $CDCl_3$) δ 11.8, 11.9, 12.8, 20.6, 21.3, 22.6 (2C), 23.8, 27.8, 31.1, 39.3, 39.9, 73.9, 75.0, 103.8, 108.1, 111.7, 117.8, 123.2, 125.7, 127.6, 130.8, 147.7, 148.3, 163.3, 165.3, 198.0. HRMS (ESI) calcd for $C_{27}H_{37}O_5$ (MH^+): 441.2636; found: 441.2633.

(*S*)-1-(2,4-Dihydroxyphenyl)-2-{[2,5,7,8-tetramethyl-2-(4-methylpentyl)chroman-6-yl]oxy}ethan-1-one (22b)

According to the procedure described for the preparation of **12b**, compound **21b** (600 mg, 2.07 mmol) was converted into compound **22b** as pale yellow solid (505 mg, 55%): mp 86–87 °C; $[\alpha]_D^{25}$ −3.9 (*c* 1.11, $CHCl_3$); IR (neat): 3351 (OH), 1626 (C=O); ^{1}H NMR (500 MHz, $CDCl_3$) δ 0.87 (d, *J* = 6.9 Hz, 6H), 1.17 (dd, *J* = 14.9, 6.9 Hz, 2H), 1.24 (s, 3H), 1.37–1.61 (m, 5H), 1.73–1.85 (m, 2H), 2.09 (s, 3H), 2.14 (s, 3H), 2.18 (s, 3H), 2.57 (t, *J* = 6.6 Hz, 2H), 4.93 (s, 2H), 6.28 (br s, 1H), 6.37 (dd, *J* = 8.9, 2.3 Hz, 1H), 6.42 (d, *J* = 2.3 Hz, 1H), 7.50 (d, *J* = 9.2 Hz, 1H), 12.38 (s, 1H); ^{13}C NMR (125 MHz, $CDCl_3$) δ 11.8, 11.9, 12.8, 20.6, 21.3, 22.6 (2C), 23.8, 27.8, 31.1, 39.3, 39.9, 73.9, 75.0, 103.8, 108.1, 111.7, 117.8, 123.2, 125.7, 127.6, 130.8, 147.7, 148.3, 163.1, 165.3, 198.0. Anal. calcd. for $C_{27}H_{36}O_5$: C, 73.61; H, 8.24. Found: C, 73.39; H, 8.49.

(*R*)-7-Hydroxy-3-{[2,5,7,8-tetramethyl-2-(4-methylpentyl)chroman-6-yl]oxy}-4*H*-chromen-4-one (14a)

According to the procedure described for the preparation of **1b**, compound **22a** (100 mg, 0.227 mmol) was converted into compound **14a** as white solid (23.0 mg, 23%): mp 255–258 °C; $[\alpha]_D^{25}$ +5.3 (*c* 0.40, THF); IR (neat): 3265 (OH); ^{1}H NMR (500 MHz, THF-d_8) δ 2.69 (d, *J* = 2.9 Hz, 3H), 2.70 (d, *J* = 2.9 Hz, 3H), 3.01 (dd, *J* = 14.9, 6.9 Hz, 2H), 3.06 (s, 3H), 3.26–3.43 (m, 5H), 3.56–3.68 (m, 2H), 3.82 (s, 3H), 3.86 (s, 3H), 3.89 (s, 3H), 4.44 (t, *J* = 6.9 Hz, 2H), 8.47 (d, *J* = 2.3 Hz, 1H), 8.64 (dd, *J* = 8.6, 2.3 Hz, 1H), 8.84 (s, 1H), 9.87 (d, *J* = 8.6 Hz, 1H), 11.19 (s, 1H); ^{13}C NMR (125 MHz, THF-d_8) δ 10.9, 11.1, 11.8, 20.4, 21.4, 22.0 (2C), 23.2, 27.9, 31.1, 39.5, 39.9, 74.9, 101.9, 114.1, 117.5, 118.0, 123.2, 125.2, 126.9, 127.3, 139.2, 143.4, 143.8, 148.9, 157.6, 162.4, 170.0. Anal. calcd. for $C_{28}H_{34}O_5 \cdot 0.1$EtOAc: C, 74.25; H, 7.64. Found: C, 74.12; H, 7.61.

(*S*)-7-Hydroxy-3-{[2,5,7,8-tetramethyl-2-(4-methylpentyl)chroman-6-yl]oxy}-4*H*-chromen-4-one (14b)

According to the procedure described for the preparation of **1b**, compound **22b** (100 mg, 0.227 mmol) was converted into compound **14b** as white solid (22.7 mg, 22%): mp 255–258 °C; $[\alpha]_D^{25}$ −5.1 (*c* 0.52, THF); IR (neat): 3147 (OH); ^{1}H NMR (500 MHz, THF-d_8) δ 2.69 (d, *J* = 2.9 Hz, 3H), 2.70 (d, *J* = 2.9 Hz, 3H), 3.01 (dd, *J* = 14.9, 6.9 Hz, 2H), 3.06 (s, 3H), 3.26–3.43 (m, 5H), 3.56–3.68 (m, 2H), 3.82 (s, 3H), 3.86 (s, 3H), 3.89 (s, 3H), 4.44 (t, *J* = 6.9 Hz, 2H), 8.47 (d, *J* = 2.3 Hz, 1H), 8.64 (dd, *J* = 8.6, 2.3 Hz, 1H), 8.84 (s, 1H), 9.87 (d, *J* = 8.6 Hz, 1H), 11.20 (s, 1H); ^{13}C NMR (125 MHz, THF-d_8) δ 10.9, 11.1, 11.8, 20.4, 21.4, 22.0 (2C), 23.2, 27.9,

31.1, 39.5, 39.9, 74.9, 101.9, 114.1, 117.5, 118.0, 123.2, 125.2, 126.9, 127.3, 139.2, 143.3, 143.8, 148.9, 157.6, 162.4, 170.0. Anal. calcd. for $C_{28}H_{34}O_5$: C, 74.64; H, 7.61. Found: C, 74.33; H, 7.74.

Screening by the Chemical Array

Photoaffinity linker-coated (PALC) slides were prepared according to previous reports using amine-coated slides and the photoaffinity proline linker [16]. A solution of compounds (2.5 mg/mL in DMSO) from the in-house chemical library (NPDepo, RIKEN) was immobilized onto the PALC glass slides with a chemical arrayer equipped with 24 stamping pins. The slides were exposed to UV irradiation of 4 J/cm^2 at 365 nm using a CL-1000L UV crosslinker (UVP, CA). The slides were washed successively with DMSO, DMF, acetonitrile, THF, dichloromethane, EtOH, and ultra-pure water (5 min, 3 times each), and dried. D- or L-MDM2^{TMR} (3 μM in 1% skim-milk-TBS-T) was incubated with the glass slide for 1 h, and then washed with TBS-T (10 mM Tris-HCl, pH 8.0, 150 mM NaCl, 0.05% Tween-20) (5 min, 3 times). The slides were dried and scanned at 532 nm on a GenePix scanner. The fluorescence signals were quantified with GenePixPro.

FP Assay

FP assays were carried out in PBS containing 2% DMSO and 0.005% Tween-20 using a fluorescein-labeled p53 (P4) peptide (0.5–1.0 nM) and MDM2$^{25-109}$ (10 nM) in black 96-well non-binding surface assay plates (Corning) [16]. The potential inhibitors and FAM-labeled P4 peptide in DMSO were diluted five-fold with PBS in advance. The protein (90 μL) was preincubated with the compound solution (5 μL) for 30 min. Then, the fluorescein-labeled P4 peptide (5 μL) was added and incubated for 30 min. The P4 peptide was used as the positive control. FP signals were analyzed using an EnVision Xcite plate reader (Perkin Elmer) with a 480-nm excitation filter and a 535-nm emission filter.

SPR Analysis

SPR Analyses of p53 binding to synthetic MDM2$^{25-109}$ and MDM2^{TMR} were carried out using Biacore T200 SPR instrument. PBS (Nacalai Tesque, pH 7.4) containing 0.05% Tween-20 was used as the running buffer at 25 °C. Biotinylated wild-type p53 peptides (biotinyl-aminocaproyl-GSGSSQETFSDLWKLLPEN-NH_2) were immobilized on a streptavidin (SA) sensor chip (L-p53: 45.1 RU, D-p53: 46.4 RU). All analytes were evaluated for 2 min as contact time, followed by 2 min dissociation at a flow rate of 30 μL/min.

For competitive inhibition assays, L-MDM2$^{25-109}$ (30 nM) in the presence of varying concentration of inhibitors in PBS containing 0.05% Tween-20 and 1% DMSO were injected on SA sensor chip, where biotinylated wild-type L-p53 peptide was immobilized (127.3 RU).

Competitive Binding Inhibition Assay by a Standard ELISA

ELISA assays were carried out in HEPES buffer [20 mM HEPES (pH 7.4), 100 mM NaCl, 0.05% Tween-20, 0.1% BSA]. Precoated streptavidin 96-well plates (Nunc) were incubated with 300 μL/well of HEPES buffer containing 3% BSA for 1 h. After three washes, biotinylated wild-type p53 peptide (100 nM) in HEPES buffer

(100 μL/well) was added and incubated for 2 h. After three washes, 100 nM MDM2 (recombinant human MDM2, untagged, Sigma) in the presence of varying concentration of inhibitors in HEPES buffer containing 1% DMSO (100 μL/well) was added and incubated for 1 h. After three washes, 1:1000 dilution of anti-MDM2 rabbit IgG antibody (N-20, Santa Cruz] in HEPES buffer (100 μL/well) was added and incubated for 1 h. After three washes, 1:5000 dilution of HRP-conjugated anti-rabbit IgG antibody (Promega) in HEPES buffer (100 μL/well) was added and incubated for 1 h. After three washes, TMB (3,3′,5,5′-Tetramethylbenzidine) solution (WAKO, 100 μL/well) was added and incubated for 1 h. Then, aqueous 2N H_2SO_4 (10 μL/well) was added. Absorbance at 450 nm was measured for each well using an EnVision Xcite plate reader. The IC_{50} values were calculated by using GraphPad Prizm (GraphPad software, San Diego, CA).

Cell Growth Inhibition Assay

SJSA-1 and H1299 cells were cultured in RPMI-1640 medium (high glucose) (WAKO) supplemented with 10% (v/v) FBS at 37 °C in a 5% CO_2-incubator. Cell-based assays using SJSA-1 and H1299 cells were performed in 96-well plates (BD Falcon). Both cells were seeded at 500 cells/well in 50 μL of DMEM, and placed for 6 h. Chemical compounds in DMSO were diluted 250-fold with the culture medium in advance. Following the addition of the fresh culture medium (40 μL), the chemical diluents (30 μL) were also added to the cell cultures. The final volume of DMSO in the medium was equal to 0.1% (v/v). The cells under chemical treatment were incubated for a further 72 h. The wells in the plates were washed with the cultured medium without phenol-red twice. After 1 h of incubation with 100 μL of the medium, the cell culture in each well was supplemented with the MTS reagent (20 μL, Promega), followed by incubation for an additional 40 min. Absorbance at 490 nm was measured for each well using an EnVision Xcite plate reader. The GI_{50} values were calculated by using GraphPad Prizm (GraphPad software, San Diego, CA).

References

1. (a) Toledo F, Wahl GM (2006) Regulating the p53 pathway: in vitro hypotheses, in vivo veritas. Nat Rev Cancer 6:909–923; (b) Wade M, Wang YV, Wahl GM (2010) The p53 orchestra: Mdm2 and Mdmx set the tone. Trends Cell Biol 20:299–309
2. (a) Cahilly-Snyder L, Yang-Feng T, Francke U, George DLS (1987) Molecular analysis and chromosomal mapping of amplified genes isolated from a transformed mouse 3T3 cell line. Cell Mol Genet 13:235–244; (b) Momand J, Zambetti GP, Olson DC, George D, Levine AJ (1992) The mdm-2 oncogene product forms a complex with the p53 protein and inhibits p53-mediated transactivation. Cell 69:1237–1245; (c) Oliner JD, Pietenpol JA, Thiagalingam S, Gyuris J, Kinzler KW, Vogelstein B (1993) Oncoprotein MDM2 conceals the activation domain of tumour suppressor p53. Nature 362:857–860l; (d) Shvarts A, Steegenga WT, Riteco N, van Laar T, Dekker P, Bazuine M, van Ham RC, van der Houven van OW, Hateboer G, van der Eb AJ, Jochemsen AG (1996) MDMX: a novel p53-binding protein with some functional properties of MDM2. EMBO J, 15:5349–5357
3. Honda R, Tanaka H, Yasuda H (1997) Oncoprotein MDM2 is a ubiquitin ligase E3 for tumor suppressor p53. FEBS Lett 22:25–27; (b) Haupt Y, Maya R, Kazaz A, Oren M (1997) Mdm2

promotes the rapid degradation of p53. Nature 387:296–299; (c) Micheal D, Oren M (2003) The p53-Mdm2 module and the ubiquitin system. Semin Cancer Biol 13:49–58; (d) Stommel JM, Wahl GM (2005) A new twist in the feedback loop: stress-activated MDM2 destabilization is required for p53 activation. Cell Cycle 4:411–417
4. Sharp DA, Kratowicz SA, Sank MJ, George DL (1999) Stabilization of the MDM2 oncoprotein by interaction with the structurally related MDMX protein. J Biol Chem 274:38189–38196; (b) Marine JCW, Dyer MA, Jochemsen AG (2007) MDMX: from bench to bedside. J Cell Sci 120:371–378; (c) Wang X (2011) p53 regulation: teamwork between RING domains of Mdm2 and MdmX. Cell Cycle 10:4225–4229; (d) Wang X, Wang J, Jiang X (2011) MdmX protein is essential for Mdm2 protein-mediated p53 polyubiquitination. J Biol Chem 286:23725–23734
5. Wade M, Li YC, Wahl GM (2013) MDM2, MDMX and p53 in oncogenesis and cancer therapy. Nat Rev Cancer 13:83–96
6. Vassilev LT, Vu BT, Graves B, Carvajal D, Podlaski F, Filipovic Z, Kong N, Kammlott U, Lukacs C, Klein C, Fotouhi N, Liu EA (2004) In vivo activation of the p53 pathway by small-molecule antagonists of MDM2. Science 303:844–848
7. Reed D, Shen Y, Shelat AA, Arnold LA, Ferreira AM, Zhu F, Mills N, Smithson DC, Regni CA, Bashford D, Cicero SA, Schulman BA, Jochemsen AG, Guy RK, Dyer MA (2010) Identification and characterization of the first small molecule inhibitor of MDMX. J Biol Chem 285:10786–10796
8. Pazgier M, Liu M, Zou G, Yuan W, Li C, Li C, Li J, Monbo J, Zella D, Tarasov SG, Lu W (2009) Structural basis for high-affinity peptide inhibition of p53 interactions with MDM2 and MDMX. Proc Natl Acad Sci U S A 106:4665–4670
9. Liu M, Pazgier M, Li C, Yuan W, Li C, Lu W (2010) A left-handed solution to peptide inhibition of the p53-MDM2 interaction. Angew Chem Int Ed 49:3649–3652
10. Tsuganezawa K, Nakagawa Y, Kato M, Taruya S, Takahashi F, Endoh M, Utata R, Mori M, Ogawa N, Honma T, Yokoyama S, Hashizume Y, Aoki M, Kasai T, Kigawa T, Kojima H, Okabe T, Nagano T, Tanaka A (2013) A fluorescent-based high-throughput screening assay for small molecules that inhibit the interaction of MdmX with p53. J Biomol Screen 18:191–198
11. Czarna A, Popowicz GM, Pecak A, Wolf S, Dubin G, Holak TA (2009) High affinity interaction of the p53 peptide-analogue with human Mdm2 and Mdmx. Cell Cycle 8:1176–1184
12. Joseph TL, Madhumalar A, Brown CJ, Lane DP, Verma CS (2010) Differential binding of p53 and nutlin to MDM2 and MDMX: computational studies. Cell Cycle 9:1167–1181
13. Hu B, Gilkes DM, Faroogi B, Sebti SM, Chen J (2006) MDMX overexpression prevents p53 activation by the MDM2 inhibitor Nutlin. J Biol Chem 281:33030–33035
14. Danovi D, Meulmeester E, Pasini D, Migliorini D, Capra M, Frenk R, Graaf P, Francoz S, Gasparini P, Gobbi A, Helin K, Pelicci PG, Jochemsen AG, Marine JC (2004) Amplification of Mdmx (or Mdm4) directly contributes to tumor formation by inhibiting p53 tumor suppressor activity. Mol Cell Biol 24:5835–5843
15. Kondoh Y, Honda K, Osada H (2015) Construction and application of a photo-cross-linked chemical array. Methods Mol Biol 1263:29–41
16. Noguchi T, Oishi S, Honda K, Kondoh Y, Saito T, Kubo T, Kaneda M, Ohno H, Osada H, Fujii N (2013) Affinity-based screening of MDM2/MDMX-p53 interaction inhibitors by chemical array: identification of novel peptidic inhibitors. Bioorg Med Chem Lett 23:3802–3805
17. Oliner JD, Kinzler KW, Meltzer PS, George DL, Vogelstein B (1992) Amplification of a gene encoding a p53-associated protein in human sarcomas. Nature 358:80–83
18. Lin DL, Chang C (1996) p53 is a mediator for radiation-repressed human TR2 orphan receptor expression in MCF-7 cells, a new pathway from tumor suppressor to member of the steroid receptor superfamily. J Biol Chem 271:14649–14652
19. (a) Wang P, Dong S, Shieh JH, Peguero E, Hendrickson R, Moore MA, Danishefsky SJ (2013) Erythropoietin derived by chemical synthesis. Science 342:1357–1760; (b) Seenaiah M, Jbara M, Mali SM, Brik A (2015) Convergent versus sequential protein synthesis: the case of ubiquitinated and glycosylated H2B. Angew Chem Int Ed 54:12374–12378
20. Kent SBH, Milton SCF, Milton RCD (1993) D-enzyme compositions and methods of their use. Patent WO 9325667

21. Sankaranarayanan S, Sharma A, Chattopadhyay S (2002) Synthesis of the 1,5-dimethylic chiron enantiomers, 3,7,11-trimethyldodec-10-en-1-ol: application to enantiomeric syntheses of tribolure and a marine fatty acid. Tetrahedron Asymmetry 13:1373–1378
22. Cohen N, Scott CG, Neukom C, Lopresti RJ, Weber G, Saucy G (1981) Total Synthesis of All Eight Stereoisomers of α-Tocopheryl Acetate. Determination of their diastereoisomeric and enantiomeric purity by gas chromatography. Helv Chim Acta 64:1158–1173
23. Muller T, Coowar D, Hanbali M, Heushling P, Luu B (2006) Improved synthesis of tocopherol fatty alcohols and analogs: microglial activation modulators. Tetrahedron 62:12025–12040

Chapter 3
Synthesis of Grb2 SH2 Domain Proteins for Mirror-Image Screening Systems

Abstract Growth factor receptor-bound protein 2 (Grb2) is an adaptor protein that mediates cellular signal transduction. Grb2 contains an SH2 domain that interacts with phosphotyrosine-containing sequences in epidermal growth factor receptor (EGFR) and other signaling molecules, and it is a promising molecular target for anticancer agents. To identify novel inhibitors of the Grb2 SH2 domain from natural products and their mirror-image isomers, screening systems using both enantiomers of a synthetic Grb2 SH2 domain protein were established. A pair of synthetic procedures for the proteins were investigated: one employed a single native chemical ligation (NCL) of two segment peptides, and the other used the N-to-C-directed NCL of three segment peptides for easier preparation. Labeling at the N-terminus or the Ala^{115} residue of the Grb2 SH2 domain provided functional probes to detect binding to a phosphotyrosine-containing peptide. The resulting synthetic-protein-based probes were applied to bioassays including chemical array analysis and enzyme-linked immunosorbent assays (ELISAs).

Keywords Grb2 SH2 domain protein · Chemical protein synthesis · Mirror-image protein technology

Grb2 functions as an adaptor protein in signal transduction pathways that are triggered by activation of receptor tyrosine kinases (RTKs). The Grb2 SH2 domain recognizes the phosphotyrosine (pTyr)-containing sequence in epidermal growth factor receptor (EGFR) [1] and Shc adaptor proteins [2], leading to activation of the Ras-mitogen-activated protein kinase (MAPK) pathway [3] and the Gab1-mediated PI3K-Akt pathway [4]. The Grb2 SH2 domain also interacts with fibroblast growth factor receptor (FGFR) substrate 2 (FRS2) to regulate the FGFR signaling pathway [5]. Moreover, the Grb2 SH2 domain interacts with the non-RTK chimeric Bcr-Abl protein, which constitutively activates Abl tyrosine kinase activity to induce chronic myeloid leukemia [6]. Because of these pivotal roles in cell growth and differentiation signaling pathways, the Grb2 SH2 domain is a promising molecular target for anticancer agents [7].

To date, a variety of inhibitors against the Grb2 SH2 domain have been reported via structure-activity relationship studies (Fig. 3.1) [8]. Peptides with a pYXNX

© Springer Nature Singapore Pte Ltd. 2018

T. Noguchi, *Development of Chemistry-Based Screening Platform for Access to Mirror-Image Library of Natural Products*, Springer Theses,
https://doi.org/10.1007/978-981-10-6623-8_3

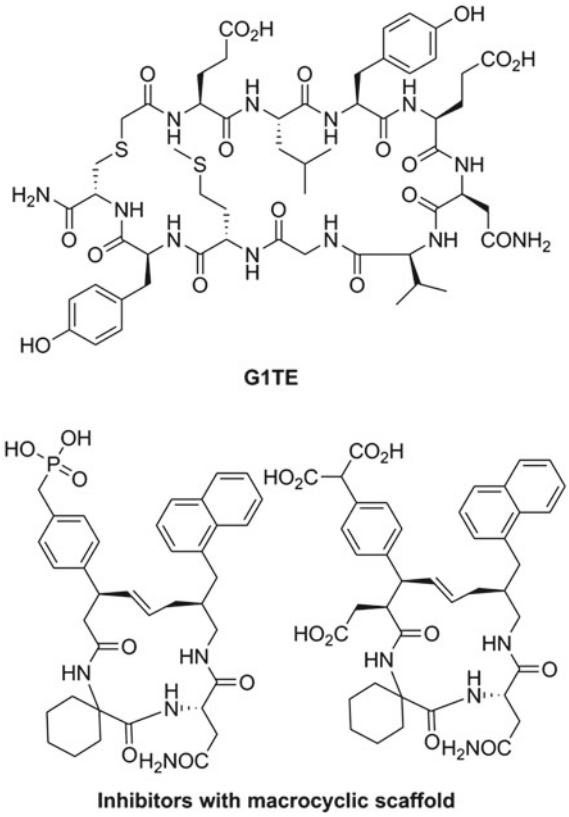

Fig. 3.1 Structures of Grb2 SH2 domain inhibitors

motif, which were identified by affinity-based purification on agarose beads from a mixture of phosphorylated peptides, exhibited selective binding for the Grb2 SH2 domain [9]. To discover more potent and selective peptides, rapid screening of an extensive library of pTyr peptides was performed [10]. Phage display libraries were also employed to identify potent phosphorylated peptides [11] or cyclic peptides G1TE [12]. After revealing the bioactive β-turn conformation of potent peptide ligands in the binding pockets of Grb2 SH2 domain [13], a number of inhibitors with a macrocyclic scaffold were designed [14]. These include nonphosphorus-containing analogues with resistance against phosphatase-mediated degradation and favorable cell permeability [15].

Despite a number of phosphopeptide-based inhibitors, there have been a limited number of reports on natural product-based Grb2 SH2 domain inhibitors (Fig. 3.2). Asterriquinones were identified by screening extracts from *Aspergillus candidus* as Grb2 SH2 domain inhibitors that disrupt the Grb2-EGFR interaction [16]. Sclerotiorinamine derivatives [17] and actinomycin derivatives [18] were reported to be Grb2 SH2 domain inhibitors that interfere with the Grb2-Shc interaction.

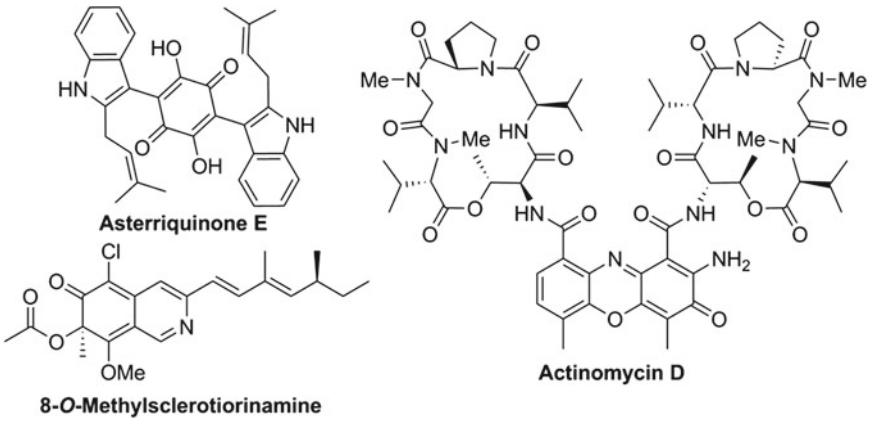

Fig. 3.2 Structures of Grb2 SH2 domain inhibitors from natural products

To validate the mirror-image screening strategy [19], the author chose the Grb2 SH2 domain and planned to apply both Grb2 SH2 domain enantiomers (L-Grb2 and D-Grb2) for the screening to identify the novel natural product-based inhibitors from both enantiomers of chiral natural products.

For synthesis of the Grb2 SH2 domain ($Grb2^{53–154}$), the author focused on two Gly-Ala sites (Gly^{81}-Ala^{82} and Gly^{114}-Ala^{115}) as the ligation sites (Fig. 3.3). Peptides with a C-terminal Gly thioester are readily ligated with N-terminal Cys peptides [20] and chemical conversion of Cys to Ala is achievable by metal-free-desulfurization (MFD) [21]. Therefore, the author planned to employ a single or N-to-C-directed NCL strategy for synthesis of Grb2 SH2 domains. In a single NCL strategy, the N-terminal segment of $Grb2^{53–81}$ and the C-terminal segment of $Grb2^{82–154}$ were ligated to produce [Cys^{82}]-$Grb2^{53–154}$ (Fig. 3.3a). This simple synthetic strategy required the solid-phase synthesis of the long C-terminal segment. In the alternative N-to-C-directed NCL strategy, three segments were successively ligated from the N-terminal $Grb2^{53–81}$ segment to the C-terminal $Grb2^{115–154}$ segment to provide [Cys^{82}/Cys^{115}]-$Grb2^{53–154}$ (Fig. 3.3b). Although this strategy required an additional NCL process, three segments with ≤ 40 residues could be synthesized by solid-phase synthesis more easily.

Initially, the author synthesized a native sequence of the Grb2 SH2 domain (L-$Grb2^{53–154}$) via NCL using two segments ($Grb2^{53–81}$ and $Grb2^{82–154}$) (Fig. 3.4). An N-terminal segment for L-$Grb2^{53–81}$ (**L-1a**) was synthesized by standard Fmoc-based solid-phase peptide synthesis (SPPS) using HBTU/HOBt/(i-Pr)$_2$NEt activation on CLEAR amide resin with a first-generation Dawson linker [22]. After chain assembly, the Dawson linker was converted to the benzimiadazol-2-one form by treatment with 4-nitrophenyl chloroformate and (i-Pr)$_2$NEt. Final deprotection and cleavage from resin was achieved by treatment with 4-mercaptophenyl acetic acid (MPAA) and provided the expected thioester **L-1a**. The C-terminal segment L-$Grb2^{82–154}$ (**L-2a**) was synthesized by standard Fmoc-based SPPS using HBTU/HOBt/(i-Pr)$_2$NEt activation

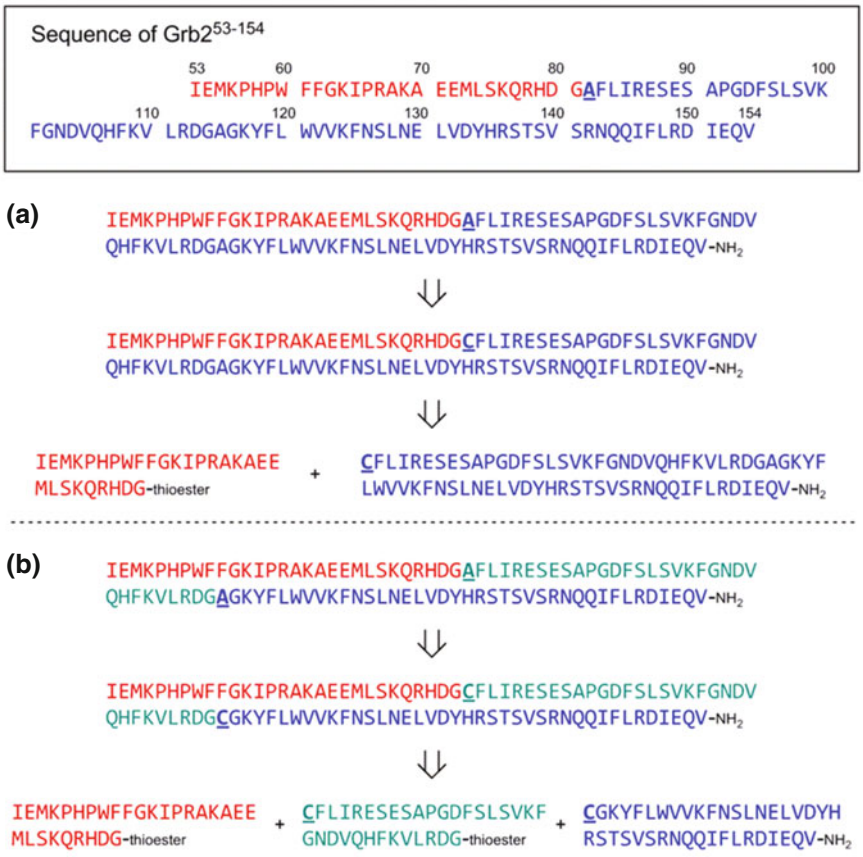

Fig. 3.3 Sequence of the Grb2 SH2 domain. Ligation sites (Gly^{81}-Ala^{82}, Gly^{114}-Ala^{115}) are underlined and in bold type. **a** Retrosynthetic analysis of $Grb2^{53–154}$ via a single NCL strategy. **b** Retrosynthetic analysis of $Grb2^{53–154}$ via the N-to-C-directed NCL strategy

on H-Rink Amide ChemMatrix amide resin. Ligation of **L-1a** and **L-2a** proceeded smoothly at room temperature to give [Cys^{82}]-L-$Grb2^{53–154}$ (**L-3a**). The radical-mediated metal-free-desulfurization of **L-3a** with VA-044 produced native sequence L-$Grb2^{53–154}$ (**L-4a**) at high purity (Fig. 3.5). MESNa was used as a thiol additive instead of glutathione [23] because the author found the reaction completed faster.

For synthetic $Grb2^{53–154}$ to be applied to chemical array screening, a tetramethylrhoramine (TMR)-labeled Grb2 SH2 domain protein was designed and synthesized (Fig. 3.6). On the basis of the previous reports in which an N-terminal GST-fused Grb2 SH2 domain was expressed [24], the author designed a TMR-labeled [Cys^{82}]-$Grb2^{53–154}$ (L-$Grb2^{TMR}$) with modification at the N-terminus of the Grb2 SH2 domain. After solid-phase synthesis of the N-terminal $Grb2^{53–81}$ segment, the TMR moiety was introduced by on-resin modification at the N-terminus via

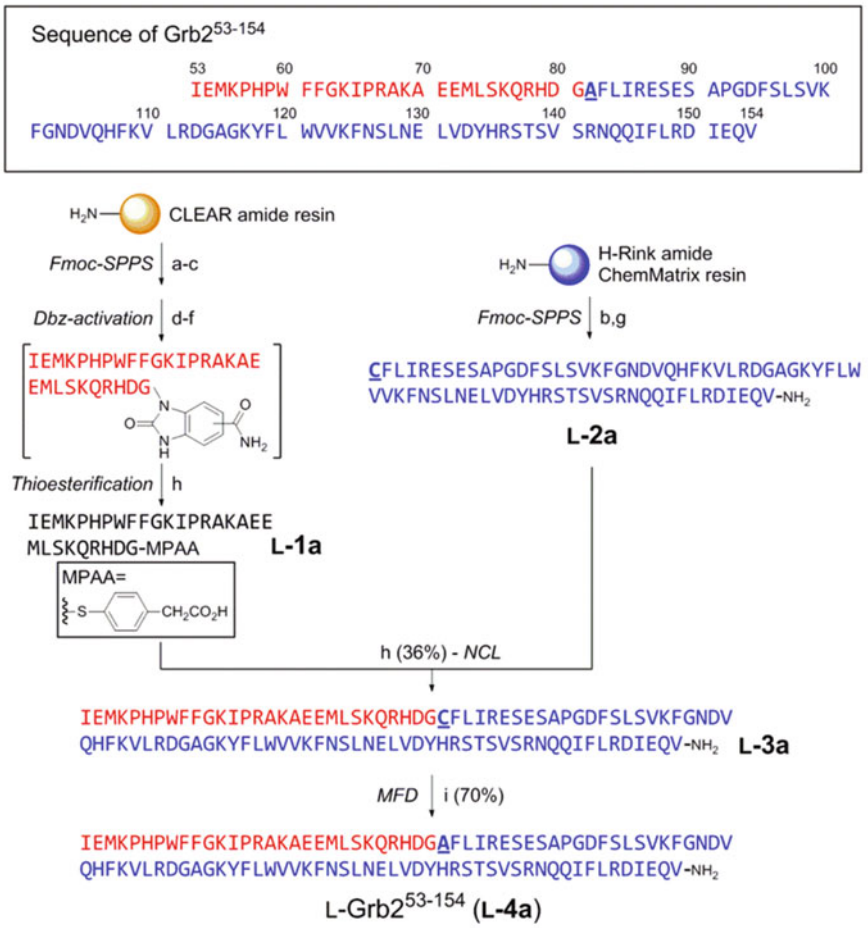

Fig. 3.4 Synthesis of Grb2$^{53–154}$. Sequence of Grb2$^{53–154}$ and the synthetic scheme. Ligation sites (Cys^{82} and Ala^{82}) are underlined and in bold type. *Reagents and conditions*: **a** Fmoc-Dbz-OH, HBTU, HOBt, (*i*-Pr)$_2$NEt, DMF, then 20% piperidine/DMF; **b** Fmoc-Xaa-OH, HBTU, HOBt, (*i*-Pr)$_2$NEt, DMF, then 20% piperidine/DMF; **c** Boc-Ile-OH, HBTU, HOBt, (*i*-Pr)$_2$NEt, DMF; **d** 0.3 M 4-nitrophenyl chloroformate in DCM; **e** 0.5 M (*i*-Pr)$_2$NEt in DMF; **f** TFA/H_2O/*m*-cresol/thioanisole (80:10:5:5); **g** TFA/H_2O/*m*-cresol/thioanisole/EDT (80:5:5:5:5); **h** 6 M Gu · HCl, 200 mM MPAA, 20 mM TCEP · HCl in PBS (pH 7.0); **i** 6 M Gu · HCl, 100 mM Na_2HPO_4, 200 mM TCEP · HCl, 20 mM VA-044 · 2HCl, 40 mM MESNa (pH 6.5). Abbreviations: Dbz = 3,4-diaminobenzoic acid, Gu · HCl = guanidine hydrochloride, MES = 2-mercaptoethanesulfonic acid, TCEP = tris(2-carboxyethyl)-phosphine

a diglycine linker. Subsequent thioester formation using the identical protocol provided the TMR-labeled N-terminal segment **L-1b**. The ligation of **L-1b** and **L-2a** proceeded efficiently to afford the expected L-Grb2^{TMR} (**L-3b**) at high purity (Fig. 3.7). Because the TMR moiety could be unstable under radical-mediated

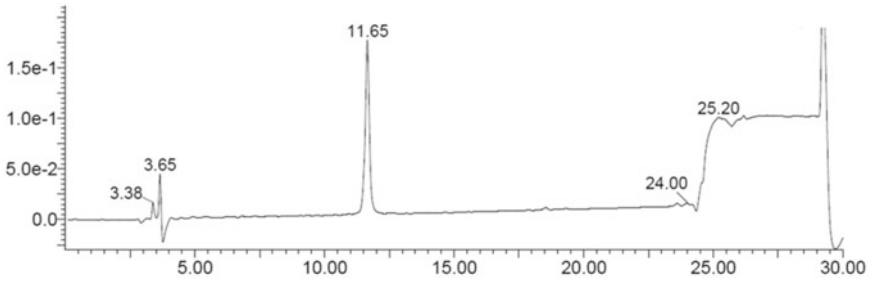

Fig. 3.5 Analytical HPLC chromatogram of purified **L-4a**. HPLC analysis was performed at 25 °C with a linear gradient of 30–50% CH_3CN containing 0.1% TFA at a flow rate of 1 mL/min over 20 min

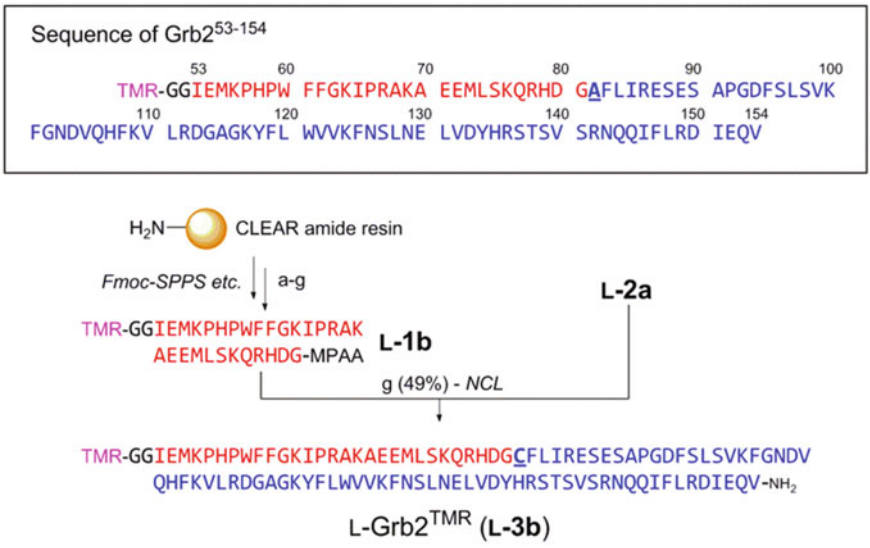

Fig. 3.6 Synthesis of TMR-labeled [Cys^{82}]-$Grb2^{53–154}$ (L-$Grb2^{TMR}$). (A) Sequence of L-$Grb2^{TMR}$ and the synthetic scheme. Ligation sites (Cys^{82}) are underlined and in bold type. *Reagents and conditions*: **a** Fmoc-Dbz-OH, HBTU, HOBt, $(i\text{-Pr})_2$NEt, DMF, then 20% piperidine/DMF; **b** Fmoc-Xaa-OH, HBTU, HOBt, $(i\text{-Pr})_2$NEt, DMF, then 20% piperidine/DMF; **c** TMR, HOBt, DIPCI, DMF; **d** 0.3 M 4-nitrophenyl chloroformate in DCM; **e** 0.5 M $(i\text{-Pr})_2$NEt in DMF; **f** TFA/H_2O/*m*-cresol/thioanisole (80:10:5:5); **g** 6 M Gu · HCl, 200 mM MPAA, 20 mM TCEP · HCl in PBS (pH 7.0)

MFD conditions, L-$Grb2^{TMR}$ (**L-3b**) was used for the biological studies without further conversion to the native sequence. The mirror-image protein (**D-3b**) was also synthesized using identical procedures.

This two segment-based approach for $Grb2^{53–154}$ needed to be improved for the large scale preparation of proteins that are required to screen a number of compounds, because the yields of the two segments were quite low (up to 2% yield from the

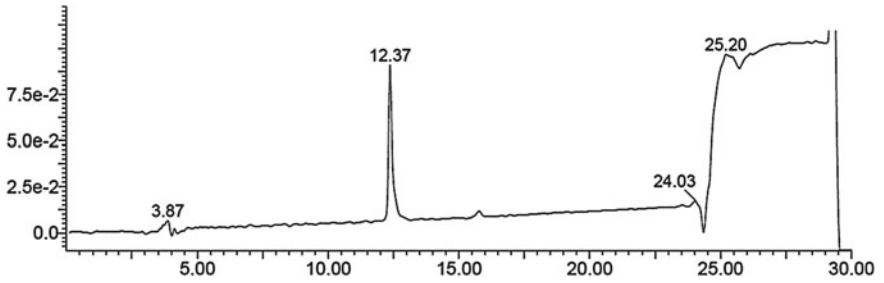

Fig. 3.7 Analytical HPLC chromatogram of purified L-Grb2^{TMR} (**L-3b**). HPLC analysis was performed at 25 °C with a linear gradient of 30–50% CH_3CN containing 0.1% TFA at a flow rate of 1 mL/min over 20 min

starting resin). The low yields of N- and C-terminal segments were because of undesirable cleavage in the activation process of the Dawson linker and low efficiencies at the late stage of couplings, respectively. To overcome these problems, the author investigated an alternative synthetic strategy for Grb2$^{53–154}$ via N-to-C-directed NCL using three segments (Grb2$^{53–81}$, Grb2$^{82–114}$ and Grb2$^{115–154}$) (Fig. 3.8) [25]. To synthesize peptide hydrazides for the N-terminal and middle segments (Grb2$^{53–81}$ and Grb2$^{82–114}$), a hydrazine linker was attached to Wang-PEG resin by treatment of 4-nitrophenyl chloroformate and hydrazine. The peptide sequences were constructed by standard Fmoc-based SPPS using HBTU/HOBt/(*i*-Pr)$_2$NEt activation. Cleavage from resin and final deprotection using a TFA cocktail followed by HPLC purification afforded the peptide hydrazides **L-1c** and **L-5c** at yields of more than 10%. The C-terminal segment **L-6c** was also obtained at a satisfactory yield by the standard protocol. Next, sequential N-to-C-directed NCL was investigated. The first NCL was conducted by $NaNO_2$-mediated activation of **L-1c** followed by the addition of **L-5c** in the presence of MPAA to provide the first NCL product **L-7c**. The second NCL was conducted by the same protocol using the hydrazide **L-7c** and the C-terminal segment **L-6c** to provide the full sequence **L-3c** with Cys^{82}/Cys^{115} substitutions. To obtain the native sequence, global desulfurization was performed to provide L-Grb2$^{53–154}$ (**L-4a**) (Fig. 3.9). Although solid-phase synthesis of three segments and two ligation processes were needed in this strategy, the overall yield of the target protein (0.91%) was improved compared with the previous synthesis using two segments (0.25%). The mirror-image protein, D-Grb2$^{53–154}$ (**D-4a**), was also synthesized in the same manner.

Prior to assaying the biological activities of the synthetic Grb2 SH2 domain proteins, structural and functional analyses were performed. According to a procedure for refolding the Grb2 SH2 domain from *Escherichia. Coli* inclusion bodies [26], the author investigated the folding conditions of chemically synthesized Grb2$^{53–154}$. After the lyophilized synthetic proteins L-Grb2$^{53–154}$ (**L-4a**) and D-Grb2$^{53–154}$ (**D-4a**) were denatured in 6 M guanidine solution, the solutions were dialyzed in HEPES buffer (pH 7.4) to afford folded proteins. A similar L-Grb2$^{53–154}$ spectrum was observed compared with reported spectra of other SH2 domains [27], indicating that the synthetic Grb2 SH2 domain was correctly folded. Symmetrical circular dichroism

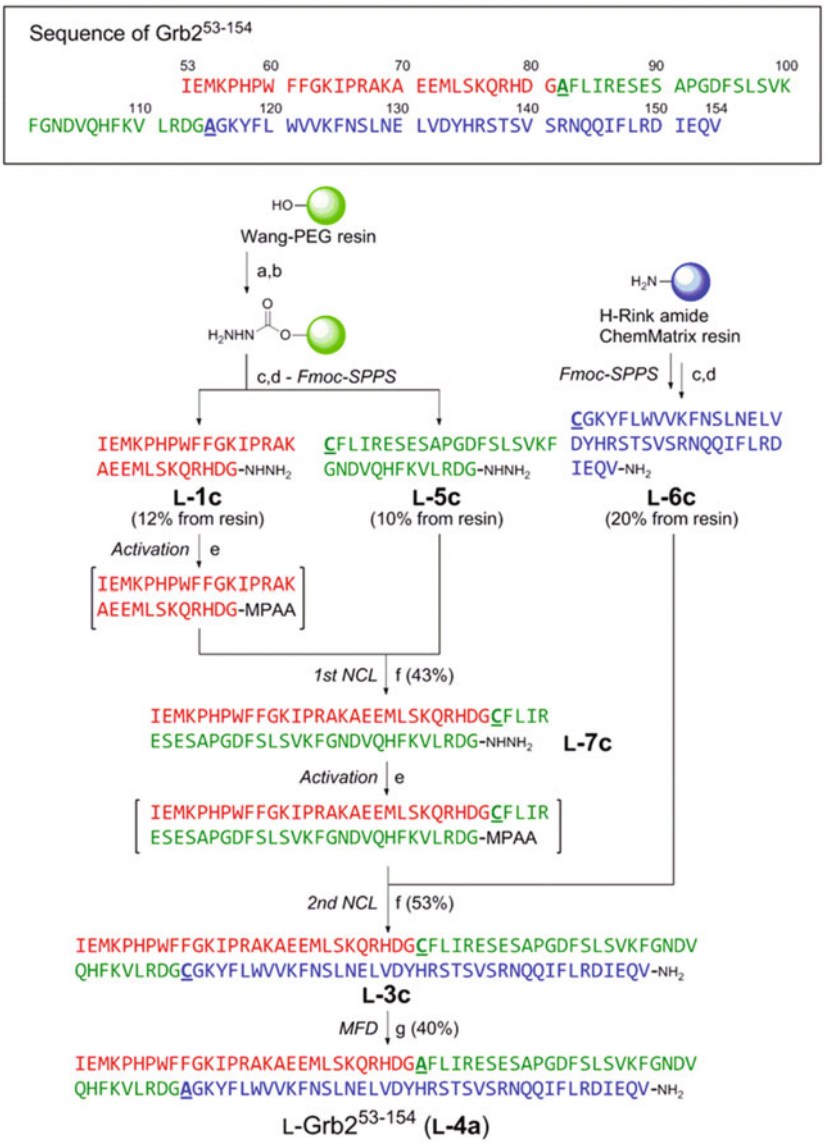

Fig. 3.8 Synthesis of L-Grb2$^{53–154}$ by three-segment hydrazide-based NCL. (A) Sequence of Grb2$^{53–154}$ and the synthetic scheme by N-to-C-directed NCL using three segments. Ligation sites are underlined and in bold type. *Reagents and conditions*: **a** 4-nitrophenyl chloroformate, pyridine in DCM; **b** $NH_2NH_2 \cdot H_2O$ in THF; **c** Fmoc-Xaa-OH, HBTU, HOBt, $(i\text{-Pr})_2$NEt, DMF, then 20% piperidine/DMF; **d** TFA/H_2O/*m*-cresol/thioanisole/EDT (80:5:5:5:5); **e** $NaNO_2$, 6 M Gu · HCl, 100 mM Na_2HPO_4 (pH 3.0); **f** 6 M Gu · HCl, 150 mM Na_2HPO_4, 100 mM MPAA (pH 6.8–7.0); **g** 6 M Gu · HCl, 100 mM Na_2HPO_4, 200 mM TCEP · HCl, 20 mM VA-044 · 2HCl, 40 mM MESNa (pH 6.5)

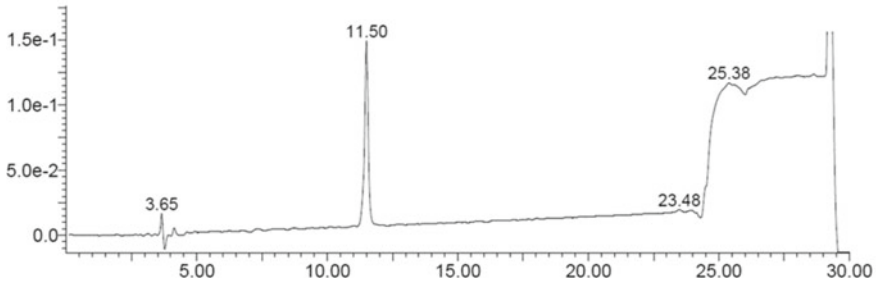

Fig. 3.9 Analytical HPLC chromatogram of purified **L-4a**. HPLC analysis was performed at 25 °C with a linear gradient of 30–50% CH_3CN containing 0.1% TFA at a flow rate of 1 mL/min over 20 min

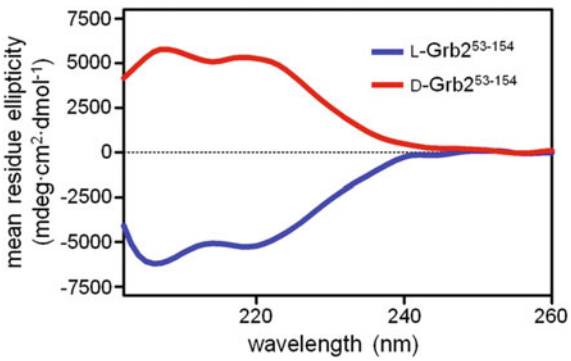

Fig. 3.10 CD spectra of folded L-Grb2$^{53–154}$ and D-Grb2$^{53–154}$

(CD) spectra of L-Grb2$^{53–154}$ and D-Grb2$^{53–154}$ supported the mirror-image structures of both Grb2 SH2 domain enantiomers (Fig. 3.10).

To validate the biological activities of the folded Grb2 SH2 domain proteins, their binding affinities toward both enantiomers of a pTyr-containing EGFR-derived peptide, biotin-EGFR$^{1060–1076}$ (biotin-DTELPVPEpYINQSVPKR-NH_2), were evaluated by surface plasmon resonance (SPR) analysis. The selective binding of L-Grb2$^{53–154}$ toward L-EGFR$^{1060–1076}$ was observed with a KD value of 329 nM, while no binding was observed toward D-EGFR$^{1060–1076}$ (Fig. 3.11). The selective binding of D-Grb2$^{53–154}$ toward D-EGFR$^{1060–1076}$ was observed with a KD value of 447 nM, while no binding was observed toward L-EGFR$^{1060–1076}$, as well. The author also evaluated the binding activity of [Cys^{82}]-L-Grb2$^{53–154}$, which was obtained by folding **L-3a**. The binding affinity toward L-EGFR$^{1060–1076}$ was identical (KD: 327 nM), suggesting that the Ala82Cys mutation in the Grb2 SH2 domain had little effect on the binding toward the target pTyr-containing sequence, presumably because Ala^{82} is buried in the interior of the Grb2 SH2 domain [28].

The author next evaluated the binding activities of TMR-labeled Grb2 SH2 domains (L-Grb2^{TMR} and D-Grb2^{TMR}) toward pTyr-containing sequences by SPR analysis (Fig. 3.12). L-Grb2^{TMR} and D-Grb2^{TMR} bound to L-EGFR$^{1060–1076}$

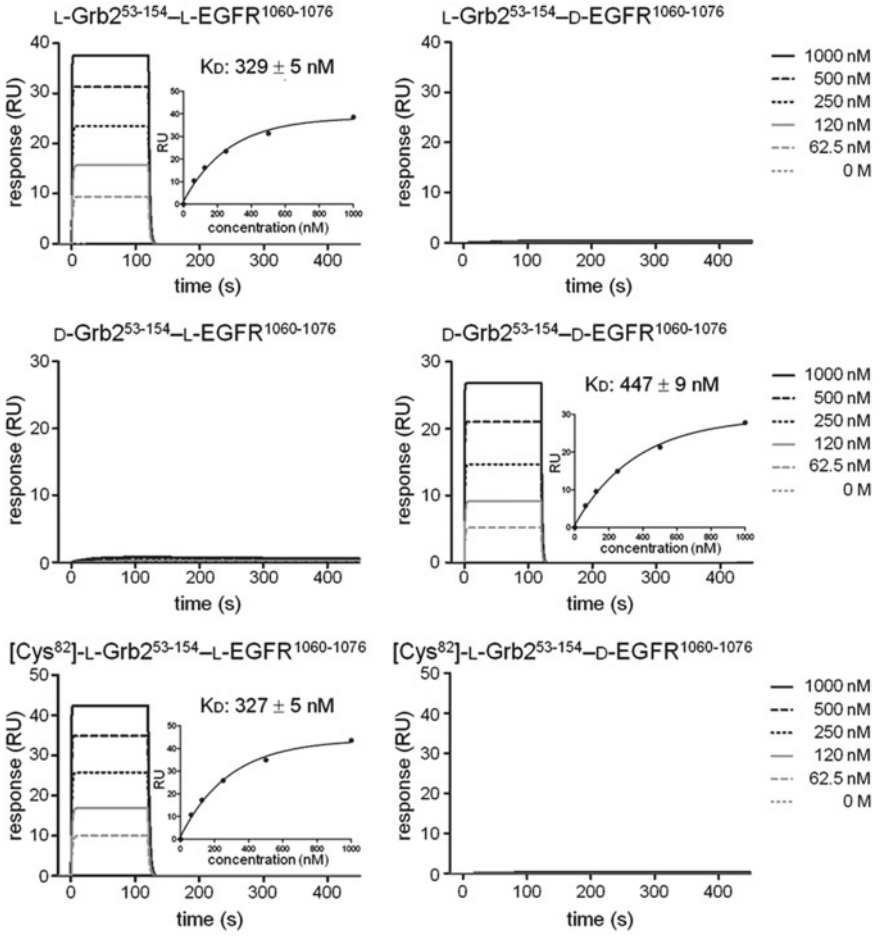

Fig. 3.11 Representative data of SPR analysis of folded L-Grb2$^{53–154}$ and [Cys^{82}]-L-Grb2$^{53–154}$ for binding to N-terminally biotinylated L-EGFR$^{1060–1076}$ and D-EGFR$^{1060–1076}$ peptides. The steady-state bindings were evaluated from triplicate analyses

and D-EGFR$^{1060–1076}$ with KD values of 180 and 242 nM, respectively. In contrast, no interaction was observed for L-Grb2^{TMR}-D-EGFR$^{1060–1076}$ and D-Grb2^{TMR}-L-EGFR$^{1060–1076}$. These data suggested that TMR labeling at the N-terminus of the Grb2 SH2 domain did not interfere with binding or chiral recognition of pTyr-containing sequences.

The author also assessed the binding of TMR-labeled Grb2 SH2 proteins toward EGFR$^{1060–1076}$ peptides, which were immobilized on a chemical array via carbene-medi-ated covalent bond formation. Both L-Grb2^{TMR} and D-Grb2^{TMR} showed selective binding to L-EGFR$^{1060–1076}$ and D-EGFR$^{1060–1076}$ peptides, respectively, at different concentrations of spotted peptides (Fig. 3.13). As such, these synthetic

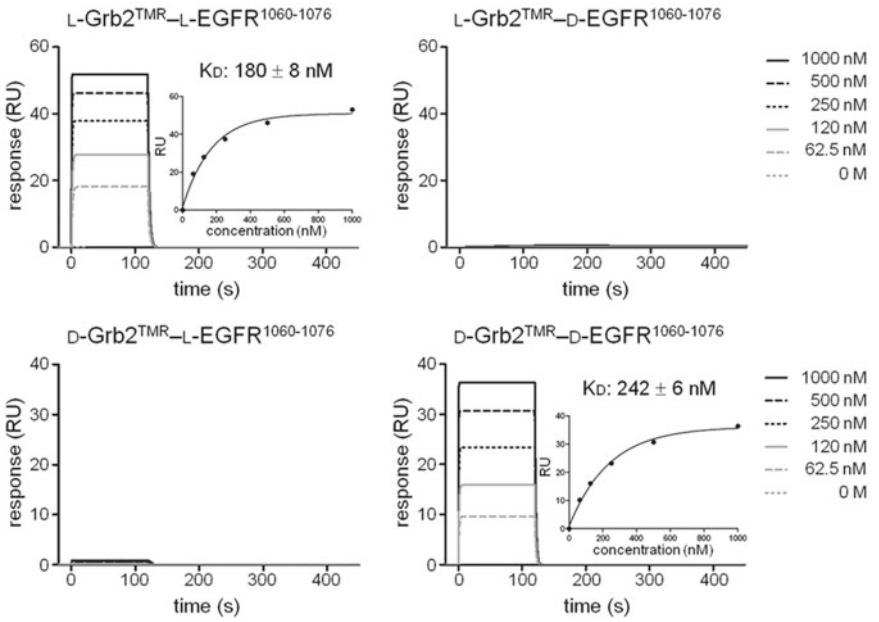

Fig. 3.12 Representative data of SPR analysis of folded L-Grb2^{TMR} and D-Grb2^{TMR} toward L-EGFR$^{1060-1076}$ and D-EGFR$^{1060-1076}$ peptides. The steady-state binding affinities were evaluated from triplicate assays

TMR-labeled Grb2 proteins, with good chiral recognition ability, could be employed for chemical array screenings.

Using the both enantiomers of TMR-labeled Grb2 SH2 domains, chemical array screening for Grb2 SH2 domain was performed for 29,707 compounds from the Natural Products Depository (NPDepo in RIKEN) and our in-house library. Of these, 198 molecules and 503 molecules showed selective binding to L-Grb2^{TMR} and D-Grb2^{TMR}, respectively. The other 634 compounds exhibited binding to both L-Grb2^{TMR} and D-Grb2^{TMR}.

The chemically synthesized, functional Grb2 SH2 domain proteins should be applicable to chemical array technologies for the screening of a number of compounds. However, the hit compounds from chemical array analysis may bind to various pockets or to the surface of the SH2 domain. To identify compound(s) that binds to the pTyr-binding pocket of the Grb2 SH2 domain, thereby inhibiting the Grb2-EGFR interaction, the author next investigated synthetic Grb2$^{53-154}$ in other bioassay systems. To date, a number of ELISA systems have been employed to test for inhibitory activity against interaction between the Grb2 SH2 domain and the pTyr peptide in EGFR. The majority of systems uses pTyr-containing peptides of EGFR or Shc immobilized on plates. The binding of the Grb2 SH2 domain is monitored by indirect detection using a GST-fused Grb2, an anti-GST antibody and an anti-IgG antibody conjugated with peroxidase [29]. These ELISA

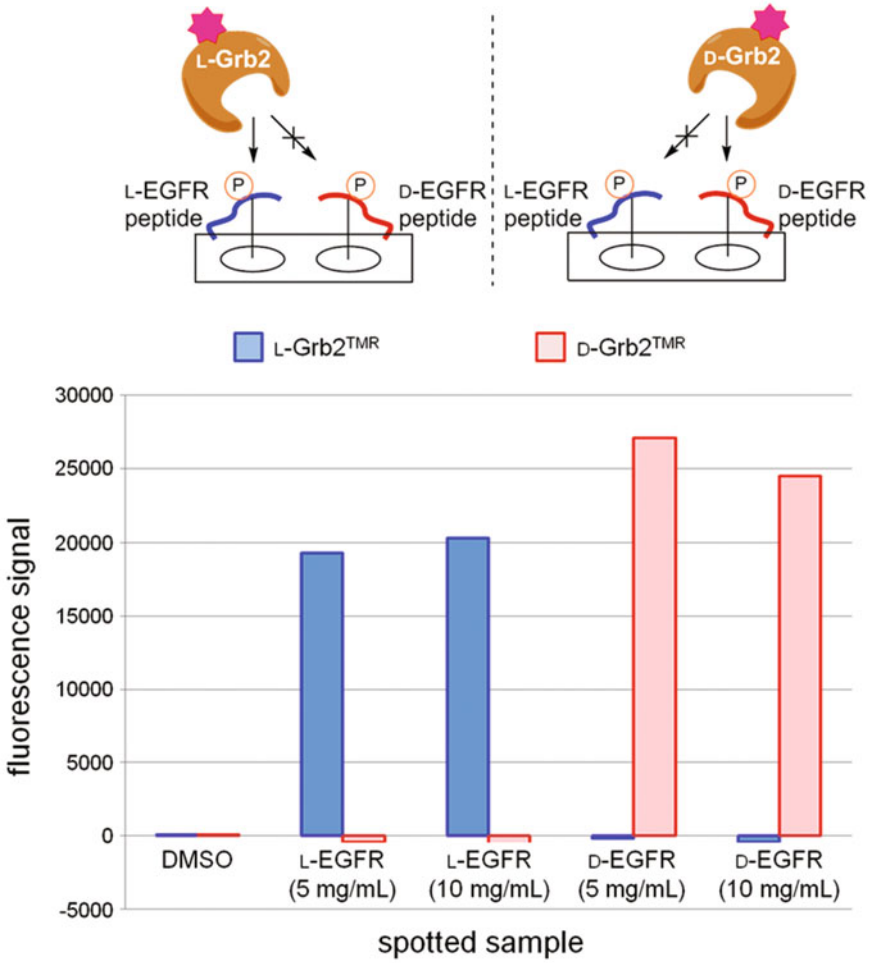

Fig. 3.13 Binding acitivities of Grb2 SH2 domain proteins toward pTyr-containing peptides immobilized on a chemical array. The bindings of L-Grb2^{TMR} and D-Grb2^{TMR} were assessed using a chemcial array, where L-EGFR$^{1060-1076}$ or D-EGFR$^{1060-1076}$ peptides were spotted at various concentrations

systems cannot be applied to mirror-image screening because commercially available antibodies cannot be used to detect mirror-image proteins and tag sequences consisting of D-amino acids. To establish a simple ELISA system for D-Grb2–D-EGFR interaction, native-form tags would be favorable for labeling D-Grb2 SH2 domain proteins and their counterpart pTyr-containing peptide (Fig. 3.14). That is, D-Grb2 SH2 domain proteins with a D-biotin tag (native form) were designed for immobilization on a streptavidin (SA)-coated plate. The mirror-image D-pTyr-containing sequence, D-EGFR$^{1060-1076}$ was labeled with a native 3×FLAG tag

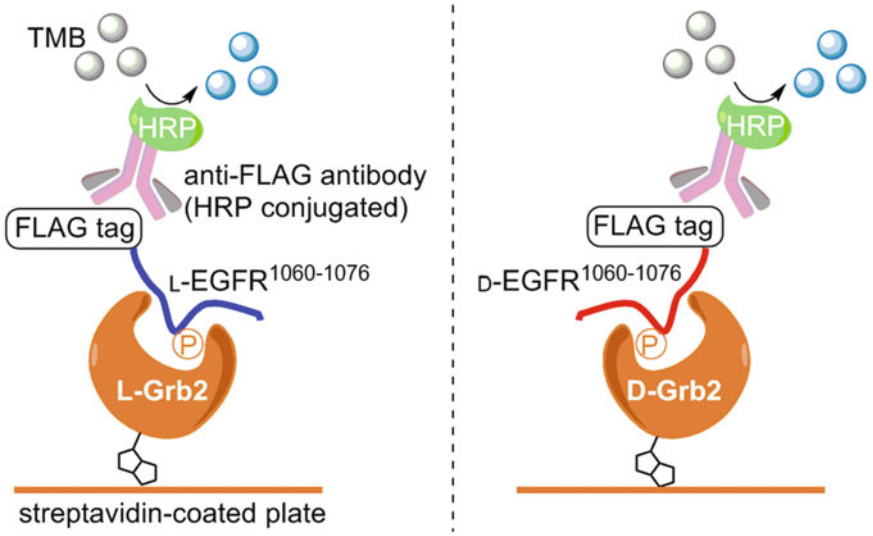

Fig. 3.14 Schematic representation of the ELISA principle using synthetic proteins. Biotinylated L-Grb2 or D-Grb2 is immobilized on a streptavidin-coated plate. The binding of EGFR-derived pTyr peptide with a FLAG tag is detected by an HRP-conjugated anti-FLAG antibody and TMB substrate. Abbreviations: HRP = horseradish peroxidase, TMB = 3,3′,5,5′-tetramethylbenzidine

consisting of L-amino acids (sequence: DYKDHDGDYKDHDIDYKDDDDK). In this system, mirror-image protein–protein interaction between D-Grb2 and D-EGFR was assessed using a commercially available anti-FLAG antibody.

For this purpose, two biotinylated Grb2 SH2 domain proteins were designed and synthesized. On the basis of successful N-terminal TMR labeling of the Grb2 SH2 domain, biotin conjugation was attempted at the N-terminus via a diglycine linker (L-Grb2$^{\text{N-biotin}}$, **L-4d**). Additionally, the author chose the Ala^{115} residue, which is surface-located and away from the pTyr binding pocket, according to the crystal structure of the Grb2 SH2 domain (Fig. 3.15), as an alternative position for biotin labeling.

L-Grb2$^{\text{N-biotin}}$ (**L-4d**) was synthesized according to the procedure used for **L-4a** (Fig. 3.16). Briefly, the first NCL using a biotinylated N-terminal segment **1d** provided a peptide hydrazide of [Cys^{82}]-L-Grb2$^{53–114,\ \text{N-biotin}}$ (**L-7d**) at a yield of 39%. The second ligation using the C-terminal segment **L-6c** provided [Cys^{82}, Cys^{115}]-L-Grb2$^{53–154,\ \text{N-biotin}}$ (**L-3d**) at a yield of 47%. The subsequent desulfurization of **L-3d** afforded the expected **L-4d** at high purity (Fig. 3.17). The mirror-image protein (D-Grb2$^{\text{N-biotin}}$; **D-4d**) was also synthesized in the same manner using mirror-image materials except for native D-biotin.

The synthesis of L-Grb2$^{115\text{-biotin}}$ (**L-4e**) with biotin labeling at the Ala^{115} position of the Grb2 SH2 domain began with desulfurization of Cys^{82} in **L-7c**, which was

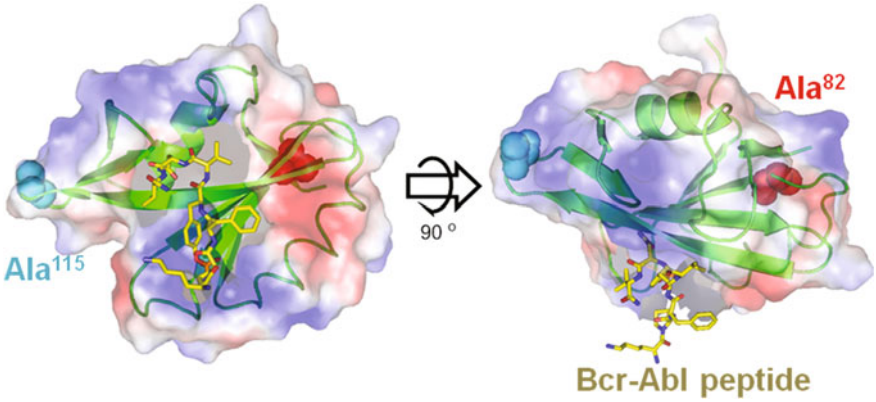

Fig. 3.15 Structure of the Grb2 SH2 domain (PDB ID: 1TZE) [28]. Ala^{82} (red) and Ala^{115} (cyan) are represented as spheres. The Bcr-Abl peptide bound to the Grb2 SH2 domain is represented as sticks

employed as an intermediate for the synthesis of native sequence **L-7a**, to give a peptide hydrazide of L-$Grb2^{53–114}$ (**L-7e**). The subsequent NCL with **L-6c** provided [Cys^{115}]-L-$Grb2^{53–154}$ (**L-3e**) at a yield of 42%. The expected L-$Grb2^{115\text{-biotin}}$ (**L-4e**) was synthesized by conjugation with biotin-PEG_2-maleimide **8** at Cys^{115} under acidic conditions (Fig. 3.16). In this process, two stepwise NCLs and desulfurization of the intermediate facilitated the site-specific biotin labeling after all segments were assembled (Fig. 3.17). This approach would be applicable to labeling proteins at the late stage of synthesis, facilitating the easy introduction of appropriate labeling group(s) for various screening processes.

The resulting synthetic biotinylated Grb2 SH2 domains (**L-4d**, **D-4d** and **L-4e**) were subjected to folding conditions to provide bioactive proteins (Fig. 3.18). The binding affinities between biotinylated proteins and the counterpart pTyr peptides ($EGFR^{1060–1076}$ peptides) were evaluated by SPR analysis, in which the biotinylated Grb2 SH2 domain proteins were immobilized on an SA sensor chip. L-$EGFR^{1060–1076}$ peptide showed the desired binding toward L-$Grb2^{N\text{-biotin}}$ (KD: 330 nM), while no binding of the mirror image D-$EGFR^{1060–1076}$ peptide was observed, suggesting that N-terminal biotin labeling did not prevent chiral recognition at the binding pocket for the pTyr peptide. Also, D-$EGFR^{1060–1076}$ peptide showed the desired binding toward D-$Grb2^{N\text{-biotin}}$ (KD: 221 nM), while no binding of the mirror image L-$EGFR^{1060–1076}$ peptide was observed. The affinity between the L-$Grb2^{115\text{-biotin}}$ and L-$EGFR^{1060–1076}$ peptide was similar to that of L-$Grb2^{N\text{-biotin}}$ (KD: 364 nM). These data indicated that both the N-terminus and Ala^{115} in $Grb2^{53–154}$ would be appropriate positions for biotin labeling without impairing the Grb2 SH2 domain–pTyr peptide and biotin–streptavidin interactions in the ELISA systems.

Using the biotinylated Grb2 SH2 protein, ELISAs were established using L-$Grb2^{N\text{-biotin}}$ and D-$Grb2^{N\text{-biotin}}$ to measure the inhibitory activity of potential Grb2 SH2 domain inhibitors. Initially, L-$Grb2^{N\text{-biotin}}$ (1.8 ng/well) was immobi-

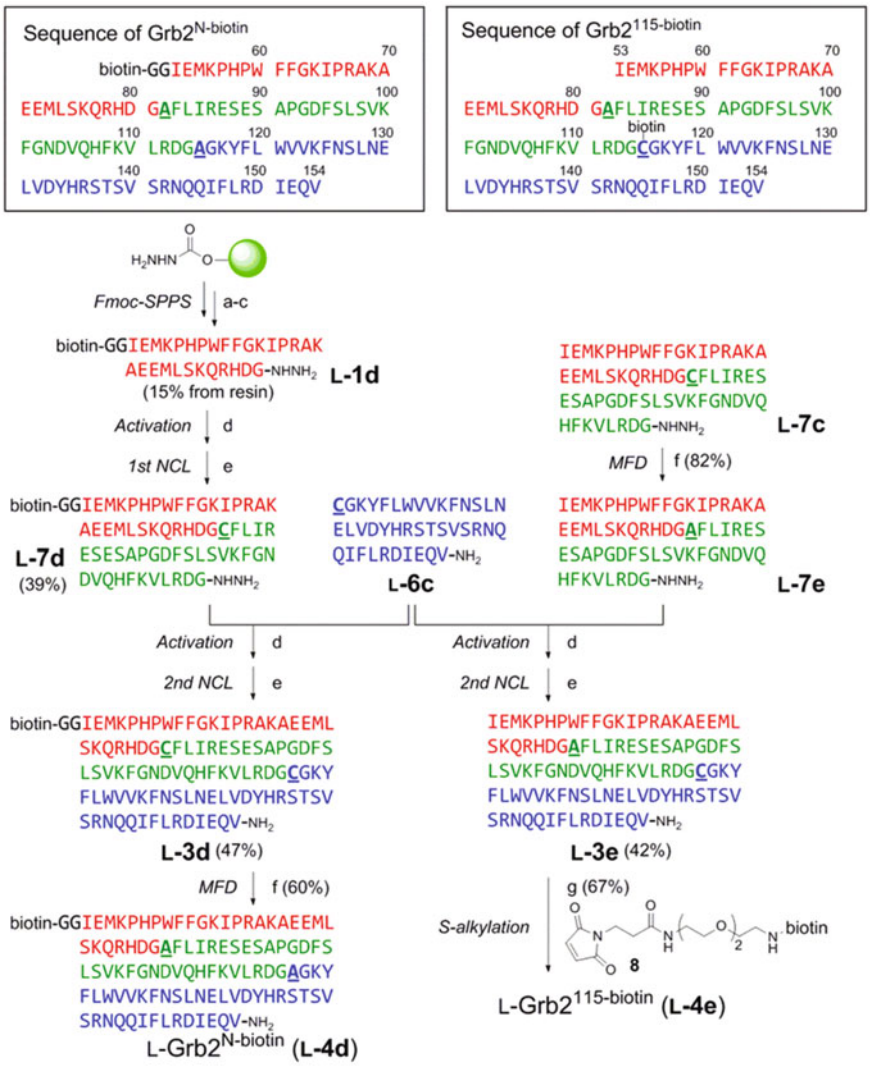

Fig. 3.16 Design and synthesis of biotinylated Grb2 SH2 proteins. (A) Synthetic schemes for L-Grb2$^{N\text{-biotin}}$ (**L-4d**) and L-Grb2$^{115\text{-biotin}}$ (**L-4e**). Amino acid sequences of Grb2$^{N\text{-biotin}}$ and Grb2$^{115\text{-biotin}}$. Ligation sites (Ala^{82}, Ala^{115}) are underlined and in bold type. *Reagents and conditions*: **a** Fmoc-Xaa-OH, HBTU, HOBt, $(i\text{-Pr})_2$NEt, DMF, then 20% piperidine/DMF; **b** biotin, HBTU, HOBt, $(i\text{-Pr})_2$NEt, DMF; **c** TFA/H_2O/*m*-cresol/thioanisole/EDT (80:5:5:5:5); **d** $NaNO_2$, 6 M Gu · HCl, 100 mM Na_2HPO_4 (pH 3.0); **e** 6 M Gu · HCl, 150 mM Na_2HPO_4, 100 mM MPAA (pH 6.8–7.0); **f** 6 M Gu · HCl, 100 mM Na_2HPO_4, 200 mM TCEP · HCl, 20 mM VA-044 · 2HCl, 40 mM MESNa (pH 6.5); **g 8**, AcOH/DMSO/H_2O (1:2:1)

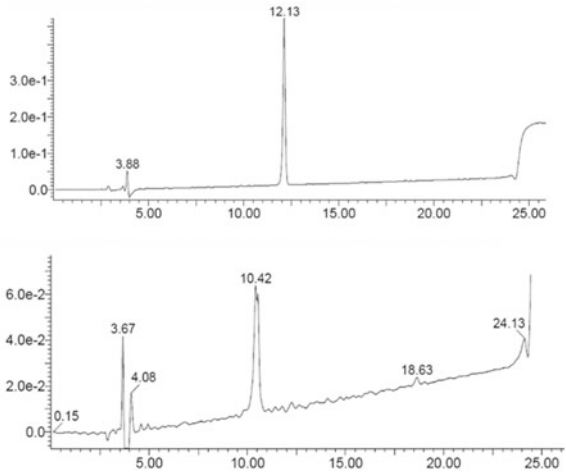

Fig. 3.17 Analytical HPLC chromatograms of purified **L-4d** (above) and **L-4e** (below). HPLC analysis was performed at 25 °C with a linear gradient of 30–50% CH_3CN containing 0.1% TFA at a flow rate of 1 mL/min over 20 min

lized on streptavidin-coated 96-well plates. Subsequently, the L-EGFR$^{1060-1076}$ peptide, which possessed a FLAG tag at the N-terminus, was added (100 nM). The binding ratio of FLAG-labeled L-EGFR$^{1060-1076}$ peptide to L-Grb2$^{N\text{-biotin}}$ protein was detected using an HRP-conjugated anti-FLAG antibody and TMB substrate. The mirror-image interaction between D-Grb2$^{N\text{-biotin}}$ and D-EGFR$^{1060-1076}$ was also monitored in the same manner. The bioactivity of a reported Grb2 SH2 domain inhibitor, pY1068, which is a pTyr-containing peptide of EGFR$^{1060-1076}$, was evaluated for inhibitory activity against the L-Grb2$^{N\text{-biotin}}$–L-EGFR$^{1060-1076}$ interaction (Fig. 3.19 and Table 3.1). L-pY1068 potently inhibited the native interaction with an IC_{50} value of 0.60 μM, while D-pY1068 did not. Similarly, D-pY1068 inhibited the mirror-image interaction between D-Grb2$^{N\text{-biotin}}$-D-EGFR$^{1060-1076}$ with an IC_{50} of 0.39 μM. Taken together, both enantiomers of chemically synthesized Grb2 SH2 domain proteins were successfully applied to the ELISA-based competition assays to identify inhibitors of Grb2-EGFR interaction.

In this study, the author investigated the chemical synthesis of Grb2 SH2 domain proteins and their application to the development of in vitro assay systems for Grb2 SH2 domain inhibitors. Initial attempt by single NCL at the Ala^{82} position using two segments produced synthetic Grb2 SH2 domain protein at moderate yield. When N-to-C-directed sequential NCL of three segments was employed, the desired Grb2 SH2 proteins were obtained with higher efficiency. To the best of the author's knowledge, this is the first report of the chemical synthesis of SH2 domain proteins. Based on these protocols, several labeled Grb2 SH2 proteins including Grb2^{TMR}, Grb2$^{N\text{-biotin}}$ and Grb2$^{115\text{-biotin}}$, were synthesized. The synthetic proteins, which were subjected to folding under the appropriate conditions, exhibited the expected potent binding to phosphorylated EGFR peptide in chemical array analysis, SPR analysis,

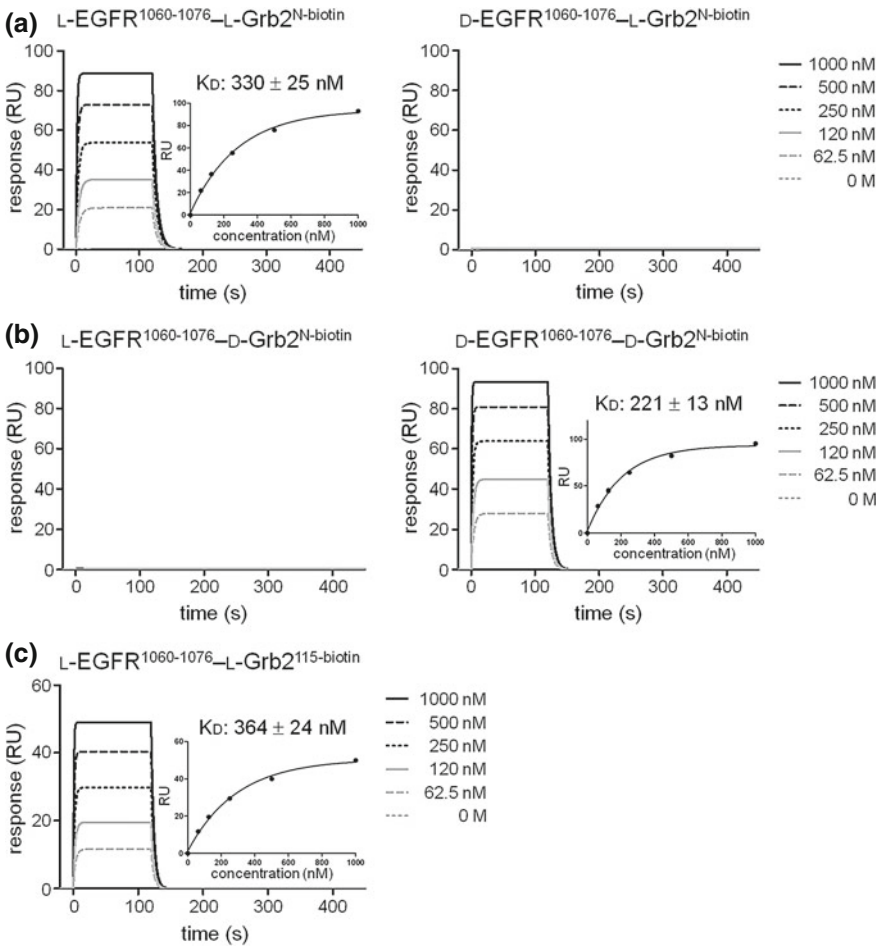

Fig. 3.18 SPR analysis of biotinylated Grb2 SH2 domain proteins. Representative data of L-EGFR$^{1060-1076}$ peptide binding to L-Grb2$^{N\text{-biotin}}$ (**a**); D-EGFR$^{1060-1076}$ binding to L-Grb2$^{N\text{-biotin}}$ (**b**); and L-EGFR$^{1060-1076}$ binding to L-Grb2$^{115\text{-biotin}}$ (**c**). The steady-state bindings affinities were evaluated from triplicate assays

and ELISA. The L-Grb2 SH2 and D-Grb2 SH2 proteins selectively interacted with L-peptide and D-peptide of phosphorylated EGFR(1060–1076), respectively, suggesting that these proteins distinguish the native sequence and the mirror-image structure. In Sect. 2, of Chap. 1, chemical array screening and subsequent competitive fluorescence polarization assays using both enantiomers of synthetic L-MDM2 and D-MDM2 proteins identified novel inhibitors against MDM2-p53 interaction [1]. This mirror-image screening facilitated the identification process from a virtual library of mirror-image natural products. The in vitro assay systems using these chemically synthesized Grb2 SH2 domain proteins would be applicable to facile

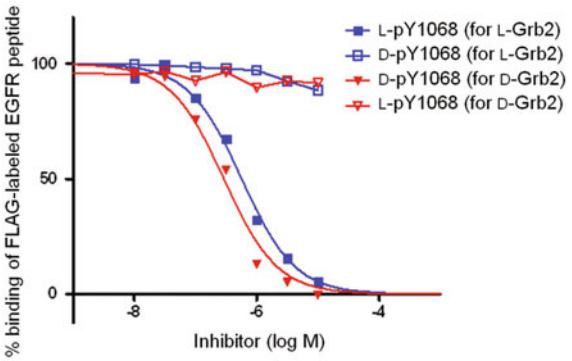

Fig. 3.19 ELISA-based competition assays for Grb2 SH2 domain inhibitors. Representative dose-response curves of the assay using L-Grb2$^{N\text{-biotin}}$ or D-Grb2$^{N\text{-biotin}}$ are shown

Table 3.1 Inhibitory activities of mirror-image pTyr-containing peptides (pY1068) against Grb2$^{N\text{-biotin}}$-EGFR$^{1060-1076}$ interactions in ELISAs

Compound	IC_{50} (μM)[a]	
	L-Grb2 SH2	D-Grb2 SH2
L-pY1068	0.60 ± 0.03	>10
D-pY1068	>10	0.39 ± 0.08

[a]The inhibitory activities were evaluated by ELISA-based competitive assays using L-Grb2$^{N\text{-biotin}}$ or D-Grb2$^{N\text{-biotin}}$. IC_{50} values were calculated from triplicate assays

drug screening for the identification of novel Grb2 SH2 domain inhibitors from chiral substances (chiral natural products and L-peptides from phage display) and the virtual mirror-image compounds.

SH2 domains, which consist of a central antiparallel β-sheet flanked by two α-helices, are characteristic structural motifs common to a variety of critical intracellular signaling proteins. Because these mediate distinct signaling pathways [30], selective inhibitors to impairing key intracellular SH2-mediated protein-protein interactions would be promising pharmaceutical agents [31]. The developed synthetic protocols in this section are applicable to the preparation of a number of other SH2 domains, and their application in screening virtual mirror-image libraries will facilitate the identification of selective agents for these structurally conserved domains.

3.1 Experimental Section

General Methods

Fmoc-protected amino acids were purchased from Watanabe Chemical Industries, Ltd. (Hiroshima, Japan) or Kokusan Chemical Co. Ltd. (Kanagawa, Japan). For

analytical HPLC, Cosmosil 5C18-AR300 column (4.6 × 250 mm, Nacalai Tesque Inc.) was employed with a linear gradient of CH_3CN containing 0.1% (v/v) TFA at a flow rate of 1 mL/min. The products were detected by UV absorbance at 220 nm. For preparative HPLC, Cosmosil 5C18-AR300 column (20 × 250 mm, Nacalai Tesque Inc.) was employed with a linear gradient of CH_3CN containing 0.1% (v/v) TFA at a flow rate of 8 mL/min unless otherwise stated. All peptides were characterized by micromass ZQ LC-MS (Waters).

General Procedure for the Synthesis of Peptide Amides

Peptide chain elongation was performed on H-Rink Amide ChemMatrix resin (0.4–0.6 mmol/g) using an automatic peptide synthesizer (PSSM-8, Shimadzu) by Fmoc-based solid-phase peptide synthesis. For the side-chain protection, *t*-Bu ester for Asp and Glu; 2, 2, 4, 6, 7-pentamethyldihydrobenzofuran-5-sulfonyl (Pbf) for Arg; *t*-Bu for Thr, Tyr and Ser; Boc for Lys and Trp; and Trt for Gln, Asn, His, and Cys were employed for side-chain protection. Fmoc-protected amino acids (5 eq) were coupled by using HBTU (5 eq), HOBt (5 eq) and $(i\text{-Pr})_2NEt$ (10 eq) in DMF for 45 min twice. Fmoc-protecting group was removed by treatment with 20% piperidine in DMF for 5 min. The resulting protected peptide resin was treated with a TFA cocktail [TFA/H_2O/*m*-cresol/thioanisole/EDT (80:5:5:5:5)] for 2 h. After the removal of the resin by filtration, the filtrate was poured into ice-cold dry Et_2O. The resulting powder was collected by centrifugation and washed three times with ice-cold dry Et_2O. The crude product was purified by RP-HPLC to afford the expected peptide.

Peptide L-2a

By the standard procedure for peptide synthesis on H-Rink Amide ChemMatrix resin (160 mg, ca. 0.08 mmol), peptide **L-2a** was synthesized (8.43 mg, 1% yield). MS (ESI): Calcd for $C_{384}H_{588}N_{106}O_{110}S_3$: 8481.62; observed: $[M+10H]^{10+}$ *m/z* = 849.04, $[M+9H]^{9+}$ *m/z* = 944.03, $[M+8H]^{8+}$ *m/z* = 1061.32, $[M+7H]^{7+}$ *m/z* = 1213.18, $[M+6H]^{6+}$ *m/z* = 1414.90.

Peptide D-2a

By the standard procedure for peptide synthesis on H-Rink Amide ChemMatrix resin (160 mg, ca. 0.08 mmol), peptide **D-2a** was synthesized (16.0 mg, 2% yield). MS (ESI): Calcd for $C_{384}H_{588}N_{106}O_{110}S_3$: 8481.62; observed: $[M+10H]^{10+}$ *m/z* = 849.18, $[M+9H]^{9+}$ *m/z* = 943.60, $[M+8H]^{8+}$ *m/z* = 1061.29, $[M+7H]^{7+}$ *m/z* = 1212.92, $[M+6H]^{6+}$ *m/z* = 1415.46.

Peptide L-6c

By the standard procedure for peptide synthesis, peptide **L-6c** was synthesized (19.5 mg, 20% yield) from H-Rink Amide ChemMatrix resin (40 mg, ca. 0.02 mmol). MS (ESI): Calcd for $C_{219}H_{337}N_{61}O_{61}S$: 4832.53; observed: $[M+6H]^{6+}$ *m/z* = 806.45, $[M+5H]^{5+}$ *m/z* = 967.69, $[M+4H]^{4+}$ *m/z* = 1209.21.

Peptide D-6c

By the standard procedure for peptide synthesis, peptide **D-6c** was synthesized (22.2 mg, 12% yield) from H-Rink Amide ChemMatrix resin (80.0 mg, ca. 0.04 mmol). MS (ESI): Calcd for $C_{219}H_{337}N_{61}O_{61}S$: 4832.53; observed: $[M+6H]^{6+}$ *m/z* = 806.50, $[M+5H]^{5+}$ *m/z* = 967.46, $[M+4H]^{4+}$ *m/z* = 1209.26.

Synthesis of Peptide MPAA Thioesters: Peptide L-1a

Fmoc-Dbz-OH (300 mg, 0.8 mmol) was loaded on CLEAR amide resin (0.32 mmol/g, 500 mg, 0.16 mmol) by HBTU (303 mg, 0.8 mmol), HOBt·H_2O (123 mg, 0.8 mmol) and (i-Pr)$_2$NEt (279 μL, 1.6 mmol) in DMF for 2 h (three times). After the loading of the Dbz group on resin, the resins were split into eight portions (0.02 mmol each). The solid-phase peptide synthesis was performed using automatic peptide synthesizer by the standard protocol. For the coupling of an N-terminal Ile in peptide **1a**, Boc-Ile-OH (23.1 mg, 0.1 mmol) was employed with HBTU (37.9 mg, 0.1 mmol), HOBt · H_2O (15.3 mg, 0.1 mmol) and (i-Pr)$_2$NEt (34.8 μL, 0.2 mmol) for 2 h using the 2 vessels (0.02 mmol × 2). After chain assembly, the resins were combined and treated with 0.3 M 4-nitrophenyl chloroformate in DCM (2.00 mL) for 2 h followed by 0.5 M (i-Pr)$_2$NEt in DMF (2.00 mL) for 1 h. Global deprotection and cleavage from resin was performed by treatment with a TFA cocktail [TFA/H_2O/m-cresol/thioanisole (80:10:5:5)] for 2 h. After removal of the resin by filtration, the filtrate was poured into ice-cold dry Et_2O. The resulting powder was collected by centrifugation and washed three times with ice-cold dry Et_2O. The resulting precipitate was dissolved in minimum amount of ligation buffer (6 M Gu · HCl, 200 mM MPAA, 20 mM TCEP · HCl in PBS, pH 7.0) for 30 min. Purification by RP-HPLC provided the peptide **1a** (2.96 mg, 2% yield). MS (ESI): Calcd for $C_{165}H_{249}N_{45}O_{41}S_3$: 3615.26; observed: $[M+6H]^{6+}$ m/z = 603.25, $[M+5H]^{5+}$ m/z = 724.00, $[M+4H]^{4+}$ m/z = 904.79, $[M+3H]^{3+}$ m/z = 1205.95.

Peptide Thioester L-1b

By the identical procedure described for the synthesis of peptide **L-1a**, thioester **L-1b** was synthesized (2.85 mg, 1% yield) from Clear amide resin (156 mg, 0.05 mmol). TMR (64.6 mg, 0.15 mmol) was coupled by using DIPCI (23.2 μL, 0.15 mmol), HOBt · H_2O (23.0 mg, 0.15 mmol) in DMF for 3 h. MS (ESI): Calcd for $C_{194}H_{275}N_{49}O_{47}S_3$: 4141.81; observed: $[M+7H]^{7+}$ m/z = 592.43, $[M+6H]^{6+}$ m/z = 691.32, $[M+5H]^{5+}$ m/z = 829.46, $[M+4H]^{4+}$ m/z = 1036.63, $[M+3H]^{3+}$ m/z = 1381.67.

Peptide Thioester D-1b

By the identical procedure described for the synthesis of peptide **L-1a** and **L-1b**, thioester **D-1b** was synthesized (1.95 mg, 1% yield) from Clear amide resin (125 mg, 0.04 mmol). MS (ESI): Calcd for $C_{194}H_{275}N_{49}O_{47}S_3$: 4141.81; observed: $[M+7H]^{7+}$ m/z = 593.22, $[M+6H]^{6+}$ m/z = 691.44, $[M+5H]^{5+}$ m/z = 829.48, $[M+4H]^{4+}$ m/z = 1036.78, $[M+3H]^{3+}$ m/z = 1381.94.

Preparation of Hydrazide Linker for the Solid-phase Synthesis of Peptide Hydrazides

4-Nitrophenyl chloroformate (1.01 g, 5.00 mmol) was added to the suspension of Wang-PEG resin (0.31 mmol/g, 1.60 g, 0.500 mmol) in dry pyridine (404 μL, 5.00 mmol) and dry DCM (16 mL), and the suspension was agitated for 2 h. After filtration, the resin was treated with 1 M NH_2NH_2 · H_2O in THF (16 mL) for 2 h.

Peptide Hydrazide L-1c

By the standard procedure for peptide synthesis, hydrazide **L-1c** was synthesized (20.7 mg, 12% yield) from Wang-PEG resin (161 mg, 0.05 mmol). MS (ESI): Calcd for $C_{157}H_{245}N_{47}O_{39}S_2$: 3479.10; observed: $[M+6H]^{6+}$ *m/z* = 580.70, $[M+5H]^{5+}$ *m/z* = 696.65, $[M+4H]^{4+}$ *m/z* = 870.72, $[M+3H]^{3+}$ *m/z* = 1160.61.

Peptide Hydrazide D-1c

By the standard procedure for peptide synthesis, hydrazide **D-1c** was synthesized (4.90 mg, 14% yield) from Wang-PEG resin (32.3 mg, 0.01 mmol). MS (ESI): Calcd for $C_{157}H_{245}N_{47}O_{39}S_2$: 3479.10; observed: $[M+6H]^{6+}$ *m/z* = 580.83, $[M+5H]^{5+}$ *m/z* = 696.88, $[M+4H]^{4+}$ *m/z* = 871.05, $[M+3H]^{3+}$ *m/z* = 1160.87.

Peptide Hydrazide L-1d

By the standard procedure for peptide synthesis, hydazide **L-1d** was synthesized (29.2 mg, 15% yield) from Wang-PEG resin (161 mg, 0.05 mmol). Biotin (61.1 mg, 0.25 mmol) was coupled by using HBTU (94.8 mg, 0.25 mmol), HOBt · H_2O (38.3 mg, 0.25 mmol) and (*i*-Pr)$_2$NEt (89.1 μL, 0.5 mmol) in DMF for 2 h. MS (ESI): Calcd for $C_{171}H_{271}N_{51}O_{43}S_3$: 3819.50; observed: $[M+6H]^{6+}$ *m/z* = 637.66, $[M+5H]^{5+}$ *m/z* = 764.98, $[M+4H]^{4+}$ *m/z* = 956.01, $[M+3H]^{3+}$ *m/z* = 1274.14.

Peptide Hydrazide D-1d

By the standard procedure for peptide synthesis, hydazide **D-1d** was synthesized (10.9 mg, 14%) from Wang-PEG resin (64.5 mg, 0.02 mmol). MS (ESI): Calcd for $C_{171}H_{271}N_{51}O_{43}S_3$: 3819.50; observed: $[M+6H]^{6+}$ *m/z* = 637.45, $[M+5H]^{5+}$ *m/z* = 764.95, $[M+4H]^{4+}$ *m/z* = 955.88, $[M+3H]^{3+}$ *m/z* = 1274.09.

Peptide Hydrazide L-5c

By the standard procedure for peptide synthesis, hydrazide **L-5c** was synthesized (30.5 mg, 10% yield) from Wang-PEG resin (258 mg, 0.08 mmol). MS (ESI): Calcd for $C_{165}H_{255}N_{47}O_{49}S$: 3713.20; observed: $[M+5H]^{5+}$ *m/z* = 743.93, $[M+4H]^{4+}$ *m/z* = 929.33, $[M+3H]^{3+}$ *m/z* = 1238.69.

Peptide Hydrazide D-5c

By the standard procedure for peptide synthesis, hydrazide **D-5c** was synthesized (10.5 mg, 7% yield) from Wang-PEG resin (129 mg, 0.04 mmol). MS (ESI): Calcd for $C_{165}H_{255}N_{47}O_{49}S$: 3713.20; observed: $[M+4H]^{4+}$ *m/z* = 929.28, $[M+3H]^{3+}$ *m/z* = 1238.64.

Native Chemical Ligation Using Peptide MPAA Thioester: Synthesis of Peptide L-3a

MPAA-thioester segment **L-1a** (1.40 mg, 0.387 μmol) and C-terminal segment **L-2a** (2.00 mg, 0.236 μmol) were dissolved in the ligation buffer (6 M Gu · HCl, 200 mM MPAA, 20 mM TCEP · HCl in PBS, pH 7.0; 470 μL), and the reaction was monitored by LC-MS. After reaction was completed, TCEP · HCl (13.5 mg, 47.0 μmol) was added to the reaction mixture, and the mixture was stirred for 30 min at room temperature. The crude products were purified by preparative HPLC to afford peptide **L-3a** (1.02 mg, 36% yield). MS (ESI): Calcd for $C_{541}H_{829}N_{151}O_{149}S_3$: 11928.67; observed: $[M+15H]^{15+}$ *m/z* = 796.67, $[M+14H]^{14+}$ *m/z* = 853.13, $[M+13H]^{13+}$ *m/z* = 918.72,

$[M+12H]^{12+}$ *m/z* = 995.28, $[M+11H]^{11+}$ *m/z* = 1085.77, $[M+10H]^{10+}$ *m/z* = 1194.04, $[M+9H]^{9+}$ *m/z* = 1326.84.

Peptide L-3b

By the identical procedure described for the synthesis of peptide **L-3a**, peptide **L-1b** (1.50 mg, 0.362 μmol) and peptide **L-2a** (1.40 mg, 0.165 μmol) were converted into the peptide **L-3b** (1.00 mg, 49% yield). MS (ESI): Calcd for $C_{570}H_{855}N_{155}O_{155}S_3$: 12455.22; observed: $[M+15H]^{15+}$ *m/z* = 831.50, $[M+14H]^{14+}$ *m/z* = 891.31, $[M+13H]^{13+}$ *m/z* = 959.32, $[M+12H]^{12+}$ *m/z* = 1039.15, $[M+11H]^{11+}$ *m/z* = 1133.59, $[M+10H]^{10+}$ *m/z* = 1246.82, $[M+9H]^{9+}$ *m/z* = 1385.89.

Peptide D-3b

By the identical procedure described for the synthesis of peptide **L-3a**, peptide **D-1b** (1.95 mg, 0.471 μmol) and peptide **D-2a** (1.84 mg, 0.217 μmol) were converted into the peptide **D-3b** (1.40 mg, 52% yield). MS (ESI): Calcd for $C_{570}H_{855}N_{155}O_{155}S_3$: 12455.22; observed: $[M+15H]^{15+}$ *m/z* = 831.90, $[M+14H]^{14+}$ *m/z* = 890.86, $[M+13H]^{13+}$ *m/z* = 959.27, $[M+12H]^{12+}$ *m/z* = 1039.32, $[M+11H]^{11+}$ *m/z* = 1133.98, $[M+10H]^{10+}$ *m/z* = 1246.68.

Native Chemical Ligation Using Peptide-hydrazide: Synthesis of Peptide L-3c

$NaNO_2$ solution (200 mM, 8.40 μL, 1.68 μmol) was added to a solution of hydrazide **L-7c** (1.00 mg, 0.140 μmol) in activation buffer (6 M Gu · HCl, 100 mM Na_2HPO_4, pH 3.0; 139 μL) at -20 °C [24]. After the mixture was stirred for 30 min, peptide **L-6c** (680 μg, 1.41 μmol) was added to the mixture in MPAA solution (6 M Gu · HCl, 200 mM MPAA, 200 mM Na_2HPO_4, pH 7.0; 139 μL) The mixture was warmed to room temperature and pH was adjusted to 6.8–7.0. After reaction was completed, TCEP · HCl (8.18 mg, 0.0285 mmol) was added to the reaction mixture to a final concentration of 100 mM. The crude products were purified by preparative HPLC to afford peptide **L-3c** (900 μg, 53% yield). MS (ESI): Calcd for $C_{541}H_{829}N_{151}O_{149}S_4$: 11960.73; observed: $[M+15H]^{15+}$ *m/z* = 798.04, $[M+14H]^{14+}$ *m/z* = 855.34, $[M+13H]^{13+}$ *m/z* = 921.34, $[M+12H]^{12+}$ *m/z* = 997.92, $[M+11H]^{11+}$ *m/z* = 1088.70, $[M+10H]^{10+}$ *m/z* = 1197.22, $[M+9H]^{9+}$ *m/z* = 1330.61.

Peptide D-3c

By the identical procedure described for the synthesis of peptide **L-3c**, peptide **D-7c** (1.45 mg, 0.203 μmol) and peptide **D-6c** (1.47 mg, 0.304 μmol) were converted into the peptide **D-3c** (1.10 mg, 45% yield). MS (ESI): Calcd for $C_{541}H_{829}N_{151}O_{149}S_4$: 11960.73; observed: $[M+15H]^{15+}$ *m/z* = 798.55, $[M+14H]^{14+}$ *m/z* = 855.43, $[M+13H]^{13+}$ *m/z* = 921.37, $[M+12H]^{12+}$ *m/z* = 998.07, $[M+11H]^{11+}$ *m/z* = 1088.59, $[M+10H]^{10+}$ *m/z* = 1197.72, $[M+9H]^{9+}$ *m/z* = 1330.64.

Peptide L-3d

By the identical procedure described for the synthesis of peptide **L-3c**, peptide **L-7d** (3.95 mg, 0.537 μmol) and peptide **L-6c** (3.31 mg, 0.685 μmol) were converted into the peptide **L-3d** (3.10 mg, 47% yield). MS (ESI): Calcd for $C_{555}H_{849}N_{155}O_{153}S_5$: 12301.13; observed: $[M+15H]^{15+}$ *m/z* = 821.27, $[M+14H]^{14+}$ *m/z* = 879.82, $[M+13H]^{13+}$ *m/z* = 947.59, $[M+12H]^{12+}$ *m/z* = 1026.47, $[M+11H]^{11+}$ *m/z* = 1119.56, $[M+10H]^{10+}$ *m/z* = 1231.55, $[M+9H]^{9+}$ *m/z* = 1367.79.

Peptide D-3d

By the identical procedure described for the synthesis of peptide **L-3d**, peptide **D-7d** (1.08 mg, 0.144 μmol) and peptide **D-6c** (900 μg, 0.187 μmol) were converted into the peptide **D-3d** (850 μg, 47% yield). MS (ESI): Calcd for $C_{555}H_{849}N_{155}O_{153}S_5$: 12301.13; observed: $[M+15H]^{15+}$ *m/z* = 821.50, $[M+14H]^{14+}$ *m/z* = 879.54, $[M+13H]^{13+}$ *m/z* = 947.51, $[M+12H]^{12+}$ *m/z* = 1026.20, $[M+11H]^{11+}$ *m/z* = 1119.43, $[M+10H]^{10+}$ *m/z* = 1230.97, $[M+9H]^{9+}$ *m/z* = 1368.69.

Peptide L-3e

By the identical procedure described for the synthesis of peptide **L-3c**, peptide **L-7e** (1.55 mg, 0.217 μmol) and peptide **L-6c** (1.37 mg, 0.283 μmol) were converted into the peptide **L-3e** (1.09 mg, 42% yield). MS (ESI): Calcd for $C_{541}H_{829}N_{151}O_{149}S_3$: 11928.67; observed: $[M+15H]^{15+}$ *m/z* = 796.30, $[M+14H]^{14+}$ *m/z* = 853.26, $[M+13H]^{13+}$ *m/z* = 918.75, $[M+12H]^{12+}$ *m/z* = 995.29, $[M+11H]^{11+}$ *m/z* = 1085.66, $[M+10H]^{10+}$ *m/z* = 1194.14, $[M+9H]^{9+}$ *m/z* = 1326.83.

Peptide L-7c

By the identical procedure described for the synthesis of peptide **L-3c**, peptide **L-1c** (5.96 mg, 1.75 μmol) and peptide **L-5c** (5.00 mg, 1.35 μmol) were converted into the peptide **L-7c** (4.20 mg, 43% yield). MS (ESI): Calcd for $C_{322}H_{496}N_{92}O_{88}S_3$: 7160.25; observed: $[M+11H]^{11+}$ *m/z* = 652.07, $[M+10H]^{10+}$ *m/z* = 717.11, $[M+9H]^{9+}$ *m/z* = 796.59, $[M+8H]^{8+}$ *m/z* = 895.97, $[M+7H]^{7+}$ *m/z* = 1023.89, $[M+6H]^{6+}$ *m/z* = 1194.66, $[M+5H]^{5+}$ *m/z* = 1433.28.

Peptide D-7c

By the identical procedure described for the synthesis of peptide **L-3c**, peptide **D-1c** (3.00 mg, 0.881 μmol) and peptide **D-5c** (2.50 mg, 0.677 μmol) were converted into the peptide **D-7c** (1.45 mg, 30% yield). MS (ESI): Calcd for $C_{322}H_{496}N_{92}O_{88}S_3$: 7160.25; observed: $[M+10H]^{10+}$ *m/z* = 717.19, $[M+9H]^{9+}$ *m/z* = 796.86, $[M+8H]^{8+}$ *m/z* = 896.19, $[M+7H]^{7+}$ *m/z* = 1024.15, $[M+6H]^{6+}$ *m/z* = 1194.25, $[M+5H]^{5+}$ *m/z* = 1433.24.

Peptide L-7d

By the identical procedure described for the synthesis of peptide **L-3c**, peptide **L-1d** (6.70 mg, 1.75 μmol) and peptide **L-5c** (5.00 mg, 1.35 μmol) were converted into the peptide **L-7d** (3.95 mg, 39% yield). MS (ESI): Calcd for $C_{336}H_{516}N_{96}O_{92}S_4$: 7500.64; observed: $[M+10H]^{10+}$ *m/z* = 751.15, $[M+9H]^{9+}$ *m/z* = 834.62, $[M+8H]^{8+}$ *m/z* = 938.69, $[M+7H]^{7+}$ *m/z* = 1072.76, $[M+6H]^{6+}$ *m/z* = 1251.64.

Peptide D-7d

By the identical procedure described for the synthesis of peptide **L-3c**, peptide **D-1d** (2.67 mg, 0.700 μmol) and peptide **D-5c** (2.00 mg, 0.538 μmol) were converted into the peptide **D-7d** (1.42 mg, 35% yield). MS (ESI): Calcd for $C_{336}H_{516}N_{96}O_{92}S_4$: 7500.64; observed: $[M+10H]^{10+}$ *m/z* = 750.72, $[M+9H]^{9+}$ *m/z* = 834.54, $[M+8H]^{8+}$ *m/z* = 938.66, $[M+7H]^{7+}$ *m/z* = 1072.71, $[M+6H]^{6+}$ *m/z* = 1251.02.

Desulfurization of Cysteine Residues: Synthesis of Peptide L-4a

[23] VA-044 · 2HCl (2.20 mg, 6.80 μmol) was added to a solution of peptide **L-3a** (660 μg, 0.0553 μmol) in the desulfurization buffer (6 M Gu · HCl, 100 mM

Na_2HPO_4, 200 mM TCEP · HCl, 40 mM MESNa, pH 6.5; 340 μL). The mixture was incubated at 37 °C and the reaction was monitored by LC-MS. After the reaction was completed, the crude products were purified by preparative HPLC to afford peptide **L-4a** (460 μg, 70% yield). MS (ESI): Calcd for $C_{541}H_{829}N_{151}O_{149}S_2$: 11896.61; observed: $[M+14H]^{14+}$ *m/z* = 850.76, $[M+13H]^{13+}$ *m/z* = 916.25, $[M+12H]^{12+}$ *m/z* = 992.62, $[M+11H]^{11+}$ *m/z* = 1082.79, $[M+10H]^{10+}$ *m/z* = 1190.99, $[M+9H]^{9+}$ *m/z* = 1322.74.

Peptide L-4a from Peptide L-3c

By the identical procedure described for the synthesis of peptide **L-4a** from **L-3a**, peptide **L-3c** (600 μg, 0.0502 μmol) was converted into the peptide **L-4a** (240 μg, 40% yield). MS (ESI): Calcd for $C_{541}H_{829}N_{151}O_{149}S_2$: 11896.61; observed: $[M+15H]^{15+}$ *m/z* = 794.45, $[M+14H]^{14+}$ *m/z* = 851.03, $[M+13H]^{13+}$ *m/z* = 916.30, $[M+12H]^{12+}$ *m/z* = 992.72, $[M+11H]^{11+}$ *m/z* = 1082.89, $[M+10H]^{10+}$ *m/z* = 1191.42.

Peptide D-4a

By the identical procedure described for the synthesis of peptide **L-4a**, peptide **D-3c** (1.10 mg, 0.0920 μmol) was converted into the peptide **D-4a** (670 μg, 61% yield). MS (ESI): Calcd for $C_{541}H_{829}N_{151}O_{149}S_2$: 11896.61; observed: $[M+15H]^{15+}$ *m/z* = 794.58, $[M+14H]^{14+}$ *m/z* = 851.01, $[M+13H]^{13+}$ *m/z* = 916.29, $[M+12H]^{12+}$ *m/z* = 992.65, $[M+11H]^{11+}$ *m/z* = 1082.90, $[M+10H]^{10+}$ *m/z* = 1191.11, $[M+9H]^{9+}$ *m/z* = 1323.09.

Peptide L-4d

By the identical procedure described for the synthesis of peptide **L-4a**, peptide **L-3d** (3.10 mg, 0.252 μmol) was converted into the peptide **L-4d** (1.86 mg, 60% yield). MS (ESI): Calcd for $C_{555}H_{849}N_{155}O_{153}S_3$: 12237.01; observed: $[M+15H]^{15+}$ *m/z* = 816.97, $[M+14H]^{14+}$ *m/z* = 875.28, $[M+13H]^{13+}$ *m/z* = 942.47, $[M+12H]^{12+}$ *m/z* = 1020.91, $[M+11H]^{11+}$ *m/z* = 1113.61, $[M+10H]^{10+}$ *m/z* = 1225.03, $[M+9H]^{9+}$ *m/z* = 1361.02.

Peptide D-4d

By the identical procedure described for the synthesis of **L-4a**, peptide **D-3d** (850 μg, 0.0691 μmol) was converted into the peptide **D-4d** (490 μg, 57% yield). MS (ESI): Calcd for $C_{555}H_{849}N_{155}O_{153}S_3$: 12237.01; observed: $[M+14H]^{14+}$ *m/z* = 875.03, $[M+13H]^{13+}$ *m/z* = 942.37, $[M+12H]^{12+}$ *m/z* = 1020.72, $[M+11H]^{11+}$ *m/z* = 1113.45, $[M+10H]^{10+}$ *m/z* = 1224.75, $[M+9H]^{9+}$ *m/z* = 1360.98.

Peptide L-7e

By the identical procedure described for the synthesis of peptide **L-4a**, peptide **L-7c** (2.00 mg, 0.279 μmol) was converted into the peptide **L-7e** (1.66 mg, 82% yield). MS (ESI): Calcd for $C_{322}H_{496}N_{92}O_{88}S_2$: 7128.19; observed: $[M+10H]^{10+}$ *m/z* = 713.74, $[M+9H]^{9+}$ *m/z* = 793.14, $[M+8H]^{8+}$ *m/z* = 892.20, $[M+7H]^{7+}$ *m/z* = 1019.45, $[M+6H]^{6+}$ *m/z* = 1189.38, $[M+5H]^{5+}$ *m/z* = 1426.82.

Biotin Labeling on the Cys Residue: Synthesis of Peptide L-4e

The solution of maleimide-linked biotin **8** (132 μg, 0.251 μmol) in DMSO (15 μL) was added to the solution of peptide **L-3e** (300 μg, 0.0251 μmol) in AcOH (30 μL)

and H_2O (15 μL), and the mixture was incubated at 37 °C overnight. The crude product was purified by preparative HPLC to afford peptide **L-4e** (210 μg, 67% yield). MS (ESI): Calcd for $C_{564}H_{864}N_{156}O_{156}S_4$: 12454.29; observed: $[M+14H]^{14+}$ *m/z* = 831.33, $[M+13H]^{13+}$ *m/z* = 890.68, $[M+12H]^{12+}$ *m/z* = 959.08, $[M+11H]^{11+}$ *m/z* = 1039.03, $[M+10H]^{10+}$ *m/z* = 1133.47, $[M+9H]^{9+}$ *m/z* = 1246.53.

L-pY1068 (EGFR$^{1060-1076}$: H-DTELPVPEpYINQSVPKR-NH$_2$)

By the standard procedure for peptide synthesis, L-pY1068 was synthesized (6.27 mg, 15% yield) from NovaSyn®TGR resin (76.9 mg, 0.02 mmol). Fmoc-Tyr[PO(OBzl)OH]-OH (57.4 mg, 0.1 mmol) was coupled by using TBTU (32.1 mg, 0.1 mmol), HOBt · H_2O (15.3 mg, 0.1 mmol) and (*i*-Pr)$_2$NEt (34.8 μL, 0.2 mmol) in DMF for 3 h. MS (ESI): Calcd for $C_{92}H_{145}N_{24}O_{29}P$: 2082.29; observed: $[M+3H]^{3+}$ *m/z* = 694.86, $[M+2H]^{2+}$ *m/z* = 1042.25.

D-pY1068

By the identical procedure described for the synthesis of L-pY1068, D-pY1068 was synthesized (7.50 mg, 18% yield) from NovaSyn®TGR resin (76.9 mg, 0.02 mmol). MS (ESI): Calcd for $C_{92}H_{145}N_{24}O_{29}P$: 2082.29; observed: $[M+3H]^{3+}$ *m/z* = 695.01, $[M+2H]^{2+}$ *m/z* = 1042.12.

Biotin-labeled L-EGFR$^{1060-1076}$ (biotin-DTELPVPEpYINQSVPKR-NH$_2$)

By the identical procedure described for the synthesis of L-pY1068, biotin-labeled L-EGFR$^{1060-1076}$ was synthesized (5.6 mg, 24% yield) from NovaSyn®TGR resin (38.5 mg, 0.01 mmol). Biotin (12.2 mg, 0.05 mmol) was coupled by using HBTU (19.0 mg, 0.05 mmol) HOBt · H_2O (7.66 mg, 0.05 mmol) and (*i*-Pr)$_2$NEt (17.4 μL, 0.1 mmol) in DMF for 2 h. MS (ESI): Calcd for $C_{102}H_{159}N_{26}O_{31}PS$: 2308.58; observed: $[M+3H]^{3+}$ *m/z* = 770.49, $[M+2H]^{2+}$ *m/z* = 1155.36.

Biotin-labeled D-EGFR$^{1060-1076}$

By the identical procedure described for the synthesis of biotin-labeled L-EGFR$^{1060-1076}$, biotin-labeled D-EGFR$^{1060-1076}$ was synthesized (14.0 mg, 30% yield) from NovaSyn®TGR resin (76.9 mg, 0.02 mmol). MS (ESI): Calcd for $C_{102}H_{159}N_{26}O_{31}PS$: 2308.58; observed: $[M+3H]^{3+}$ *m/z* = 770.50, $[M+2H]^{2+}$ *m/z* = 1155.35.

FLAG-labeled L-EGFR$^{1060-1076}$ (H-DYKDHDGDYKDHDIDYKDDDDK-DTELPV-PEpYINQSVPKR-NH$_2$)

By the identical procedure described for the synthesis of L-pY1068, FLAG-labeled L-EGFR$^{1060-1076}$ was synthesized (3.00 mg, 3% yield) from H-Rink Amide ChemMatrix resin (40 mg, ca. 0.02 mmol). MS (ESI): Calcd for $C_{207}H_{303}N_{54}O_{76}P$: 4794.98; observed: $[M+6H]^{6+}$ *m/z* = 800.26, $[M+5H]^{5+}$ *m/z* = 960.20, $[M+4H]^{4+}$ *m/z* = 1199.89.

FLAG-labeled D-EGFR$^{1060-1076}$

By the identical procedure described for the synthesis of FLAG-labeled L-EGFR$^{1060-1076}$, FLAG-labeled D-EGFR$^{1060-1076}$ was synthesized (34.8 mg, 9% yield) from H-Rink Amide ChemMatrix resin (160 mg, ca. 0.08 mmol). MS (ESI):

Calcd for $C_{207}H_{303}N_{54}O_{76}P$: 4794.98; observed: $[M+6H]^{6+}$ m/z = 800.25, $[M+5H]^{5+}$ m/z = 960.14, $[M+4H]^{4+}$ m/z = 1199.79.

Folding of Grb2 SH2 Domain Proteins

Lyophilized peptide was dissolved in denaturing buffer (6 M Gu · HCl, 20 mM HEPES, 100 mM NaCl, pH 8.5) at the concentration of 0.5 mg/mL. The solution was dialyzed three times against a 200-fold volume of a folding buffer (20 mM HEPES, 100 mM NaCl, 0.5 mM TCEP · HCl, pH 7.4) at 4 °C for 2 h using MWCO 3000 membrane.

Evaluation of Binding Activity on a Chemical Array

Photoaffinity linker-coated (PALC) slides were prepared according to previous reports using amine-coated slides and the photoaffinity PEG linker [19]. A solution of compounds in DMSO was spotted onto the PALC glass slides with a chemical arrayer equipped with 24 stamping pins or a MultiSPRinter spotter (Toyobo) equipped with single stamping pin. The slides were exposed to UV irradiation of 4 J/cm^2 at 365 nm using a CL-1000L UV crosslinker (UVP, CA) for immobilization. The slides were washed successively with DMSO, DMF, acetonitrile, THF, dichloromethane, EtOH, and ultrapure water (5 min, three times each), and dried. L-Grb2^{TMR} or D-Grb2^{TMR} (3 μM in 1% skimmed-milk-TBS-T) was incubated with the glass slide for 1 h, and then washed with TBS-T [10 mM Tris-HCl (pH 8.0), 150 mM NaCl, 0.05% Tween-20] (5 min, three times). The slides were dried and scanned at 532 nm on a GenePix scanner. The fluorescence signals were quantified with GenePixPro.

CD Spectra of L-Grb2$^{53–154}$ and D-Grb2$^{53–154}$

CD spectra of L-Grb2$^{53–154}$ and D-Grb2$^{53–154}$ were recorded in 5 mM HEPES buffer containing 0.1 mM TCEP · HCl, pH 7.4 on a JASCO J-720 circular dichroism spectrometer at 20 °C.

SPR Analysis

SPR analyses of EGFR$^{1060–1076}$ peptide binding to synthetic Grb2 and its derivatives were carried out using a Biacore T200 SPR instrument. 20 mM HEPES buffer containing 100 mM NaCl and 0.05% Tween-20 (pH 7.4) was used as the running buffer at 25 °C. For evaluation of unlabeled and TMR-labeled Grb2 SH2 domain proteins, biotinylated EGFR$^{1060–1076}$ peptide was immobilized on an SA sensor chip (L-EGFR$^{1060–1076}$ peptide: 26.1 RU, D-EGFR$^{1060–1076}$ peptide: 26.0 RU). For the evaluation of biotin-labeled Grb2 SH2 proteins, biotinylated Grb2 was immobilized on an SA sensor chip (L-Grb2$^{N\text{-}biotin}$: 1306.8 RU, D-Grb2$^{N\text{-}biotin}$: 1279.5 RU, L-Grb2$^{115\text{-}biotin}$: 1312.5 RU). All analytes were evaluated for 2 min of contact time, followed by 2 min dissociation at a flow rate of 30 μL/min. KD values were calculated by steady-state bindings from triplicate assays.

Competitive Binding Inhibition Assay by ELISA

ELISAs were performed in 20 mM HEPES buffer (pH 7.4) containing 100 mM NaCl, 0.05% Tween-20, 0.1% BSA. Precoated streptavidin 96-well plates (Nunc) were incubated with HEPES buffer containing 3% BSA (300 μL/well) for 1 h. After three washes, Grb2$^{N\text{-}biotin}$ (1.5 nM) in HEPES buffer (100 μL/well) was added and

incubated for 2 h. After three washes, 100 nM FLAG-labeled $EGFR^{1060-1076}$ peptide in the presence of varying concentration of inhibitors in HEPES buffer containing 1% DMSO (100 μL/well) was added and incubated for 1 h. After three washes, a 1:10,000 dilution of HRP-conjugated anti-FLAG antibody (Sigma) in HEPES buffer (100 μL/well) was added and incubated for 1 h. After three washes, TMB solution (Wako, 100 μL/well) was added and incubated for 1 h. Next, aqueous 2 N H_2SO_4 (10 μL/well) was added. Absorbance at 450 nm was measured for each well using an EnVision Xcite plate reader. The IC_{50} values were calculated using GraphPad Prizm (GraphPad software, San Diego, CA).

References

1. (a) Downward J, Parker P, Waterfield MD (1984) Autophosphorylation sites on the epidermal growth factor receptor. Nature 311:483–485; (b) Margolis BL, Lax I, Kris R, Dombalagian M, Honegger AM, Howk R, Givol D, Ullrich A, Schlessinger J (1989) All autophosphorylation sites of epidermal growth factor (EGF) receptor and HER2/neu are located in their carboxyl-terminal tails. Identification of a novel site in EGF receptor. J Biol Chem 264:10667–10671; (c) Batzer AG, Rotin D, Ureña JM, Skolnik EY, Schlessinger J (1994) Hierarchy of binding sites for Grb2 and Shc on the epidermal growth factor receptor. Mol Cell Biol 14:5192–5201
2. Salcini AE, McGlade J, Pelicci G, Nicoletti I, Pawson T, Pelicci PG (1994) Formation of Shc-Grb2 complexes is necessary to induce neoplastic transformation by overexpression of Shc proteins. Oncogene 9:2827–2836
3. (a) Lowenstein EJ, Daly RJ, Batzer AG, Li W, Margolis B, Lammers R, Ullrich A, Skolnik EY, Bar-Sagi D, Schlessinger J (1992) The SH2 and SH3 domain-containing protein GRB2 links receptor tyrosine kinases to ras signaling. Cell 70:431–442; (b) Gale NW, Kaplan S, Lowenstein EJ, Schlessinger J, Bar-Sagi D (1993) Grb2 mediates the EGF-dependent activation of guanine nucleotide exchange on Ras. Nature 363:88–92
4. Rodrigues GA, Falasca M, Zhang Z, Ong SH, Schlessinger J (2000) A novel positive feedback loop mediated by the docking protein Gab1 and phosphatidylinositol 3-kinase in epidermal growth factor receptor signaling. Mol Cell Biol 20:1448–1459
5. Kouhara H, Hadari YR, Spivak-Kroizman T, Schilling J, Bar-Sagi D, Lax I, Schlessinger J (1997) A lipid-anchored Grb2-binding protein that links FGF-receptor activation to the Ras/MAPK signaling pathway. Cell 89:693–702
6. Pendergast AM, Quilliam LA, Cripe LD, Bassing CH, Dai Z, Li N, Batzer A, Rabun KM, Der CJ, Schlessinger J, Gishizky ML (1993) BCR-ABL-induced oncogenesis is mediated by direct interaction with the SH2 domain of the GRB-2 adaptor protein. Cell 75:175–185
7. (a) Pawson T (1995) Protein modules and signalling networks. Nature 373:573–580; (b) Vidal M, Gigoux V, Garbay C (1995) SH2 and SH3 domains as targets for anti-proliferative agents. Crit Rev Oncol Hematol 40:175–186
8. (a) Burke TR (2006) Development of Grb2 SH2 Domain Signaling Antagonists: A Potential New Class of Antiproliferative Agents. Int J Pept Res Ther 12:33–48; (b) Kraskouskaya D, Duodu E, Arpin CC, Gunning PT (2013) Progress towards the development of SH2 domain inhibitors. Chem Soc Rev 42:3337–3370
9. Songyang Z, Shoelson SE, McGlade J, Olivier P, Pawson T, Bustelo XR, Barbacid M, Sabe H, Hanafusa H, Yi T, Ren R, Baltimore D, Ratnofsky S, Feldman R, Cantley LC (1994) Specific motifs recognized by the SH2 domains of Csk, 3BP2, fps/fes, GRB-2, HCP, SHC, Syk, and Vav. Mol Cell Biol 14:2777–2783
10. (a) Müller K, Gombert FO, Manning U, Grossmüller F, Graff P, Zaegel H, Zuber JF, Freuler F, Tschopp C, Baumann G (1996) Rapid identification of phosphopeptide ligands for SH2

domains. Screening of peptide libraries by fluorescence-activated bead sorting. J Bio Chem 271:16500–16505; (b) Kessels HW, Ward AC, Schumacher TN (2002). Specificity and affinity motifs for Grb2 SH2-ligand interactions. Proc Natl Acad Sci U S A 99:8524–8529; (c) Lee JY, Miraglia S, Yan X, Swartzman E, Cornell-Kennon S, Mellentin-Michelotti J, Bruseo C, France DS (2003) Oncology drug discovery applications using the FMAT 8100 HTS system. J Biomol Screen 8:81–88; (d) Luzy JP, Chen H, Gril B, Liu WQ, Vidal M, Perdereau D, Burnol AF, Garbay C (2008) Development of binding assays for the SH2 domain of Grb7 and Grb2 using fluorescence polarization. J Biomol Screen 13:112–119; (e) Krishnamoorthy S, Liu Z, Hong A, Zhu R, Chen H, Li T, Zhou X, Gao X (2013) A Novel Phosphopeptide Microarray Based Interactome Map in Breast Cancer Cells Reveals Phosphoprotein-GRB2 Cell Signaling Networks. PLos One 8:e67634

11. Gram H, Schmitz R, Zuber JF, Baumamn G (1997) Identification of phosphopeptide ligands for the Src-homology 2 (SH2) domain of Grb2 by phage display. Eur J Biochem 246:633–637
12. Oligino L, Lung FD, Sastry L, Bigelow J, Cao T, Curran M, Burke TR Jr, Wang S, Krag D, Roller PP, King CR (1997) Nonphosphorylated peptide ligands for the Grb2 Src homology 2 domain. J Biol Chem 272:29046–29052
13. Rahuel J, Gay B, Erdmann D, Strauss A, Gracía-Echeverría C, Fruet P, Caravatti G, Fretz H, Schoepfer J, Grütter MG (1996) Structural basis for specificity of Grb2-SH2 revealed by a novel ligand binding mode. Nat Struct Biol 3:586–589
14. (a) Wei CQ, Gao Y, Lee K, Guo R, Li B, Zhang M, Yang D, Burke TR Jr (2003) Macrocyclization in the design of Grb2 SH2 domain-binding ligands exhibiting high potency in whole-cell systems. J Med Chem 46:244–254; (b) Oishi S, Karki RG, Kang SU, Wang X, Worthy KM, Bindu LK, Nicklaus MC, Fisher RJ, Burke TR Jr (2005) Design and synthesis of conformationally constrained Grb2 SH2 domain binding peptides employing alpha-methylphenylalanyl based phosphotyrosyl mimetics. J Med Chem 48:764–772; (c) Oishi S, Shi ZD, Worthy KM, Bindu LK, Fisher RJ, Burke TR Jr (2005) Ring-closing metathesis of C-terminal allylglycine residues with an N-terminal beta-vinyl-substituted phosphotyrosyl mimetic as an approach to novel Grb2 SH2 domain-binding macrocycles. ChemBioChem 6:668–674; (d) Oishi S, Karki RG, Shi ZD, Worthy KM, Bindu L, Chertov O, Esposito D, Frank P, Gillette WK, Maderia M, Hartley J, Nicklaus MC, Barchi JJ Jr, Fisher RJ, Burke TR Jr (2005) Evaluation of macrocyclic Grb2 SH2 domain-binding peptide mimetics prepared by ring-closing metathesis of C-terminal allylglycines with an N-terminal beta-vinyl-substituted phosphotyrosyl mimetic. Bioorg Med Chem 13:2431–2438
15. (a) Yao ZJ, King CR, Cao T, Kelley J, Milne GW, Voigt JH, Burke TR Jr (1999) Potent inhibition of Grb2 SH2 domain binding by non-phosphate-containing ligands. J Med Chem 42:25–35; (b) Shi ZD, Wei CQ, Lee K, Liu H, Zhang M, Araki T, Roberts LR, Worthy KM, Fisher RJ, Neel BG, Kelley JA, Yang D, Burke TR Jr (2004) Macrocyclization in the design of non-phosphorus-containing Grb2 SH2 domain-binding ligands. J Med Chem 47:2166–2169
16. Alvi KA, Pu H, Luche M, Rice A, App H, McMahon G, Dare H, Margolis B (1999) Asterriquinones produced by Aspergillus candidus inhibit binding of the Grb-2 adapter to phosphorylated EGF receptor tyrosine kinase. J Antibiot 52:215–223
17. Nam JY, Son KH, Kim HK, Han MY, Kim SU, Choi JD, Kwon BM (2000) Sclerotiorin and Isochromophilone IV : Inhibitors of Grb2-Shc Interaction , Isolated from Penicillium multicolor F1753. J Microbiol Biotechnol 10:544–546 and the references cited therein
18. Kim HK, Nam JY, Han MY, Son KH, Choi JD, Kwon BM, Takusagawa HL, Huang Y, Takusagawa F (2000) Natural and synthetic analogues of actinomycin D as Grb2-SH2 domain blockers. Bioorg Med Chem Lett 10:1455–1457 and the references cited therein
19. Noguchi T, Oishi S, Honda K, Kondoh Y, Saito T, Ohno H, Osada H, Fujii N (2016) Screening of a virtual mirror-image library of natural products. Chem Commun 52:7653–7656
20. Hackeng TM, Griffin JH, Dawson PE (1999) Protein synthesis by native chemical ligation: expanded scope by using straightforward methodology. Proc Natl Acad Sci U S A 96:10068–10073

21. Wan Q, Danishefky SJ (2007) Free-radical-based, specific desulfurization of cysteine: a powerful advance in the synthesis of polypeptides and glycopolypeptides. Angew Chem Int Ed 46:9248–9252
22. Blanco-Canosa JB, Dawson PE (2008) An efficient Fmoc-SPPS approach for the generation of thioester peptide precursors for use in native chemical ligation. Angew Chem Int Ed 47:6851–6855
23. Weinstock MT, Jacobsen MT, Kay MS (2014) Synthesis and folding of a mirror-image enzyme reveals ambidextrous chaperone activity. Proc Natl Acad Sci U S A 111:11679–11684
24. (a) Müller K, Gombert FO, Manning U, Grossmüller F, Graff P, Zaegel H, Zuber JF, Freuler F, Tschopp C, Baumann G (1996) Rapid identification of phosphopeptide ligands for SH2 domains. Screening of peptide libraries by fluorescence-activated bead sorting. J Bio Chem 271:16500–16505; (b) Kessels HW, Ward AC, Schumacher TN (2002) Specificity and affinity motifs for Grb2 SH2-ligand interactions. Proc Natl Acad Sci U S A 99:8524–8529; (c) Lee JY, Miraglia S, Yan X, Swartzman E, Cornell-Kennon S, Mellentin-Michelotti J, Bruseo C, France DS (2003) Oncology drug discovery applications using the FMAT 8100 HTS system. J Biomol Screen 8:81–88
25. Fang GM, Li YM, Shen F, Huang YC, Li JB, Lin Y, Cui HK, Liu L (2011) Protein chemical synthesis by ligation of peptide hydrazides. Angew Chem Int Ed 50:7645–7649
26. Ettmayer P, France D, Gounarides J, Jarosinski M, Martin MS, Rondeau JM, Sabio M, Topiol S, Weidmann B, Zurini M, Bair KW (1999) Structural and conformational requirements for high-affinity binding to the SH2 domain of Grb2(1). J Med Chem 42:971–980
27. (a) Panayotou G, Bax B, Gout I, Federwisch M, Wroblowski B, Dhand R, Fry MJ, Blundell TL, Wollmer A, Waterfield MD (1992) Interaction of the p85 subunit of PI 3-kinase and its N-terminal SH2 domain with a PDGF receptor phosphorylation site: structural features and analysis of conformational changes. EMBO J 11:4261–4272; (b) Shoelson SE, Sivaraja M, Williams KP, Hu P, Schlessinger J, Weiss MA (1993) Specific phosphopeptide binding regulates a conformational change in the PI 3-kinase SH2 domain associated with enzyme activation. EMBO J 12:795–802; (c) Haan S, Hermmann U, Hassiepen U, Schaper F, Schneider-Mergener J, Wollmer A, Heinrich PC, Grötzinger J (1999) Characterization and binding specificity of the monomeric STAT3-SH2 domain. J Biol Chem 274:1342–1348
28. Rahuel J, Gay B, Erdmann D, Strauss A, Gracía-Echeverría C, Fruet P, Caravatti G, Fretz H, Schoepfer J, Grütter MG (1996) Structural basis for specificity of Grb2-SH2 revealed by a novel ligand binding mode. Nat Struct Biol 3:586–589
29. (a) Liu WQ, Vidal M, Gresh N, Rogues BP, Garbay C (1999) Small peptides containing phosphotyrosine and adjacent alphaMe-phosphotyrosine or its mimetics as highly potent inhibitors of Grb2 SH2 domain. J Med Chem 42:3737–3741; (b) Gao Y, Luo J, Yao ZJ, Guo R, Zou H, Kelley J, Voigt JH, Yang D, Burke TR Jr (2000) Inhibition of Grb2 SH2 domain binding by non-phosphate-containing ligands. 2. 4-(2-Malonyl)phenylalanine as a potent phosphotyrosyl mimetic. J Med Chem 43:911–920; (c) Furet P, Gay B, Caravatti G, Gracía-Echeverría C, Rahuel J, Schoepfer J, Fretz H (1998) Structure-based design and synthesis of high affinity tripeptide ligands of the Grb2-SH2 domain. J Med Chem 41:3442–3449
30. Pawson T, Nash P (2003) Assembly of cell regulatory systems through protein interaction domains. Science 300:445–452
31. Cody WL, Lin Z, Panek RL, Rose DW, Rubin JR (2000) Progress in the development of inhibitors of SH2 domains. Curr Pharm Des 6:59–98

Chapter 4
Conclusions

Abstract In summary, the author developed a screening process from a virtual mirror image library of natural products using synthetic D-protein technology. In contrast to conventional screening approaches, this process could identify hit compounds from unavailable mirror-image chiral natural products, thus providing unprecedented lead compounds for drug discovery.

Keywords Mirror-image screening · D-protein technology · Chemical protein synthesis · *ent*-Natural products

1. The author has established screening protocols for binding compounds of MDM2 and MDMX by chemical array technology using synthetic fluorescent proteins. The preliminary screening of an in-house chemical library identified a number of peptidic binding compounds towards MDM2 and MDMX. The subsequent FP assay identified three dual inhibitors of MDM2–p53 and MDMX–p53 interactions.
2. The author has established a novel screening process for MDM2-p53 inhibitors from a virtual mirror-image library of chiral natural products and derivatives. Chemically synthesized mirror-image MDM2 was applied for chemical array screening of a library of natural product derivatives, identifying novel tocopherol derivative NP843 as a D-MDM2–D-p53 interaction inhibitor. Chemical synthesis of the enantiomeric compound enabled the validation of the inhibitory activity of *ent*-NP843 against the L-MDM2–L-p53 interaction. The selective recognition by MDM2 was attributed to the stereochemistry of the tetra substituted carbon on the chromane skeleton of *ent*-NP843. The aliphatic side chain of three isoprene units was also needed for the inhibitory activity.
3. The author investigated the chemical synthesis of Grb2 SH2 domain proteins and application to the development of in vitro assay systems for Grb2 SH2 domain inhibitors. Several labeled Grb2 SH2 proteins including $Grb2^{TMR}$, $Grb2^{N\text{-biotin}}$ and $Grb2^{115\text{-biotin}}$ were synthesized. Screening systems using both enantiomers

© Springer Nature Singapore Pte Ltd. 2018

T. Noguchi, *Development of Chemistry-Based Screening Platform for Access to Mirror-Image Library of Natural Products*, Springer Theses,
https://doi.org/10.1007/978-981-10-6623-8_4

of these proteins to some bioassays including SPR analysis, chemical array and ELISA, were developed.

In summary, the author developed a screening process from a virtual mirror-image library of natural products using synthetic D-protein technology. In contrast to conventional screening approaches, this process could identify hit compounds from unavailable mirror-image chiral natural products, thus providing unprecedented lead compounds for drug discovery.

In mirror-image screening strategy, mirror-image molecules (target proteins and hit natural products) should be prepared. These mirror-image molecules are mainly prepared by organic chemistry methods, such as total synthesis of natural products and chemical protein synthesis. Therefore, the author expects that the mirror-image screening strategy not only provides opportunities to identify novel lead compounds, but also provides new values in the field of organic chemistry. Investigation of the bioactivities and functions of virtual mirror-image molecules is achievable only by using advanced synthetic organic chemical technologies.